1-1-2016

Activatable Fluorophores for the Molecular Imaging of Cytosolic Phospholipase A2 in Breast Cancer

Michael Chiorazzo
University of Pennsylvania, mchio@mail.med.upenn.edu

Activatable Fluorophores for the Molecular Imaging of Cytosolic Phospholipase A2 in Breast Cancer

Abstract
Breast cancer is the most commonly diagnosed cancer in women and the number two cause of cancer associated death. Surgery is the first line of defense in treating breast cancer and the success of surgery has been shown to predict the probability of cancer reoccurrence. Near Infrared (NIR) fluorescence guided surgery offers the potential to increase the accuracy of surgical resection by the use of fluorescence imaging agents targeted towards cancer. Cytosolic Phospholipase A2 (cPLA2) activity is enhanced in triple negative breast cancer and is associated with resistance to therapy in luminal-like cancers. The goal of this work is to develop activatable fluorophores targeted towards cPLA2 and evaluate their use for the molecular imaging of breast cancer in order to determine their potential as contrast agents for NIR fluorescence guided surgery. A series of tricyclic fluorophores were caged through esterification with fatty acids. Arachidonic acid was utilized to generate cPLA2 selective probes and palmitic acid was used to generate control probes. In vitro, probes were shown to activate in the presence of purified PLA2 and results were used to identify the most promising probe: DDAO arachidonate. Cellular fluorescence spectroscopy and microscopy showed DDAO arachidonate activated in breast cancer cell lines expressing cPLA2, where control probe did not. Modulation of cPLA2 activity through inhibition, induction, and genetic knockdown, resulted in corresponding changes in fluorescence generation. In a panel of breast cancer cell lines, cPLA2 expression, varied based on molecular subtype and correlated with DDAO arachidonate activation. Finally, DDAO arachidonate, when painted onto human triple negative tumor mouse xenografts, resulted in selective activation of tumor but not surrounding healthy tissue. Together, these results indicate DDAO arachidonate is a useful agent for measuring cPLA2 activity in both breast cancer cells and tumors and may offer the potential to aid in the fluorescence guided surgery of triple negative breast cancer.

Degree Type
Dissertation

Degree Name
Doctor of Philosophy (PhD)

Graduate Group
Pharmacology

First Advisor
Edward J. Delikatny

Second Advisor
Anatoliy V. Popov

Keywords
Activatable Fluorescence, Breast Cancer, Fluorescence Guided Surgery

ACTIVATABLE FLUOROPHORES FOR THE MOLECULAR IMAGING OF CYTOSOLIC PHOSPHOLIPASE A2 IN BREAST CANCER

Michael Gerard Chiorazzo

A DISSERTATION

in

Pharmacology

Presented to the Faculties of the University of Pennsylvania

in

Partial Fulfillment of the Requirements for the

Degree of Doctor of Philosophy

2016

Supervisor of Dissertation

_____

E. James Delikatny, Ph.D.
Professor of Radiology

Co-Supervisor of Dissertation

_____

Anatoliy V. Popov, Ph.D.
Research Assistant Professor of Radiology

Graduate Group Chairperson

_____

Julie Blendy, Ph.D.
Professor of Pharmacology

Dissertation Committee
Andrew Tsourkas, Ph.D., Professor of Bioengineering
Ian Blair, Ph.D., A.N. Richards Professor of Pharmacology
Garret FitzGerald, M.D., F.R.S, Professor of Medicine and Pharmacology
Robert Mach, Ph.D., Britton Chance Professor of Radiology

ACTIVATABLE FLUOROPHORES FOR THE MOLECULAR IMAGING OF

CYTOSOLIC PHOSPHOLIPASE A2 IN BREAST CANCER COPYRIGHT

2016

Michael Gerard Chiorazzo

Dedicated to my Aunt,

Mary Domke

ACKNOWLEDGMENTS

First and foremost I would like to thank my advisor, Dr. Jim Delikatny for his support and guidance throughout my graduate studies. I would also like to thank Dr. Anatoliy Popov, whose chemical expertise made this work possible.

I thank my committee members: Dr. Andrew Tsourkas, Dr. Ian Blair, Dr. Garret FitzGerald, and Dr. Robert Mach for their invaluable knowledge, expertise and experimental insight.

I would also like to thank past and present members of the Delikatny lab. In addition to providing help and feedback during critical experiments, their friendships made every day more enjoyable.

I would like to thank all members of the pharmacology graduate group who I have had the pleasure of getting to know. I have no doubts that I will remain lifelong friends with many of you.

I need to also thank Samantha Murray, who I met here in Philadelphia. You make good days great and bad days more bearable.

I thank my family for their unconditional support and love. I thank my sister and best friend Jill Chiorazzo. I also thank John McSweeney and Michael Young, who I consider my brothers. Finally, I thank my parents for everything they do to help me succeed.

ABSTRACT

ACTIVATABLE FLUOROPHORES FOR THE MOLECULAR IMAGING OF CYTOSOLIC PHOSPHOLIPASE A2 IN BREAST CANCER

Michael Gerard Chiorazzo

E. James Delikatny, Ph.D.

Breast cancer is the most commonly diagnosed cancer in women and the number two cause of cancer associated death. Surgery is the first line of defense in treating breast cancer and the success of surgery has been shown to predict the probability of cancer reoccurrence. Near Infrared (NIR) fluorescence guided surgery offers the potential to increase the accuracy of surgical resection by the use of fluorescence imaging agents targeted towards cancer. Cytosolic Phospholipase A2 (cPLA2) activity is enhanced in triple negative breast cancer and is associated with resistance to therapy in luminal-like cancers. The goal of this work is to develop activatable fluorophores targeted towards cPLA2 and evaluate their use for the molecular imaging of breast cancer in order to determine their potential as contrast agents for NIR fluorescence guided surgery. A series of tricyclic fluorophores were caged through esterification with fatty acids. Arachidonic acid was utilized to generate cPLA2 selective probes and palmitic acid was used to generate control probes. *In vitro*, probes were shown to activate in the presence of purified PLA2 and results were used to identify the most promising probe: DDAO arachidonate. Cellular fluorescence spectroscopy and microscopy showed DDAO arachidonate activated in breast cancer cell lines expressing cPLA2, where control probe did not. Modulation of cPLA2 activity through inhibition, induction, and genetic

knockdown, resulted in corresponding changes in fluorescence generation. In a panel of breast cancer cell lines, cPLA2 expression, varied based on molecular subtype and correlated with DDAO arachidonate activation. Finally, DDAO arachidonate, when painted onto human triple negative tumor mouse xenografts, resulted in selective activation of tumor but not surrounding healthy tissue. Together, these results indicate DDAO arachidonate is a useful agent for measuring cPLA2 activity in both breast cancer cells and tumors and may offer the potential to aid in the fluorescence guided surgery of triple negative breast cancer.

TABLE OF CONTENTS

LIST OF TABLES

LIST OF ILLUSTRATIONS

CHAPTER 1: Introduction

1.1 Breast Cancer

In women, breast cancer is the most frequently diagnosed cancer and the second highest cause of cancer related death (DeSantis et al. 2014). Breast cancer has been shown to be not one disease, but an umbrella term for numerous cancer subtypes. Extensive study on the molecular basis of breast cancer subtypes has led to the elucidation of varying genetic signatures. This has driven the development of molecular based therapeutics, which targets these genetic signatures in each subtype. The growth of targeted therapeutics in addition to increased screening of the general population has likely been the cause of decreased mortality rates in breast cancer patients (Berry et al. 2005). Despite this, surgical resection through either mastectomy or breast conserving surgery in combination with radiation therapy remains the standard for primary treatment (DeSantis et al. 2014). The accuracy of surgery, as defined by the presence of positive margins in tissue histology, is a significant predictor for local recurrence and metastasis, suggesting complete removal of the primary tumor is necessary for enhancing the probability of relapse free survival (Singletary 2002).

Estrogen receptor (ER) positive is the most frequently diagnosed form of breast cancer (Haque et al. 2012). Commonly referred to as luminal-like, cancers expressing estrogen receptor can be classified as luminal A or luminal B. Luminal A has the most favorable prognosis of all breast cancer subtypes and is associated with the highest probability of relapse free and overall survival (Prat and Perou 2011). It is generally defined as having high levels of ER and/or progesterone receptor (PR) with no expression

of the HER2/*Neu* oncogene, low Ki67 staining (a standard marker of proliferation), and a low histological grade (Eroles et al. 2012). For breast cancer, histological grade is determined in accordance with the Nottingham grading system which evaluates tumors based on tubule formation, nuclear grade, and mitotic rate (Edge and Compton 2010). Luminal B breast cancer has high amounts of ER and/or PR along with either expressing the HER2/*Neu* oncogene or having high staining for Ki67 with a high histological grade. Unlike luminal A, luminal B breast cancer has lower rates of relapse free and overall survival (Prat and Perou 2011). In addition to surgery and radiation therapy, common adjuvant treatment of luminal-like breast cancer consists of hormonal therapy with selective estrogen receptor modifiers (SERMs). One of the most commonly used SERMs is tamoxifen, a prodrug whose biologically active metabolites result in competitive antagonism of ER (Osborne 1998).

HER2-type breast cancer is defined as expressing the HER2/*Neu* oncogene without expression of ER or PR (Eroles et al. 2012). The HER2/*Neu* gene encodes for a transmembrane tyrosine kinase receptor that falls within the epidermal growth factor receptor (EGFR) family (Ross et al. 2003). Activation of EGFR enhances homo and hetero-dimerization resulting in autophosphorylation and the initiation of various major biological signaling cascades (Normanno et al. 2006). Overexpression of HER2/*Neu* has been shown to occur in 20-30% of breast cancers and has fueled the development of anti-HER2/*Neu* therapies (Slamon et al. 1987). Most notable is the monoclonal antibody, trastuzumab, which is selective for the extracellular portion of the HER2 transmembrane protein (Hudis 2007). The anti-cancer activity of trastuzumab may result from a

combination of mechanisms including decreasing HER2 dimerization, increasing receptor endocytosis and subsequent degradation, preventing the cleavage and release of the extracellular domain, and immune activation resulting in cancer cell death (Valabrega, Montemurro, and Aglietta 2007). Regardless, significant efficacy has been shown in HER2-type breast cancer patients when used in combination with traditional chemotherapeutics (O'Sullivan et al. 2015).

Basal-like is a subtype of breast cancer which does not have elevated ER, PR, or HER2/*Neu*. Because of this, it is often referred to as triple negative breast cancer and has the lowest probability of relapse free and overall survival (Eroles et al. 2012). No molecular based therapeutics exist for this subtype and only traditional chemotherapy in addition to surgery and radiation therapy is possible. Basal-like breast cancer has a high response rate to pre-surgical neoadjuvant chemotherapy (Lehmann et al. 2011). Despite this, high rates of recurrence and metastasis result in lower probability of relapse free and overall survival, with less than 30% of basal-like patients surviving 5 years.

A further complication to this model of genetic variation and subsequent treatment of breast cancer is the increasing understanding of tumor heterogeneity. Heterogeneity within breast cancer can arise both spatially, in which several populations of cells with varying genetic signatures are present within the same tumor, or temporally, in which the genetic signatures of cells change with time in the primary tumor and metastatic lesions (Zardavas et al. 2015). Certain basal-like tumors have been shown to contain distinct populations of luminal-like progenitors (Lim et al. 2009). In addition,

differences in expression of ER, PR, and HER2 have been seen between primary tumor and metastatic lesions (Aurilio et al. 2014).

It is likely that tumor heterogeneity, in addition to the limited number of molecular therapeutics, contributes to the problem of breast cancer resistance, reoccurrence, and metastasis. Because of therapeutic limitations, surgical resection through either mastectomy or breast conserving surgery in combination with radiation therapy remains the primary treatment for breast cancer, being performed in 95% of cases. Improvement of surgical resection efficiency would likely have a high benefit on survival.

Near Infrared (NIR) fluorescence guided surgery has recently emerged as a powerful technique to aid surgeons during tumor resection. By administering fluorophores, which either accumulate or activate specifically in cancerous tissue, surgeons can use fluorescence as a guide for the discernment of tumor margins (Nguyen and Tsien 2013). To date, several studies have shown the ability of NIR fluorescence guided surgery to improve surgical resections in patients (Shinoda et al. 2003, van Dam et al. 2011, Day et al. 2013, Stummer et al. 2006, Keating et al. 2016, Judy et al. 2015). However, the pool of fluorescence contrast agents under study remains small and the most well studied agents rely primarily on the enhanced permeability and retention effect (EPR) of tumors. In order to expand the capabilities and efficiency of this technique, new contrast agents targeted towards distinct molecular features of cancer are urgently needed.

1.2 Phospholipases

Phospholipases are a class of enzyme responsible for the catabolism of phospholipids within biological membranes. First discovered for their role as a lytic agent in snake venom, phospholipases have since been shown to have numerous biological functions including digestion, membrane re-modeling (necessary for cell division, motility, and vesicular trafficking), and the generation of bioactive signaling molecules (Burke and Dennis 2009, Rocha et al. 2014). In cancer, increased cell division through membrane remodeling along with the production of bioactive signaling molecules that promote cancer progression have been linked to phospholipase activation.

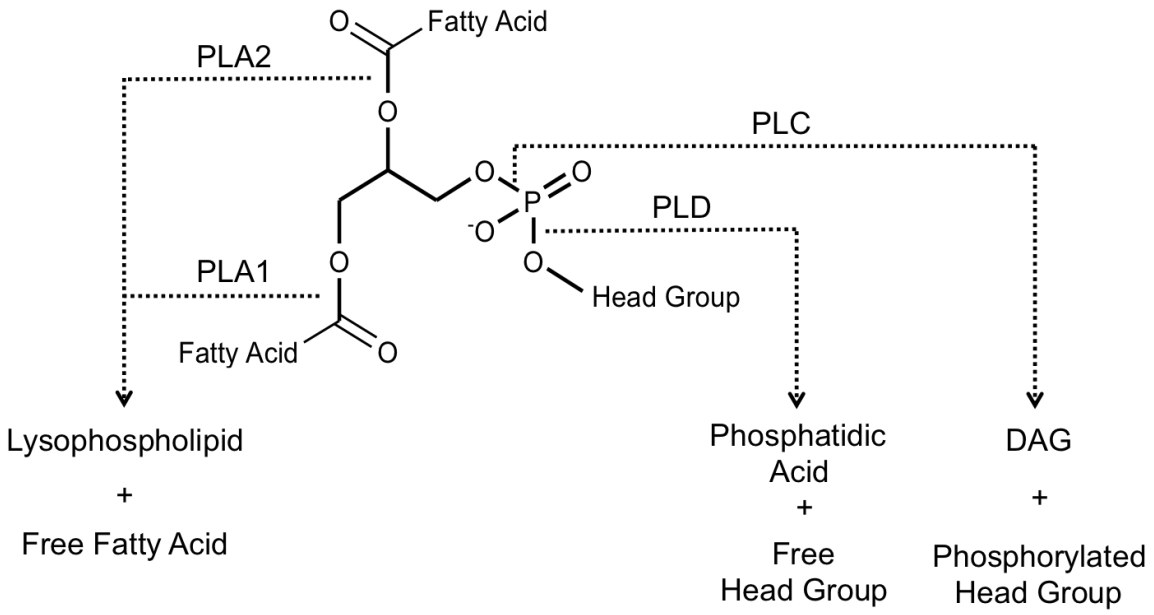

Figure 1.1. Overview of phospholipase activity. PLA1 and PLA2 cleave at the *sn*-1 and *sn*-2 ester bond respectively to generate lysophosphatidic acid and a free fatty acid. PLC cleaves at the glycerol-phosphate bond to release phosphatidic acid and a free head group. PLD cleaves at the head group-phosphate bond to generate DAG and a phosphorylated head group.

Phospholipases are grouped into four major categories based on the location in which they hydrolyze phospholipids (Figure 1.1). Phospholipase D hydrolyzes the bond linking the head group to the phosphate moiety releasing a free head group in addition to phosphatidic acid. Phospholipase D has been found elevated in several cancers including breast, colon, gastric, and kidney (Park et al. 2012). It is generally thought to promote cancer progression through the activation of RAS and mTOR by phosphatidic acid (Zhao et al. 2007, Fang et al. 2001). Phospholipase C is perhaps the most well-known phospholipase for its role in signaling. Phospholipase C hydrolyses the glycerophosphate bond of phospholipids releasing diacylglycerol (DAG) and a phosphorylated head group. When phospholipase C acts on phosphatidylinositides, inositol-1,4,5-triphosphate (IP3) is released. IP3 and DAG have been extensively studied for their role in signaling and in relation to cancer. IP3 leads to release of calcium from intracellular stores leading to modulation of numerous enzymes which are dependent on calcium binding (Berridge 2009). DAG is the principal activator of protein kinase C (PKC), which has been shown to promote the progression of cancer (Griner and Kazanietz 2007). Finally, phospholipase A1 and A2 (PLA1 and PLA2, respectively) are responsible for the release of a lysophospholipid and a free fatty acid from, respectively, either the *sn*-1 or *sn*-2 position of the glycerol backbone. Lysophospholipids are potent activators of cancer and can stimulate mobilization and subsequent invasion (Xu et al. 1995). Free fatty acids can be stored in lipid droplets, recycled into biological membranes, metabolized via beta oxidation, or used to synthesize downstream signaling molecules (Boren and Brindle 2012, Delikatny et al. 2011). Arachidonic acid release serves as the precursor to

eicosanoid signaling molecules, which have been shown to have numerous roles in cancer progression (Wang and Dubois 2010).

PLA2 can be further sub-classified into sixteen groups, each representing PLA2 enzymes with distinct biological functions. Secreted phospholipase A2 (sPLA2) enzymes (which include groups I, II, III, V, and X) are found in the extracellular space, are the largest family of phospholipases, and the first to be discovered. Though large in number, they are smallest in size, typically ranging from 14-18 kDa (with the exception of group III). sPLA2 enzymes are dependent on calcium for activity and serve a range of functions including digestion, activity in inflammatory processes, and microbial protection (Burke and Dennis 2009). sPLA2 has been shown to play a role in several diseases including rheumatoid arthritis, atherosclerosis, and cancer (Dennis et al. 2011).

Calcium independent phospholipase (iPLA2, group VI) is an intracellular PLA2 which does not require calcium for its activity (Burke and Dennis 2009). iPLA2β is the most well studied iPLA2 family member. Due to its calcium independent actions it has been long thought to function in homeostatic membrane remodeling (Winstead, Balsinde, and Dennis 2000). Recently it has been suggested that iPLA2 may also be active in several signaling processes. iPLA2 has been implicated in the development of diabetes, Barth syndrome, and NBIA/neuroaxonal dystrophy (Dennis et al. 2011).

Platelet activating factor-acetyl hydrolase (PAF-AH, group VII) acts on PAF to release acetate from the *sn*-2 position. PAF-AH is a secreted enzyme that associates with LDL and HDL in the human plasma (Tjoelker et al. 1995). Increased PAF-AH is

associated with an increased risk of coronary disease, stroke, and mortality (Oei et al. 2005). Lysosomal phospholipase A2 (LPLA2) (group XV) localizes to lysosomal compartments of cells where it acts to degrade lysosomal phospholipids. LPLA2 is highly expressed in alveolar macrophages (Abe et al. 2004). Adipose-specific phospholipase A2 (group XVI) is expressed to high levels in white adipose tissue (Duncan et al. 2008). Adipose-specific phospholipase A2 has been shown to also possess PLA1 activity and functions to release stored fatty acids for energy conversion through beta oxidation.

Cytosolic phospholipase A2 (cPLA2, group IV) is a class of phospholipases that are primarily considered signaling enzymes. Like iPLA2, cPLA2 is an intracellular phospholipase and resides in the cytosol until activated (Dennis et al. 2011). cPLA2α, the most studied isoform, was first found in platelets and neutrophils, but is now known to be ubiquitously expressed in all mammalian tissue. This 85 kDa protein contains a C2 calcium binding domain and a catalytic domain containing a unique catalytic dyad instead of the catalytic triad seen in α/β hydrolases (Dessen et al. 1999). Unlike other PLA2 enzymes, cPLA2α displays substrate specificity for arachidonic acid at the *sn*-2 position (Murakami et al. 2011). Since the discovery of cPLA2α, two additional human isoforms have been found (along with three murine isoforms). cPLA2β is a ubiquitous phospholipase, and contains a C2 domain and a catalytic domain similar to cPLA2α. Unlike cPLA2α, cPLA2β has relatively low substrate specificity and general phospholipase activity. cPLA2γ is expressed to a high degree in heart and skeletal

muscle, has low substrate specificity, and lacks a C2 domain allowing it to act independent of calcium (Dennis et al. 2011).

1.3 cPLA2 and Cancer

cPLA2α, henceforth referred to as cPLA2, is activated during calcium release from cytosolic stores. The binding of calcium to the C2 domain of cPLA2 results in translocation to the perinuclear membrane where it acts upon arachidonic acid-containing phospholipids. In addition to calcium, cPLA2 activity can be enhanced by phosphorylation through mitogen-activated protein (MAP). Ser505 phosphorylation promotes membrane binding of hydrophobic residues surrounding the active site. This allows for cPLA2 to remain bound to the membrane and active after the cytosolic calcium concentration returns to baseline (Das et al. 2003). An additional residue, Ser727 is targeted by a heterotetramer (A2t) of p11 and annexin A2, which when bound to Ser727 disrupts cPLA2 membrane binding and inhibits activity (Tian et al. 2008). Phosphorylation of Ser727 prevents targeting by the inhibitory A2t tetramer and allows full activation of cPLA2. In addition, phosphorylation of Ser515 by calmodulin-dependent kinase II has also been shown to result in cPLA2 activation (Muthalif et al. 2001). Independent of phosphorylation, several other associations result in the retainment of cPLA2 on the membrane. Phosphatidylinositol 4,5-bis phosphate (PIP2) has been found to bind residues within the catalytic domain and promote cPLA2 activity (Tucker et al. 2009). Finally, ceramide-1-phosphate (C1P) has been found to be required for translocation of cPLA2 through association with a β-groove in the C2 domain (Lin et al. 1993, Mosior, Six, and Dennis 1998, Subramanian et al. 2005, Lamour et al. 2009).

cPLA2 functions as a signaling agent due to its ability to release free arachidonic acid. Free arachidonic acid is an important central mediator in inflammatory and replicative processes. Arachidonic acid can be acted upon by cytochrome P450 (CYPs), lipoxygenase, or cyclooxygenase to generate prostaglandins and eicosanoids, a large family of bioactive molecules involved in autocrine and paracrine signaling (Figure 1.2) (Wang and Dubois 2010). In addition to homeostatic maintenance, eicosanoids are involved in a wide range of functions including vasodilation and constriction of vascular smooth muscle, aggregation and declumping of platelets, contraction of uterine smooth muscle, bone resorption, ovulation, pain response, fever generation, and inflammation (Funk 2001). Dysregulation of eicosanoids has been implicated in several diseases including rheumatoid arthritis, hypertension, atherosclerosis, and cancer.

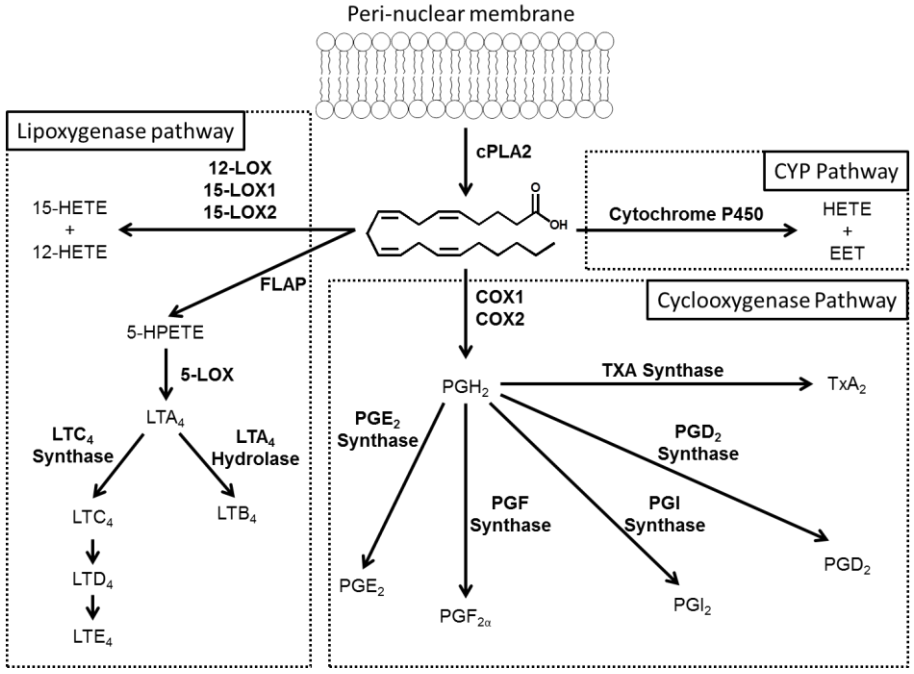

Figure 1.2. Eicosanoid Signaling Pathway.

CYPs are best known for their involvement in the detoxification of compounds in the liver. Blockage of these enzymes can result in the prolonged half-life of drugs, resulting in increased delivery of many compounds, including anticancer drugs (Panigrahy et al. 2010). In contrast, certain anticancer prodrugs rely on the actions of CYPs and increasing their activity may increase efficacy (Lu, Chen, and Waxman 2009). In addition, the action of CYPs on endogenous substrates such as arachidonic acid are thought to play a role in tumor progression (Nebert and Dalton 2006). Arachidonic acid metabolism through CYPs occurs through either the ω-hydroxylase pathway, resulting in the formation of hydroxyeicosatetraenoic acids (HETEs), or the epoxygenase pathway, resulting in formation of epoxyeicosatrienoic acids (EETs) (Panigrahy et al. 2010). 20-HETE, the primary metabolite of the ω-hydroxylase pathway, has pro-inflammation and pro-angiogenic associations. Inhibition of CYPs in the 20-HETE pathway has been shown to reduce tumor growth in triple negative breast cancer, mouse tumor xenografts (Borin et al. 2014). EETs have also been shown to promote angiogenesis and have a role in epithelial cell proliferation (Harris et al. 1990). CYP J2J, involved in EET synthesis has been found to be elevated in 77% of carcinomas (Jiang et al. 2005).

Lipoxygenase activity results in the formation of HETEs and leukotrienes, which have been shown to have several roles in cancer (Wang and Dubois 2010). LTB4 has been shown to be increased in colon and prostate cancer (Larre et al. 2008, Dreyling et al. 1986). Pancreatic cancer has increased LTB4 receptors, and administration of LTB4 increases growth of pancreatic cancer cells (Hennig et al. 2002). LTA4 hydrolase has been shown to be elevated in esophageal cancer through analysis of patient tissue (Chen

et al. 2003). Inhibition of LTA4 hydrolase in a rat model of esophageal cancer resulted in reduced cancer growth (Chen et al. 2003).

The cyclooxygenase pathway is the most well studied pathway for arachidonic acid metabolism in relation to cancer. Cyclooxygenase has two isoforms (COX-1 and -2), with COX-1 being considered a constitutively active housekeeping enzyme whereas COX-2 is inducible in response to various stimuli (Simmons, Botting, and Hla 2004). In cancer, overexpression of COX-2 has been shown in numerous cancers including colon, prostate, head and neck, lung, cervical, and breast cancer (Eberhart et al. 1994, Gupta et al. 2000, Khuri et al. 2001, Kulkarni et al. 2001, Lin et al. 2002, Subbaramaiah et al. 2002). Inhibition of cyclooxygenases with nonsteroidal anti-inflammatory drugs (NSAIDs) has shown some ability to prevent and treat cancer (Thun, Henley, and Patrono 2002).

Cyclooxygenase acts on arachidonic acid to generate prostaglandin H2, which is then further converted into the prostaglandins and thromboxanes. Prostaglandins have been shown to have varying activity in cancer progression. PGE2 is well known for its association with cancer, promoting proliferation, angiogenesis, metastasis, and evasion of apoptosis (Greenhough et al. 2009). In contrast, increased production of PGD2 results in decreased growth of cancer (Park et al. 2007). It has been hypothesized that this is not through the direct activity of PGD2 but due to either the association of the PGD2 product, 15dPGJ2, with PPARγ or through depletion of PGE2 through increased PGD2 synthesis (Sertznig et al. 2007, Wang and Dubois 2010).

The expression of cPLA2 and COX2 has been shown to be positively correlated in colorectal cancer, likely due to the requirement of free arachidonic acid for prostaglandin production (Panel et al. 2006). Unsurprisingly, cPLA2 has been shown to be overexpressed in a number of cancers and associated with cancer development (Hong et al. 2001, Meyer et al. 2004, Murakami et al. 2011). In breast cancer, cPLA2 activity correlates with molecular subtype (Caiazza, Harvey, and Thomas 2010). In both established cell lines and patient tissue, cPLA2 mRNA is significantly elevated in basal-like versus luminal-like breast cancer (Caiazza et al. 2011). In agreement with these observations, ^{1}H nuclear magnetic resonance (NMR) analysis of glycerophosphocholine, generated through the hydrolysis of phosphatidylcholine by cPLA2, is markedly elevated in basal-like cancers compared to luminal-like cancers (Moestue et al. 2010). In luminal-like breast cancer, it has been shown that estradiol-2 can lead to rapid phosphorylation and subsequent activation of cPLA2 through an EGFR mediated mechanism (Caiazza, Harvey, and Thomas 2010). Furthermore, a correlation between cPLA2 mRNA and EGFR mRNA has been shown in both basal-like and luminal-like breast cancers (Caiazza et al. 2011). It has been suggested that cPLA2 activation through EGFR is a possible mechanism for the development of resistance to estrogen receptor therapy. In support of this claim, it has been shown that luminal-like patients with higher levels of cPLA2 have a significantly lower rate of overall survival (Caiazza et al. 2011). As a result, cPLA2 is emerging as a useful biomarker for the differentiation of breast cancer subtypes and a predictor for the likelihood of resistance generation to estrogen receptor therapy.

1.4 Molecular Imaging and Cancer

There are a number of platforms for cancer imaging currently in clinical and preclinical use, including X-ray computed tomography (CT), ultrasound, magnetic resonance imaging/spectroscopy (MRI/MRS), positron emission tomography (PET), and fluorescence. Depending on the technique employed, anatomical, physiological, and/or molecular information about cancer can be obtained. Imaging may be performed with the use of exogenous contrast agents or may rely on the distinction of endogenous features visualized through energy/tissue interfaces. Molecular imaging of cancer offers the potential to provide phenotypic and genotypic information in addition to anatomical tumor location. Real-time knowledge of the molecular characteristics of tumors allows for the determination, monitoring, and possible alteration of treatment protocols (Weissleder 2006). In addition, tools that can assess cancer signatures in *in vivo* models can fuel anticancer drug design and evaluation (Willmann et al. 2008).

CT, ultrasound, and MRI are all widely used in clinical practice. Traditionally, these modalities have been used for anatomical imaging. Although this remains their primary use, research in the use of these techniques for molecular imaging has been of increased interest. Smart or targeted contrast agents have been utilized in these modalities to image molecular characteristics unique to cancer. As an example, gold nanoparticles conjugated to a prostate specific membrane antigen (PMSA) RNA aptamer were used to image PMSA expressing prostate cancer using CT (Popovtzer et al. 2008). $A_v\beta_3$ integrin targeted microbubbles have been used to image tumor associated angiogenesis using ultrasound (Willmann et al. 2010). Finally, MRI contrast agents

targeted towards the folate receptor have been used for the molecular imaging of ovarian cancer (Konda et al. 2001). Numerous other contrast agents have been targeted towards cancer-associated markers using these techniques.

MRS has been investigated in combination with MRI for molecular imaging of cancer. By defining a cancerous region of interest (ROI) with MRI, MRS has been successfully used to map the spatial distribution of many metabolites including total choline, which is elevated in cancer, providing the ability to evaluate cancer metabolism along with giving insight into intertumoral spatial heterogeneity (Horska and Barker 2010). In a separate study, the level of MR visible mobile lipids within tumors was shown to correlate with apoptosis and provided a measure of the efficacy of anti-cancer therapy (Liimatainen et al. 2008). Though MRS is a promising tool for providing molecular and functional information, low sensitivity remains problematic.

Positron emission tomography (PET) was one of the first imaging techniques to provide solely functional information on cancer. By exploiting the Warburg effect, radiolabeled fluorodeoxyglucose (^{18}F-FDG) is taken up to a higher degree in metabolically active cancers. Coupled with CT, this technique has become a standard clinical tool for the evaluation of solid tumors and the measurement of tumor response to therapy (Kelloff et al. 2005).

1.5 Optical Imaging

Optical imaging has yet to see widespread adoption in clinical practice but has become the most widely used imaging technique in research settings. This is possibly

due to the versatility of optical imaging agents, which can be engineered to provide highly specific information on various molecular targets (Weissleder and Pittet 2008). Optical imaging agents rely on the emission of photons within the visible-NIR range, either through bioluminescence or fluorescence to obtain molecular information.

Bioluminescence imaging is most commonly used in systems engineered to express the luciferase protein. When the luciferase substrate, luciferin, is added to the system, light is produced through an ATP and O_2 dependent reaction (Wilson and Hastings 1998). This reporter system has been used to measure the transcriptional regulation of various oncogenes, the activation of apoptosis, and the response of cancer associated genes to therapy (Gross and Piwnica-Worms 2005). Bioluminescence has been used as a tool for cellular analysis and an *in vivo* research tool. In mice, cancer cells expressing luciferase are often used to monitor tumor growth with time and the effect of anti-cancer therapy on tumor size (Lim, Modi, and Kim 2009).

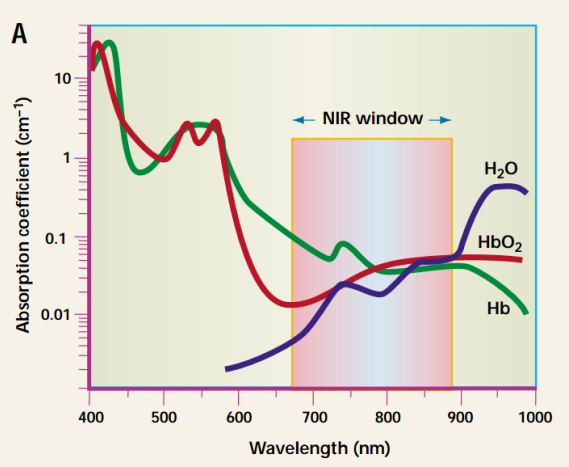

Figure 1.3. The Near Infrared (NIR) window. The NIR window (670-900 nm) is a region of the electromagnetic spectrum with minimal absorption from hemoglobin and water. Fluorophores which emit within the NIR window have greater tissue penetration and detection sensitivity. Reprinted by permission from Macmillan Publishers Ltd: Nature Biotechnology (Weissleder 2001), copyright (2001).

Fluorescence imaging relies on the detection of endogenous or exogenous fluorophores following the input of excitation energy. Similarly to luciferase, fluorescent proteins have seen widespread research use for their ability to serve as

genetic reporters (Gross and Piwnica-Worms 2005). Green fluorescent protein (GFP), which was the subject of the 2008 Nobel Prize in chemistry, was the first fluorescent protein to be designed. Due to the wavelength of GFP, applications to *in vivo* imaging are limited due to the poor tissue penetration and scattering of green light. For *in vivo* imaging, red shifted fluorescence between 650-900 nm is ideal (Weissleder 2001). This NIR window has low absorbance from hemoglobin and water allowing for maximum penetration of light and increased signal detection (Figure 1.3). In addition, light scattering, the process of absorption and re-emission of light in the non-forward direction of travel, can result in signal loss (Ntziachristos 2010). Similar to issues with light absorption, scattering is decreased at higher wavelengths, making the NIR window ideal for biological imaging. The development of longer wavelength fluorescence proteins such as red fluorescent protein (RFP), near infrared fluorescent protein (NIRFP), and Infrared Protein (IFP) have since expanded their *in vivo* capabilities (Shcherbakova and Verkhusha 2013, Shu et al. 2009).

Unlike genetic reporters, small molecule fluorophores are exogenous agents, which can be used to obtain functional information when added to cells or *in vivo* systems. Reporter fluorophores can be categorized into three groups based on their mechanism of action: Nonspecific distributing agents, targeted agents, and activatable agents (Weissleder 2001). Nonspecific distributing agents are free fluorophores, which distribute through tissue based on blood flow and perfusion. They are not targeted and therefore are most useful for the measurement of vascular perturbations. Three

fluorophores within this category, indocyanine green, fluorescein, and methylene blue have seen clinical adoption and are FDA approved for the evaluation of disease.

Indocyanine green (ICG) is a tricarbocyanine dye with fluorescence in the NIR region. ICG has no functional groups, limiting its potential for conjugation to targeting moieties, however it is highly useful in the measurement of vascular blood flow (Marshall et al. 2010). ICG is clinically approved for determining cardiac output, hepatic function and liver blood flow and for ophthalmic angiography (Nguyen and Tsien 2013).

Fluorescein is a clinically approved dye with fluorescence emission at 520 nm. Because of this lower wavelength, fluorescein has poor tissue penetration, but can be used successfully for measuring vascular flow in the eye. Fluorescein is clinically approved for diagnostic angiography or angioscopy of the retina and iris vasculature (Nguyen and Tsien 2013).

One method of improving fluorescence contrast is to conjugate fluorophores to targeting ligands. Similar to molecular imaging techniques discussed for CT, ultrasound, and MRI, this allows for selective accumulation of signal in the vicinity of the target. Targeting fluorophores results in an improved signal to background as a function of time as non-bound fluorophore clears from circulation. NIR targeted dyes have been used to image cancer signatures including folate receptor, EGFR, and HER2/*Neu* (Moon et al. 2003, Ke et al. 2003, Terwisscha van Scheltinga et al. 2011). In addition, probes have been designed targeted towards markers of apoptosis such as phosphatidylserine exposure on the outer leaflet of the cell membrane (Zhang and Zhao 2013).

Though problems faced in absorption and scattering of light can be mitigated by imaging within the NIR window, issues with detection sensitivity remain. In mouse models, fluorescence from alfalfa-containing chow can lead to high background signal in the digestive tract. This fluorescence can be significantly decreased by feeding mice purified chow with inherently low fluorescence (Inoue et al. 2008). The combination of this low fluorescence diet and NIR fluorescence has made optical imaging in mice a powerful research tool for the evaluation of cancer. Despite this, translation of these techniques to humans remains challenging due to larger tissue depths. Certain tissue is more amenable to optical imaging then others and must be taken into consideration when developing fluorescent imaging agents. Breast tissue, due to its fatty composition and compressibility has been shown to allow up to 10 cm of penetration by NIR light (Weissleder 2001).

1.6 Activatable Fluorescence

Activatable fluorescence offers a number of advantages to both free and targeted fluorophores. Targeted molecular imaging agents provide a measurement of target expression; however activatable agents can provide a measure of not only protein expression, but enzymatic activity as well. In addition, the signal to noise of an activatable agent is not solely dependent on the rate of clearance but also upon the activity of the target. Finally, in addition to providing a high degree of functional information, a single enzyme can cleave multiple substrate molecules, allowing for the amplification of a signal through increased accumulation of fluorescent product,

decreasing background signal, and thus increasing detection sensitivity (Rao, Dragulescu-Andrasi, and Yao 2007).

A commonly used research method of fluorescence activation is Föster (or Fluorescence) Resonance Energy Transfer (FRET). FRET imaging exploits non radiative energy transfer between a donor fluorophore and an acceptor chromophore (which may also be fluorescent) in close spatial proximity (Jares-Erijman and Jovin 2003). When two fluorophores are used, energy is transferred from a lower wavelength emission to a higher wavelength emission by intermediate absorption by the longer wavelength fluorophore. The intensity of the higher wavelength emission can be used as a measure for the degree of spatial interaction between the two fluorophores, since the strength of the interaction depends on the inverse sixth power of the interfluorophore distance. FRET based technologies have been utilized extensively in research and have been used to image numerous biological processes including RAS signaling and calcium signaling related to cancer (Murakoshi et al. 2004, Mochizuki et al. 2001).

Incorporation of non-fluorescent chromophores in FRET based imaging is referred to as 'dark quenching' (Jares-Erijman and Jovin 2003). Because fluorescence is dissipated through vibrational relaxation of the dark quencher, the complex remains dark when in close proximity, and only becomes fluorescent upon separation of the fluorophore from the dark quencher. One of the earliest activatable probes based on this design was developed for the detection of nucleic acids (Tyagi and Kramer 1996). This probe consisted of single strand DNA with a target strand lying in the middle of two complementary arms which annealed in solution. One arm was esterified to a

fluorophore, and the other to a complimentary dark quencher. When annealed, the complex was non-fluorescent, however following hybridization of the middle target strand to a homologous strand of DNA, the fluorophore and quencher were separated resulting in fluorescence emission.

A third mechanism of quenching useful for the development of activatable fluorophores is contact quenching. When fluorophores are within a tight spatial proximity, they can undergo stacking and result in loss of fluorescence. Recently, this quenching mechanism has been exploited for imaging of secreted phospholipase A2 using the phospholipid conjugated fluorophore, 1-palmitoyl-2-(6-((7-nitro-2-1,3-benzoxadiazol-4-yl)amino)hexanoyl)-sn-glycero-3-phosphocholine (NBD-PC). By incorporating NBD-PC into micelles at a high mole fraction, 90% quenching of fluorescence was achievable. The addition of sPLA2 resulted in disruption of the micelles and a restoration of fluorescence (Gao et al. 2015).

Several protease activatable fluorophores have been developed using both dark quenching and contact quenching. One of the earliest designed involved a graft copolymer consisting of poly-L-lysine incorporating the fluorophore, Cy 5.5, quenched through contact quenching. Cleavage of the polypeptide from lysosomal cysteine/serine proteases in tumors allowed for activation of fluorescence and imaging of cancer (Weissleder et al. 1999). Expanding from this design, a matrix metalloprotease (MMP) sensitive probe was developed conjugated to Cy 5.5 and specific to MMP-2 (Bremer, Tung, and Weissleder 2001). Probes similar to these are commercially available under the trade names ProSense and MMPSense and have been used for research on the

detection of colorectal cancer, pancreatic cancer, and the investigation of breast cancer progression (von Burstin et al. 2008, Clapper et al. 2011, Baeten et al. 2009).

Phospholipase specific probes have also been developed using dark quenching. By placing a fluorophore at the *sn*-2 position of a phospholipid and replacing the head group for a quencher, PLC selective activatable probes were generated and shown to be capable of imaging PLC in tumors (Mawn et al. 2011). Similar probes were developed for specificity towards PLA2 by incorporating a 12-carbon spacer between the fluorophore and ester linkage at the *sn*-2 position (Popov et al. 2010). In designing a $cPLA_2$ activatable fluorophore, arachidonic acid at the *sn*-2 position is necessary since $cPLA_2$ is the only phospholipase with absolute specificity for arachidonic acid at this position (Gijon and Leslie 1999). Furthermore, crystallographic analysis of $cPLA_2$ identifies a small pocket where the phospholipid head group lies during lipolysis (Dessen et al. 1999). The presence of a large quencher at this position would most likely decrease activity due to steric hindrance.

An alternate method for generating activatable fluorescence is to use chemical caging of fluorophores (Ellis-Davies 2007). This technique avoids the need for a bulky quencher, which can often interfere with enzymatic activity. In addition, this technique does not rely on spatial distances for quenching and therefore a higher percentage of quenched fluorescence can be achieved. Chemical caging involves the esterification or amidification of resonant active hydroxyls or amides resulting in altered fluorescent properties.

Such probes have been designed with photo-labile groups, which become actively fluorescent only after light is introduced into the system (Warther et al. 2010). β-galactosidase sensitive probes have also been designed using this technique through conjugation with beta galactose (Tung et al. 2004, Kamiya et al. 2007). Sulfatase sensitive probes have been developed through conjugation with sulfate (Beatty et al. 2013). Similarly activatable probes targeted towards reactive oxygen species through conjugation with aryloxyphenols have been developed (Setsukinai et al. 2003). Finally, γ-glutamyl hydroxymethyl rhodamine green was developed and found to specifically activate in the presence of γ-glutamyltranspeptidase, which is overexpressed in various cancers (Urano et al. 2011).

A phospholipase activatable fluorophore was developed previously using caged fluorescence (Huang et al. 1994). In this design, arachidonic acid was conjugated to 7-hydroxycoumarin (7-HC) through esterification of the free hydroxyl. It was shown that this probe could be activated in the presence of purified cPLA2. Intriguingly, this activation was shown to occur at an identical rate to that of endogenous substrate implying that cPLA2 activity does not require an intact phospholipid with a glycerol backbone and phosphorylated head group.

A major limitation to the design of 7-HC is the fluorescence emission of 7-HC, which occurs at a 460 nm maximum wavelength. Probes within this region of visible light have significant absorption in biological tissue due to the presence of hemoglobin (Weissleder 2001). For *in vivo* imaging, fluorescence within the NIR region (Figure 1.3) is ideal for limiting tissue absorption and allowing maximum penetration of light.

1.7 Near Infrared Fluorescence Guided Surgery

Fluorescence guided surgery is a technique rapidly gaining attention within the scientific and medical communities. Fluorophores which either accumulate in tumors or which activate specifically in tumors can provide a guide for surgeons and increase the efficacy of tumor resection, thereby minimizing the potential for tumor reoccurrence and metastasis (Nguyen and Tsien 2013). The success of surgical resection is evaluated using histology by analyzing the surgical margins of the excised tissue (Singletary 2002). 'Positive margins', the case where cancer cells lie at the cut edge, have been correlated with increased probability of recurrence and metastasis (Meric et al. 2003). Fluorophores, which accumulate in tumors are typically given intravenously and must be optimized with respect to dose and time in order to allow for systemic clearance thereby decreasing background and maximizing signal to noise (Nguyen and Tsien 2013). Activatable fluorophores allow for topical application during surgery, thereby eliminating the need for systemic administration. This reduces the time necessary to obtain suitable contrast and reduces the amount of compound that is needed, which can minimize side effects. In breast cancer specifically there is a great need for improved tumor resection as the positive surgical margin rates have been shown to range from 5-49% based on the study performed (Vahrmeijer et al. 2013).

As previously discussed, ICG and fluorescein are both under investigation for their use as contrast agents in fluorescence guided surgery (Nguyen and Tsien 2013). Because both are FDA approved, they offer reduced challenges in designing off-label clinical trials. ICG distributes diffusely and accumulates within tumors through the

presence of increased tumor vasculature (Marshall et al. 2010). ICG, injected *i.v.*, has been extensively investigated for its ability to aid the surgical resection of several carcinomas including skin, gastrointestinal, lung and breast (Schaafsma et al. 2011, Judy et al. 2015, Keating et al. 2016). Adverse effects of systemic ICG administration have been observed including anaphylaxis (Hope-Ross et al. 1994). Like ICG, fluorescein also distributes diffusely. In a study using fluorescein for the guided resection of gliomas, patients with fluorescein administered *i.v.* had a higher rate of gross total tumor resection (Shinoda et al. 2003). In addition patients who underwent gross total tumor resection had a significantly enhanced survival, giving further evidence for the value of complete tumor resection during surgery. Unlike ICG, fluorescein does not fluoresce in the NIR. Therefore, high doses were needed for tumor visualization increasing the risk of off-target effects, a potential limiting factor in future development.

Efforts to improve fluorescein accumulation in cancer, and thus increase detection sensitivity, have been carried out through conjugation to folate resulting in targeted accumulation on the folate receptor, overexpressed in numerous cancers (van Dam et al. 2011). An in human study on the surgical use of folate conjugated fluorescein in ovarian cancer demonstrated its ability to enhance the detection of tumor deposits versus visual inspection.

Antibody conjugation has also emerged as a viable means of targeting fluorophores to cancerous tissue for the aid of surgical resection. In a study investigating the surgical resection of melanoma, bevacizumab, panitumumab, tocilizumab or non-specific IgG were conjugated to an NIR fluorophore (IRDye800CW) and injected *i.v.* in

mice bearing melanoma tumor xenografts. It was determined that all antibody conjugated dyes, with the exception of IgG control, were able to discern cancerous from healthy tissue (Day et al. 2013).

5-aminolevulinic acid (5-ALA) is a precursor for porphyrin synthesis needed for the generation of hemoglobin. 5-ALA is non-fluorescent, but can be taken up by cancer cells and converted to fluorescent protoporphyrin IX as part of the synthesis of heme (Regula et al. 1995). Unlike ICG and fluorescein, 5-ALA is a prodrug and not dependent to the same degree on disrupted vasculature. 5-ALA is under investigation for fluorescence guided surgery and has shown promise for its use in the surgical resection of gliomas. In a phase III clinical study it was shown that the patient group which underwent 5-ALA guided surgery had a decreased percentage of repeat surgery and an increased 6-month progression free survival compared to the control cohort not treated with 5-ALA (Stummer et al. 2006).

The growth of activatable fluorophores can expand the capabilities of fluorescence guided surgery and decrease the reliance on vasculature fluorophore retention, which may vary between tumors. In addition, probes are also required that can identify cancerous tissue at sites distal to the primary tumor which may have more normalized vasculature and not respond to perfusion based fluorophores. Finally, agents that are selective to molecular characteristics of cancer can provide functional information while serving as a guide for resection.

1.8 Scope of Thesis

This project aims to develop cPLA2 selective activatable red-shifted fluorophores for use in the exploration of cPLA2 activity in breast cancer and for their use as a contrast agent for NIR fluorescence guided surgery. Our investigation began with the observation that 7-HC was hydrolyzed by purified cPLA2 despite the absence of a glycerol backbone and phosphorylated head group. We therefore first set out to synthesize arachidonic acid esterified fluorophores, similar in structure to 7-HC, but employing fluorophores shifted closer to the NIR window. We then evaluated the specificity of the developed probes to cPLA2 in breast cancer cell lines. Finally, we assessed the activation of cPLA2-sensitive probes *in vivo* to gauge their potential as contrast agents for surgical resection.

Chapter 2: Materials and Methods

2.1 Materials

Solvents for synthesis were purchased through Fisher Scientific. Resorufin, resorufin sodium salt, naphthofluorescein, palmitoyl chloride, porcine pancreatic phospholipase A2, arachidonyl trifluoromethyl ketone, bromoenol lactone, ionomycin, and H_2O_2 30% (w/w) were purchased from Sigma-Aldrich. 7-Hydroxy-9H-(1,3-dichloro-9,9-dimethylacridin-2- one (DDAO), arachidonoyl chloride, and LY311727 were purchased from Santa Cruz Biotechnology. 7-HC was purchased from Cayman Chemical. Syto 9 was purchased from Life Technologies. HOESCHT 333258 was generously provided by the Cellular and Molecular Imaging Core Facility (CMIC) at the Norwegian University of Science and Technology (NTNU). Egg phosphatidylcholine was purchased from Avanti Polar Lipids. AVX-235 was provided by Dr. Berit Johansen from Avexxin Pharmaceuticals (Trondheim Norway). MDA-MB-231, SKBR3, and MCF-7 cell lines were purchased from the American Type Culture Collection (ATCC). 4175-Luc+ cell line, a lung metastatic derivative of the MDA-MB-231 cell line was generously provided by Dr. Andy Minn (Minn et al. 2005). Human cPLA2 rabbit monoclonal antibody and human β-tubulin rabbit monoclonal antibody were purchased through Cell Signaling Technology. IRDye® 800 conjugated goat anti-rabbit IgG was purchased through LI-COR Biosciences. Athymic NCR nu/nu 01B7 female mice were purchased through Charles River, Production. $cPLA_2$ CRISPR/Cas9 KO Plasmid, control CRISPR/Cas9 plasmid, UltraCruz® transfection reagent and plasmid transfection media were purchased through Santa Cruz Biotechnology.

2.2 Flash Column Chromatography

A 1000 mL stopcock separation column was dried overnight under air flow. Approximately 1/3 of the column was loaded with silica gel suspended in hexanes. The walls of the column were rinsed evenly with hexanes to transfer all silica gel to the bottom. The column was packed with a hexanes mobile phase under pressurized air. A small layer of sand was added onto the silica gel to protect from physical perturbation. The sample was dissolved in the smallest possible volume of hexanes and separated under pressurized air according the procedures described.

2.3 ^{1}H NMR Spectroscopy

Samples were dried through rotary evaporation and lyophilized overnight to remove residual solvents. Samples were dissolved in the appropriate deuterated solvent based on solubility and spectra obtained on a 360 MHz Bruker Avance DMX spectrometer with gradient capabilities running the Topspin software package. Shimming was adjusted through optimization of the lock signal by adjustment of x, y, and z gradients without spinning, then adjustment of z and z^2 gradients with spinning at 20 Hz. Spectra were acquired using a zg30 pulse sequence (NS= 16, SW = 20.6 ppm). The spectra were analyzed with MestReNova software. First and second order phases were adjusted relative to the highest intensity peak and baseline was adjusted using a Whitaker baseline correction. Signals were referenced to the solvent peak.

2.4 Mass Spectrometry

Matrix-assisted laser desorption / ionization time of flight (MALDI-TOF) was performed on a Bruker MALDI-TOF. Samples were prepared in saturated solutions of either 2-(4′-hydroxybenzeneazo)benzoic acid or α- cyano-4-hydroxycinnamic acid as a

50:50 mixture (acetonitrile/ H_2O) with 0.1% trifluoroacetic acid. 1 µL of each sample was placed on an MTP AnchorChip TM 600/384 TF MALDI target (BrukerDaltonik). The mixture was dried at room temperature to allow for matrix crystallization. Spectra were generated using an Autoflex III smartbeam 1 MALDI-TOF-MS mass spectrometer (BrukerDaltonik) operating in the linear and reflectron positive ion mode. A smartbeam laser (200 Hz) was used to irradiate matrix and generate ions. Electrospray ionization (ESI) mass spectrometry was performed with a Single Quadrapole (SQ) Detector (Waters) coupled with Ultra Pure Liquid Chromatography (Acquity). Samples were dissolved in ethanol and passed through a gradient (80 - 20%) of acetonitrile in water. Results were analyzed using MestReNova for the presence of ions with predicted product mass.

2.5 Liposomal Preparation

Probe and egg phosphatidylcholine were mixed together in a 25 mL round bottom flask in chloroform at a mole fraction of 0.05-0.1. The solvent was removed under a slow stream of nitrogen gas. The resulting lipid cake was resuspended in aqueous buffer followed by sonication in a 4 °C water bath sonicator until an optically clear solution was obtained, typically 10-15 minutes. Buffer was added to result in a concentration of 100 µM probe for *in vitro* and 400 µM probe for *in vivo* analysis. Liposomes were used immediately following formation.

2.6 In Vitro sPLA2 Assay

In a 96 well plate, 80 μL of 50 mM Tris (pH 7.4) with 1.1 mM $CaCl_2$ was mixed with 0−100 units of sPLA2 Group IB (Sigma) in the presence or absence of 100 μM LY311727 (Santa Cruz Biotech) in DMSO resulting in a total volume of 90 μL per well. To initiate the reaction, 10 μL of liposomes containing activatable probe was added to each well, and fluorescence was measured as a function of time on a Spectra Max M5 fluorescent plate reader (top read; ex/em, 600/660 nm for DDAO, 595/660 nm for naphthofluorescein, and 572/585 nm for resorufin).

2.7 Cell Culture

All cell lines were maintained in Dulbecco's Modified Eagle Medium (DMEM) supplemented with 10% fetal bovine serum (HyClone Laboratories), 1% L-glutamine (Mediatech), and 1% penicillin−streptomycin (Mediatech). 4175-Luc+ cells were additionally maintained with 5 μg/mL blasticidin (Invitrogen). Frozen cells (1-2 x 10^6 cells per vial) were brought up through a rapid thaw at 37ºC and immediately placed in 10 mL of 37 °C media. DMSO containing freezing media was removed through centrifugation (1000 rpm, 4 °C, 4 min) and cell pellet was resuspended in 8 mL of media at 37 °C. Cells were expanded and maintained at 37 °C, 5% CO_2, in a humidified environment. Cells were tested immediately upon receipt and bi-annually thereafter for mycoplasma.

Cells were passaged routinely through washing 2x with 4 °C Phosphate Buffered Saline (PBS) followed by detachment from the tissue culture flask through addition of Trypsin-EDTA (0.25%) (Thermo Fisher Scientific). Following detachment, the protease was neutralized through addition of fresh 37 °C media with serum. Cells were split at a 1:10 ratio, and used for up to 20 passages before being discarded. Cells were counted on a Neubauer hemocytometer following centrifugation at 1000 rpm, resuspention in PBS and dilution (1:1) with Trypan Blue to stain for non-viable cells.

2.8 Cellular Fluorescence Activation Assay

Cells were seeded at 1.5-3.5 x 10^4 cells in a 96-well black-wall, clear-bottom plate 24 hours prior to experiment. The medium was aspirated, and cells were washed 1× in 0.1 mL of PBS (4°C, without Ca^{2+} and Mg^{2+}), and 90 µL of phenol red free DMEM containing drug treatments or vehicle control was added to each well. For phospholipase inhibition experiments, 10 µM inhibitor was incubated with cells for 4 hours (2.5 hours for AVX-235). Assays were initiated by adding 10µL of liposomes containing DDAO fluorescent probes to the wells. Fluorescence was monitored as a function of time on a Spectra Max M5 fluorescent plate reader at 37°C (bottom read, ex/em 600/660 nm). For AVX-235 inhibition and cellular comparison studies, fluorescence was monitored as a function of time on a LI-COR Odyssey® CLx Imaging System (700 nm channel, ex/em: 685/720).

2.9 Fluorescence Microscopy

Wide Field Fluorescence Microscopy

4175-Luc+ cells were seeded at 2.5×10^5 cells/mL in 0.5 mL and cultured overnight in a 24-well plate. The media was aspirated, and the cells were washed 2× in PBS. Phenol red free DMEM (450 μL) with 1 μM Syto 9 (Invitrogen) was added to each well 3 h prior to analysis. Liposomes were added either 30 minutes or 3 h prior to analysis. Immediately before analysis, DMEM was aspirated, cells were washed 1× in PBS, and fresh phenol red free DMEM was added. For live cell time course microscopy, the probe was added immediately prior to analysis, the plate was loaded into a 5% CO_2, 37 °C chamber and allowed to equilibrate for 30 minutes. Wide field fluorescence microscopy was performed on an EVOS FL Auto Cell Imaging System (Life Technologies). An LED light cube for Cy5 was used to excite DDAO fluorescence, and a GFP light cube was used to excite Syto9 fluorescence. Images were acquired at 40× magnification and analyzed with ImageJ.

Confocal Fluorescence Microscopy

Cells were seeded at 1.5-3.5 x 10^4 cells in a 96 well black-wall, clear bottom plate 24 hours prior to experiment. The medium was aspirated, and cells were washed 1× in 0.1 mL of PBS (4 °C, without Ca^{2+} and Mg^{2+}), and 90 μL of phenol red free DMEM containing drug treatments or vehicle control was added to each well. For phospholipase inhibition experiments, 10 μM AVX-235 or vehicle control was added and cells were incubated for 1.5 hours. 10 μL of probe containing liposomes in PBS was added and the

plate was incubated for 2.5 hours at 37 °C. The medium was removed and 100 µL of phenol red and FBS free media (37 °C) was added. 1 µL of HOESCHT 333258 nuclear stain was added. Confocal fluorescence microscopy was performed on a Leica SP8 imaging system and analyzed with Image J.

2.10 In Vivo Mouse Models

Anesthesia

Isoflurane was administered to achieve anesthesia. In a clean induction chamber, 1-5 mice were simultaneously induced with 1 L/min O_2 containing 4% isoflurane. Induction was assessed through loss of movement, slowed rate of breathing, and an absence to response of a toe pinch. Anesthetized mice were maintained at 1 L/min O_2 containing 2% isoflurane.

Euthanization

Mice in a cage without a filtered lid were placed in a clean CO_2 chamber and sealed. CO_2 was injected at a fill rate of 10-30% chamber volume displacement per minute for 10 minutes. Mice were monitored continuously during the procedure and assessed for lack of movement. Euthanization was confirmed through cervical dislocation.

Tumor Inoculation

Cells were expanded in T-150 tissue culture flasks to ~80% confluency. Cells were detached through trypsinization, washed 2x in 4 °C PBS, and adjusted to 2 x 10^6 cells / 100 µL of PBS. The suspension was diluted 1:1 with 4 °C Matrigel® (Corning) and placed in a 6-well plate on ice. Prior to injection, cells were resuspended and drawn

up into a 1 mL syringe with a 27-gauge needle. Air bubbles were removed through gentle tapping. The syringe was depressed until a stream of cell media was ejected consistently without air. The area of injection was sterilized with 70% isopropanol. For tumor xenograft inoculation, the cells were injected subcutaneously in the right or left lower flank or superior shoulder flank. For orthotopic inoculation, cells were injected into the mammary fat pad inferior to the lower nipple of the mouse. The mammary fat pad was located by gently pinching the skin and held in place for inoculation. Following injection, sterile gauze was used to aid in clotting. Mice were monitored the day following inoculation and every three days thereafter in order to assess tumor growth and to evaluate general health.

Probe Injections

For intravenous (*i.v.*) injection, mice were anesthetized as previously described. The tail vein was dilated through immersion of the tail in 37 °C water. Prior to injection, the compound was drawn up into a 1 mL syringe with a 30-gauge needle. Air bubbles were removed through gentle tapping. The syringe was depressed until a stream of fluid was ejected consistently without air. The tail was sterilized with 70% isopropanol. Following application of tension to the tail, the needle was inserted level with the vein.

For intraperitoneal (*i.p.*) injections, mice were used either with or without anesthesia. Prior to injection, compound was drawn up into a 1 mL syringe with a 30-gauge needle and treated as before. The area of injection was sterilized with 70% isopropanol. Injection was done in the right or left lower abdominal quadrant in order to avoid the anterior liver and bladder in the midline.

2.11 Optical Imaging

IVIS Spectrum

Fluorescence was acquired on a PerkinElmer IVIS Spectrum using a 640 nm excitation filter and a 680 nm emission filter (Bin: (M)8, FOV: 22.3 cm^2, f2, 3s exposure). For spectral unmixing, two excitation filters in combination with emission filters were used (570 nm excitation with emission 620-780 nm in 20 nm intervals and 640 nm excitation with emission 680-780 nm in 20 nm intervals). Images were processed and quantitated in LivingImage 4.4. ROIs were defined with circular shape tools. Fluorescence is reported, unless otherwise noted, as Average Radiant Efficiency, measured in photons per second and corrected for the area of the ROI and the light source efficiency at the acquired sample distance and filter settings ([p/sec/cm^2/sr]/[µW/cm^2]).

LI-COR Pearl Impulse

Fluorescence was acquired on a LI-COR Pearl Impulse scanner using the 700 nm fluorescence channel (ex/em: 685/720 nm). Images were processed and quantified in Image Studio Lite. ROIs were defined by tracing the tissue in white light mode. Fluorescence is quantified as relative fluorescence units, unless otherwise noted.

2.12 Ex Vivo Tumor Imaging

48 hours after injection of 40 nmol probe, mice were euthanized according to the previously described protocol. Tumor and organs were resected, washed in PBS, and weighed. Tissue was placed in a 24 well plate. Fluorescence was acquired (ex/em: 640/680 nm). ROIs were defined and quantified in LivingImage.

2.13 Ex Vivo Tumor Painting

Untreated mice bearing orthotopic or xenograft tumors were euthanized according to the previously described protocol and tissue was resected. Tissue was washed in PBS and sliced evenly using a razor into approximately 1 mm sections, which were weighed. The sections were placed in DMEM with serum and cultured for two hours at 37 °C, 5% CO_2. The medium was replaced with phenol red and serum free media (37 °C) prior to the addition of probe. Liposomes (100 μL containing 20 nmol probe at MF 0.05) were pipetted evenly on top of the tissue. For analysis, the plate was transferred to either the IVIS Spectrum or LI-COR Pearl Impulse imaging systems. Fluorescence was acquired at ex/em: 640/680 or 700 nm channel, respectively for each imaging system. Fluorescence emission was quantified with LivingImage or Image Studio Lite, respectively.

2.14 Protein Immunoblot

Cells were plated in 10 cm dishes at 2.5×10^5 cell/mL in 12 mL of medium 24 hours prior to the experiment. Following washing 2× with 4 °C PBS, cells were scraped on ice in radioimmunoprecipitation assay buffer containing cOmplete, mini EDTA-free protease inhibitor cocktail (Roche). Samples were vortexted and subjected to three cycles of freeze-thaw consisting of rapid freezing in liquid N_2 followed by quick thaw at 37 °C using a dry block heater. Cells were sonicated in a 4 °C water bath sonicator for 5 minutes and placed on ice for 15 minutes. Cell debris following lysis was pelleted by centrifugation (13,000 rpm for 10 min). The supernatant was removed and protein concentration was quantified using the bicinchonic acid (BCA) protein assay kit (Pierce). Samples were adjusted to equal concentrations of protein, diluted 1:1 in Laemmli loading buffer (5% 2-mercaptoethanol), and heated to 95 °C for 5 minutes. 30 μL of

approximately 25 μg protein per well was resolved on a 10% SDS-PAGE gel and transferred to a 0.45 μm pore nitrocellulose membrane (Invitrogen). The membrane was blocked in Odyssey blocking buffer (PBS) (LI-COR Biosciences) and blotted using primary antibodies for cPLA2 or β-tubulin (Cell Signaling). The membrane was imaged through incubation with secondary antibody (goat anti-rabbit) conjugated to IRDye® 800CW (LI-COR) and visualized using the LI-COR Odyssey® CLx Imaging System. Bands were quantified with Image Studio Lite.

2.15 CRISPR Gene Knockout

4175-Luc+ cells were seeded in 6 well plates at 1.5 x 10^5 cells in 3 mL of antibiotic-free DMEM and cultured for 24 hours. 2 μg of plasmid DNA was diluted in 150 μL Plasmid Transfection Media. Diluted plasma DNA was added dropwise to 150 μL of Plasmid Transfection Media containing 10 μL of UltraCruz® Transfection Reagent. The sample was vortexed and left to sit for 20 minutes at room temperature. Prior to transfection, cells were replaced with 3 mL of fresh antibiotic-free DMEM. Dropwise, plasma DNA solution was added to the well with gentle swirling. Cells were incubated for 72 hours without a media change.

Cells were separated based on GFP expression using Fluorescence-Activated Cell Sorting (FACS) on a BD FACSJAZZ. A non-transfected control was used to define a fluorescence cut-off prior to separation. Cells were expanded in T25 flasks and used for up to 5 passages before being discarded.

2.15 Statistical Analysis

All data are reported as mean ± standard deviation, unless otherwise noted. Data are listed as an average of three experimental results (n = 3), unless otherwise noted. Statistical probability (P) values were calculated using Microsoft Excel utilizing a two-tailed Students t-test. P values <0.05 were considered to be statistically significant.

Chapter 3: Chemical Synthesis

3.1 Introduction

This Chapter describes the synthesis of a series of activatable constructs that release caged fluorescence when hydrolyzed by phospholipases. A cPLA2-activatable fluorophore probe had previously been described with caged fluorescence by esterification of arachidonic acid to the resonant active hydroxyl moiety present in 7-hydroxycoumarin (7-HC) (Huang et al. 1994). Though promising, the low wavelength emission of this fluorophore (460 nm) limits its *in vivo* capabilities. Fluorophores within the NIR region of the electromagnetic spectrum (650-900 nm) have minimum absorbance from hemoglobin and water allowing for maximum penetration of light (Weissleder 2001). Therefore, we aimed to improve the design of 7-HC arachidonate using red-shifted fluorophores that emit close to or within the NIR window.

The fluorophores were selected based on several properties that would enhance detection and increase specificity. The fluorophore must possess a resonant active hydroxyl that can be esterified to result in masked fluorescence. Furthermore, the wavelength of emission should lie in the NIR window to allow for maximum tissue penetration. Finally, the fluorophore size must be small enough to allow cleavage by cPLA2. Crystallographic analysis of cPLA2 has identified a small pocket where the phospholipid head group lies during lipolysis, therefore large fluorophores would likely result in steric hindrance, preventing cPLA2 mediated cleavage (Dessen et al. 1999).

Based on these considerations, three fluorophores were chosen as potential cPLA2 imaging agents (Table 3.1).

Resorufin (ex/em: 572/585 nm) is a small tricyclic fluorophore with one available hydroxyl group. Resorufin has been shown to have ablated fluorescence upon conjugation to a photoremovable protecting group (Theriot and Mitchison 1991). Naphthofluorescein (ex/em: 595/660 nm) contains two resonant active hydroxyl groups and has been shown to have reduced fluorescence upon conjugation (Sarpara et al. 1999). These two hydroxyls are available for esterification, allowing for the synthesis of a diarachidonate probe. 7-Hydroxy-9*H*-(1,3-dichloro-9,9-dimethylacridin-2-one) (DDAO)

Table 3.1. Fluorophores used for fatty acid conjugation. Resorufin, naphthofluorescein, and DDAO were conjugated to fatty acid(s) through esterification of their free hydroxyl group(s).

Fluorophore	Structure	Excitation (nm)	Emission (nm)
7-Hydroxycoumarin	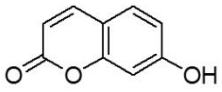	360	460
Resorufin	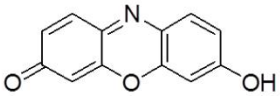	572	585
Naphthofluorescein	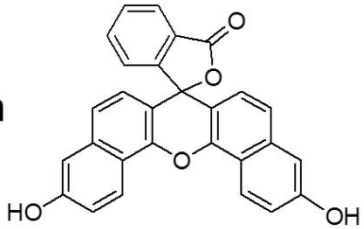	595	660
DDAO	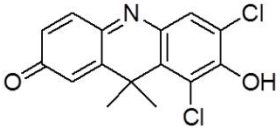	600	660

(ex/em: 600/660 nm) is an ortho-dichlorinated carbon analog of resorufin that results in redshifted fluorescence. DDAO has also been conjugated to form activatable fluorophores through conjugation of its hydroxyl group resulting in photoactivatable and sulfatase activatable probes (Beatty et al. 2013, Warther et al. 2010). In order to synthesize cPLA2 selective activatable probes, free fluorophore was conjugated to arachidonic acid. Control probes were synthesized through conjugation with palmitic acid, not expected to be cleavable by cPLA2.

3.2 Naphthofluorescein Diarachidonate

Naphthofluorescein (0.0775 mmol, 33.5 mg) was dissolved in 30 mL of pyridine at room temperature. Arachidonoyl chloride (0.31 mmol, 100 mg) was added to the solution. The flask was flushed with argon and left to stir at room temperature for 24 h. Pyridine was removed through rotary evaporation, and the resulting solid was dissolved in hexanes and filtered through a porous cotton plug to remove pyridinium salts. The solution was purified with flash column chromatography (silica gel, under N_2) in 25 mL gradients beginning with ethyl acetate/dichloromethane (DCM) (2:8, v/v), followed by ethyl acetate/DCM (7:3, v/v), ethyl acetate (pure), and methanol/ethyl acetate (3:7, v/v). The product was isolated as a dark solid (76.4 mg, 98% yield). ^{1}H NMR (360 MHz, $CDCl_3$, δ ppm) 8.51 (d, 2H, J = 9.0 Hz, -C*H*- (Ar)) 7.97 (m, 1H, -C*H*- (Ar)) 7.55 (m, 2H, -C*H*- (Ar)) 7.22 (dd, 4H, J = 9.0, 2.63 Hz, -C*H*- (Ar)), 7.05 (d, 3H, J = 2.4 Hz, -C*H*- (Ar)), 6.60 (d, 2H, J = 8.8 Hz, -C*H*- (Ar)) 5.25 (m, 16H, -C*H*=), 2.70 (m, 12H, =CH-CH_2-CH=), 2.20 (t, 4H, J = 8.0 Hz, -CH_2C(O)), 1.97 (m, 8H, -CH_2-CH_2-CH$_2$C(O)), 1.58

(quintet, 4H, J = 7.2 Hz, Bu-CH_2-CH=), 1.19 (m, 12H, CH_3-CH_2-CH_2-CH_2-), 0.77 (t, 6H, J = 6.7 Hz, CH_3-). EI-MS (m/z): 1004.51 $(M)^+$.

3.3 Resorufin Arachidonate

Resorufin (0.0775 mmol, 16.5 mg) was dissolved in 50 mL of pyridine and slightly cooled with liquid N_2. Resorufin was not completely soluble in solution. Arachidonoyl chloride (0.31 mmol, 100 mg) was added to the solution. The flask was flushed with argon and left to stir at room temperature for 24 h. Following the reaction, the solution was clear with no solids present. Pyridine was removed through rotary evaporation, and the solid was dissolved in hexanes/DCM (1:1, v/v) and filtered through a porous cotton plug to remove pyridinium salts. The solution was purified with flash column chromatography (silica gel, under N_2) in 25 mL gradients beginning with hexanes/DCM (1:1, v/v), followed by hexanes/DCM (9:1, 8:2, 7:3, 6:4, 1:1, 3:7, 1:9, v/v), DCM (pure), and DCM/ethyl acetate (19:1, v/v). The product was isolated as a yellow solid (7.7 mg, 19.9% yield). ^{1}H NMR (360 MHz, $CDCl_3$, δ ppm) 7.80 (d, 1H, J = 8.7 Hz, -C*H*- (Ar)), 7.44 (d, 1H, J = 7.4 Hz, -C*H*- (Ar)), 7.15 (d, 1H, J = 2.2 Hz, -C*H*- (Ar)) 7.12 (dd, 1H, J = 8.6, 2.5 Hz, -C*H*- (Ar)), 6.86 (dd, 1H, J = 9.8, 2.0 Hz, -C*H*- (Ar)), 6.33 (d, 1H, 2.0 Hz, -C*H*- (Ar)), 5.38 (m, 8H, -C*H*=), 2.83 (m, 6H, =CH-CH_2-CH=), 2.62 (t, 1H, J = 7.5 Hz, pro-*RS*-stereogenic -C*H*HC(O)) 2.37 (t, 1H, J = 7.5 Hz, pro-*RS*-stereogenic -CH*H*C(O)), 2.23 (q, 2H, J = 7.2 Hz, -CH_2-CH_2-CH_2C(O)) 2.14 (q, 2H, J = 7.2 Hz, Bu-CH_2-CH=), 1.86 (quintet, 1H, J = 7.5 Hz, pro-*RS*-stereogenic -CH_2-CH*H*-CH_2C(O)) 1.73 (quintet, 1H, J = 7.5 Hz, pro-*RS*-stereogenic -CH_2-C*H*H-CH_2C(O)) 1.30 (m, 6H, CH_3-CH_2-CH_2-CH_2-), 0.89 (t, 3H, J = 6.9 Hz, CH_3-). EI-MS (m/z): 500.45 $(M + 1)^+$.

3.4 DDAO Arachidonate

DDAO (0.0325 mmol, 10 mg) was dissolved in 50 mL of pyridine. Arachidonoyl chloride (0.065 mmol, 27 μL) was added to the solution, and the reaction was carried out as described above. The solid product was dissolved in hexanes/DCM (1:1, v/v), filtered, and purified with flash column chromatography using 25 mL gradients of hexanes/ DCM (3:7, 2:8,1:9, v/v), DCM (pure), and DCM/ethyl acetate (19:1, 17:3, 7:3, 4:6, and 2:8, v/v). The product was isolated as a yellow solid (12.9 mg, 65% yield). ^{1}H NMR (360 MHz, $CDCl_3$, δ ppm) 7.64 (d, 1H, J = 8.6 Hz, -C*H*- (Ar)), 7.62 (s, 1H, -C*H*- (Ar)), 7.21 (d, 1H, J = 2.4 Hz, -C*H*- (Ar)), 7.11 (dd, 1H, J = 8.6, 2.4 Hz, -C*H*- (Ar)), 5.37 (m, 8H, -C*H*=), 2.81 (m, 6H, =CH-CH_2-CH=), 2.59 (t, 2H, J = 7.5 Hz, -CH_2C(O)), 2.21 (q, 2H, J = 7.2 Hz, -CH_2-CH_2-CH_2C(O)), 2.03 (q, 2H, J = 6.8 Hz, Bu-CH_2-CH=), 1.86 (s, 6H, C(CH_3)$_2$), 1.27 (m, 8H, CH_3-CH_2-CH_2-CH_2- and -CH_2-CH_2C(O), 0.87 (t, 3H, J = 7.2 Hz, -CH_2-CH_3). MALDI-TOF-MS (m/z): 593.94 $(M)^+$.

3.5 DDAO Palmitate

DDAO (0.0325 mmol, 10 mg) was dissolved in 50 mL of pyridine. Palmitoyl chloride (0.065 mmol, 20 μL) was added to the solution. The reaction proceeded as described above, and the resulting solid was dissolved in hexanes/DCM (1:1, v/v), filtered, and purified with flash column chromatography using 25 mL gradients of DCM (pure) and DCM/ethyl acetate (19:1, 9:1, 8:2, and 1:1, v/v). The product was isolated as a yellow solid (5.9 mg, 33% yield). ^{1}H NMR (360 MHz, $CDCl_3$, δ ppm) 7.65 (d, 1H, J = 8.5 Hz, -C*H*- (Ar)), 7.62 (s, 1H, -C*H*- (Ar)), 7.21 (d, 1H, J = 2.4 Hz, -C*H*- (Ar)), 7.11 (dd, 1H, J = 8.6, 2.4 Hz, -C*H*- (Ar)), 2.57 (t, 2H, J = 7.6 Hz, -CH_2C(O)), 1.86 (s, 6H,

$C(CH_3)_2$), 1.75 (quintet, 2H, J = 7.5 Hz, -CH_2-CH_2C(O)), 1.24 (m, 24H, CH_3-CH_2-CH_2-CH_2-CH_2-CH_2-CH_2-), 0.86 (t, 3H, J = 6.9 Hz, -CH_2-CH_3). MALDI-TOF-MS (m/z): 567.24 $(M + 1 + Na)^+$.

3.6 Resorufin Palmitate

Resorufin sodium salt (0.0774 mmol, 18.2 mg) was dissolved in 80 mL of pyridine and slightly cooled with liquid N_2. Palmitoyl chloride (0.31 mmol, 95 μL) was added to the solution. The reaction proceeded as described above, and the resulting solid was dissolved in hexanes, filtered, and purified with flash column chromatography using 25 mL gradients of hexanes/DCM (9:1, 8:2, 6:4, 2:8, v/v), DCM (pure), DCM/ethyl acetate (9:1, v/v), and ethyl acetate (pure). The product was isolated as a yellow solid (5.0 mg, 14.3%). ^{1}H NMR (360 MHz, $CDCl_3$, δ ppm) 7.80 (d, 1H, J = 8.8 Hz, -C*H*- (Ar)), 7.43 (d, 1H, J = 10.1 Hz, -C*H*- (Ar)), 7.15 (d, 1H, J = 2.2 Hz, -C*H*- (Ar)), 7.12 (dd, 1H, J = 8.6, 2.5 Hz, -C*H*- (Ar)), 6.86 (dd, 1H, J = 9.8, 2.0 Hz, -C*H*- (Ar)), 6.33 (d, 1H, J = 1.8 Hz, -C*H*- (Ar)), 2.60 (t, 2H, J = 7.6 Hz, -CH_2C(O)), 1.77 (quintet, 2H, J = 7.7 Hz, -CH_2-CH_2C(O), 1.26 (m, 24H, CH_3-CH_2-CH_2-CH_2-CH_2-CH_2-CH_2-), 0.88 (t, 3H, J = 7.0 Hz, CH_3-). EI-MS (m/z): 452.21 $(M + 1)^+$.

3.7 Results

For all probes, free fluorophore was conjugated to a fatty acyl chloride through a one-step reaction in pyridine (Figure 3.1). Free fluorophore in pyridine existed as a dark red solution. Following conjugation to a fatty acid, a change in solution color to yellow was observed (Figure 3.2). This color change allowed for the visual monitoring of reaction progress. Color change occurred rapidly (within seconds) when a sufficient

amount of excess fatty acyl chloride was added to the stirring solution. The molar equivalents of fatty acyl chloride required to achieve a rapid color change varied for each given reaction. Naphthofluorescein diarachidonate, resorufin arachidonate, and resorufin palmitate required 4 equivalents of fatty acyl chloride. DDAO arachidonate and DDAO

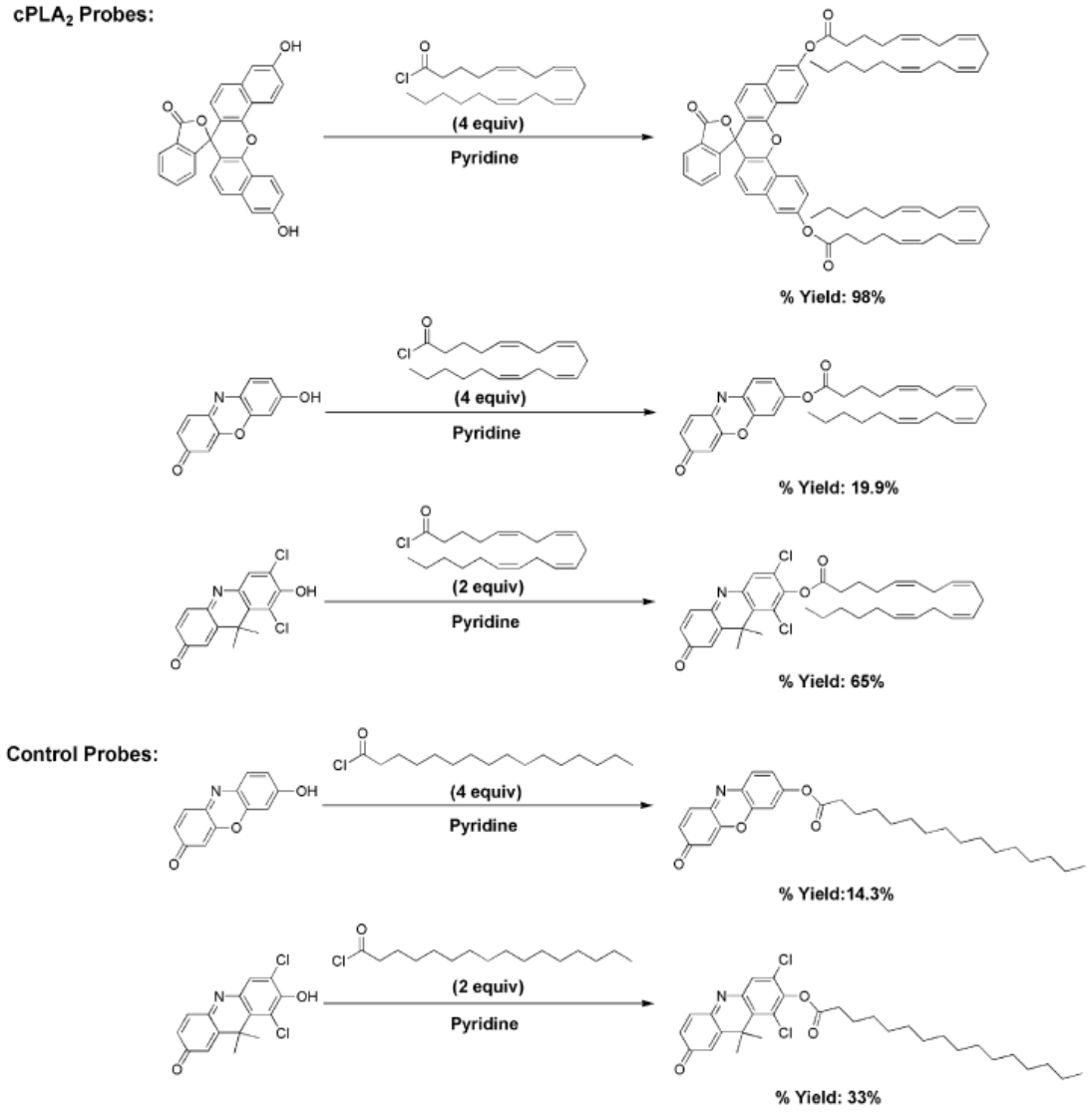

Figure 3.1. Scheme for probe synthesis. Free fluorophore was coupled with a fatty acyl chloride through a one-step reaction in pyridine. Arachidonoyl chloride was used to generate cPLA2 selective fluorophores. Palmitoyl chloride was used to generate control probes.

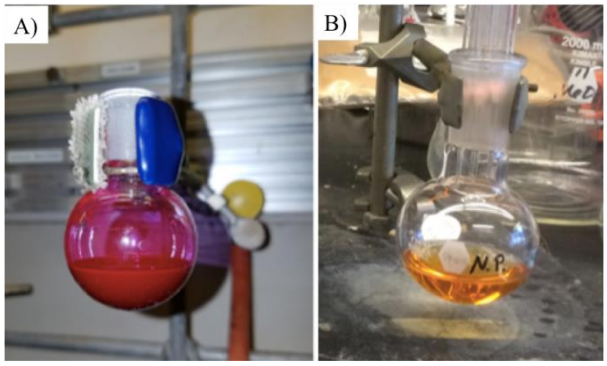

Figure 3.2. Naphthofluorescein palmitate reaction progress. A) Naphthofluorescein dissolved in pyridine resulted in a dark red solution. B) Addition of palmitoyl chloride resulted in a change to light yellow indicating successful conjugation.

palmitate required 2 equivalents of fatty acyl chloride.

Column chromatography was monitored visually with product appearing as a colored band ranging from yellow to orange for resorufin and DDAO (Figure 3.3A). Napthofluorescein diarachidonate appeared as a dark purple band. In addition, excitation with U.V. light (ex 312 nm) resulted in fluorescence of the product, which could be used to monitor the product's mobility on a silica gel column when visualized in a darkened room using a U.V. lamp (Figure 3.3B). For all probes, the product was eluted in early fractions of hexanes / ethyl acetate with slight variations between syntheses.

Naphthofluorescein displays a maximum absorbance peak at 600 nm. This absorbance was lost in naphthofluorescein diarachidonate. Addition of 200 µL 1M NaOH to naphthofluorescein diarachidonate in egg phosphatidylcholine liposomes (MF 0.1) to induce hydrolysis of the ester bond resulted in rapid (<1 min) restoration of the 600 nm absorbance peak at room temperature. Excitation at this wavelength resulted in fluorescence generation with a maximum of 660 nm. The potential for quenching of naphthofluorescein diarachidonate was determined by measuring the difference in fluorescence (ex 600, em 660) of the ionized fluorophore at pH 9 (fluorescent) versus the

protonated fluorophore at pH 3 (non fluorescent). This change to acidic pH reduced naphthofluorescein diarachidonate fluorescence by 99.4%.

Conjugation of resorufin to both arachidonic acid and palmitic acid resulted in a shift of the 572 nm resorufin absorbance peak to 450 nm. Addition of NaOH to induce hydrolysis of the ester bond resulted in a restoration of the 572 nm peak and a loss of the 450 nm peak. Excitation of resorufin at this wavelength resulted in fluorescence generation with a maximum of 585 nm. The potential percentage for quenching was determined by analyzing the difference in fluorescence (ex 600, em 660) of the ionized fluorophore at pH 9 versus the protonated fluorophore at pH 3. This was determined to be 99.8%.

DDAO contains a broad absorbance peak between 600 and 650 nm. Similar to what was observed for resorufin, conjugation to either arachidonic acid or palmitic acid resulted in a shift in absorbance resulting in a broad peak between 400 and 450 nm. In order to demonstrate the mechanism of activation for this compound, 100 Units of secreted phospholipase A2 (Group IB) was added to

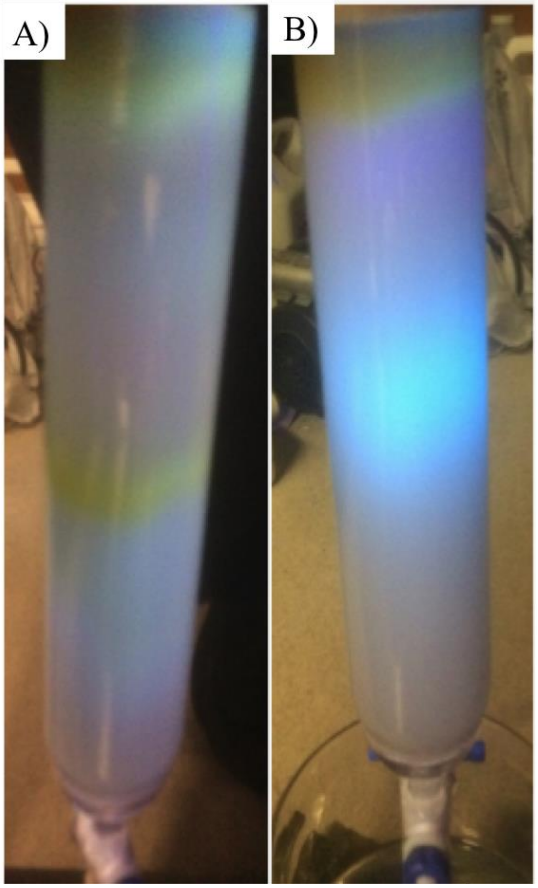

Figure 3.3. Flash column chromatography of DDAO arachidonate. A) Product can be seen as a yellow band migrating in the center of the column. B) Under U.V. light (ex 360 nm) the product fluoresces, aiding in separation from non-fluorescent compounds.

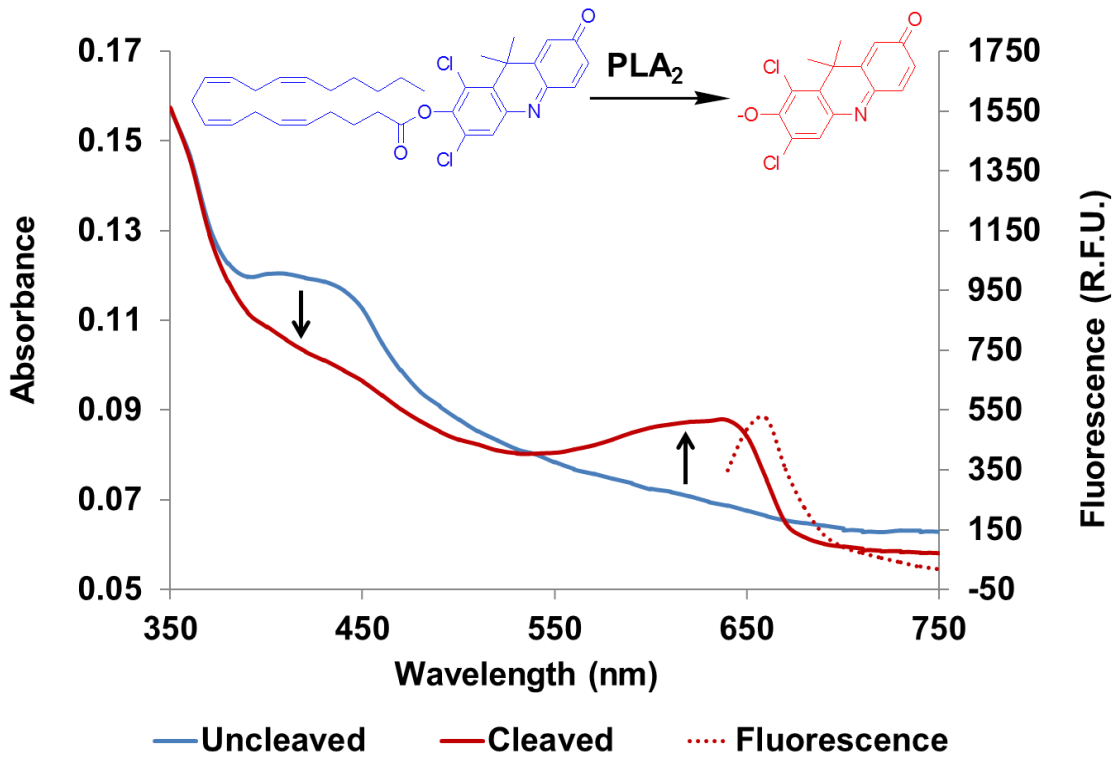

Figure 3.4. Mechanism of activation shown for DDAO arachidonate. Absorbance in the esterified quenched state is shown in solid blue. Absorbance in the unesterified state is shown in red. Cleavage of the esterified probe (10 µM) generates absorbance at 600-650 nm allowing for fluorescence (dotted red line) at 660 nm.

egg phosphatidylcholine liposomes containing DDAO arachidonate (MF 0.1) and the change in absorbance and fluorescence spectra was recorded after 4 hours of incubation at 37°C in 50 mM Tris supplemented with 1.1 mM $CaCl_2$. It was observed that following incubation, a restoration of the 600-650 absorbance peak occurred which was accompanied by a restoration of fluorescence when excited at 600 nm (Figure 3.4). Determination of the theoretical quenching was performed through comparison of the fluorescence (ex 600, em 660) of the ionized fluorophore at pH 9 versus the protonated fluorophore at pH 3 and resulted in a 98.6% quenching of fluorescence.

3.8 Discussion

This Chapter describes the synthesis of 5 caged fluorophores which were produced in high yield using a one-step esterification in pyridine. It was found that naphthofluorescein and resorufin required 4 equivalents of fatty acyl chloride to drive this reaction and achieve a color change. DDAO required only 2 equivalents of fatty acyl chloride for both arachidonate and palmitate probes. In addition, both arachidonate and palmitate reaction yields were higher for DDAO conjugation versus resorufin conjugation. This difference in reactant concentrations did not appear to correlate with reaction yield as naphthofluorescein diarachidonate had the highest yield (98 %) and resorufin palmitate had the lowest (14.3 %). However, the reaction yield did appear to be influenced by both fatty acid and fluorophore. For both resorufin and DDAO, the reaction yield was higher for arachidonate conjugates (19.9% and 65 %, respectively) versus palmitate conjugates (14.3% and 33%, respectively). Despite this observation, reaction yields are a function of many factors and the observed differences between fluorophores and fatty acid may be related to differences in starting material purity, adding temperature, side reactions such as dehydrochlorination, along with unidentified mechanisms.

The colored nature of these compounds allowed for easy visual monitoring of both reaction progress and separation using column chromatography. The use of U.V. light to monitor progress in the column increased the ability to visually separate product from starting material. Because the product traveled faster than the starting material, it was possible to adjust the ratio of hexanes/ethyl acetate in each synthesis in real time in

order to maximize separation. Following purification of individual probes with column chromatography, structures were confirmed with mass spectrometry and ^{1}H nuclear magnetic resonance (^{1}H NMR). Because of the asymmetry present in the fluorophore DDAO, two tautomeric forms arising from proton transfer between the hydroxyl and ketone groups are possible. However, despite this tautomerization, ^{1}H NMR analysis did not show a mixture of isomers indicating only one product was obtained. Previous literature indicated that substitution of the hydroxyl on the chlorinated ring occurred to a much higher extent (Warther et al. 2010, Duo, Goddard-Borger, and Withers 2014).

All fluorophores demonstrated the ability to be quenched through fluorescence measurements in protonated vs. unprotonated states. In addition, hydrolysis with NaOH demonstrated the ability to restore fluorescence for each esterified fluorophore. For DDAO arachidonate, we demonstrated that a pancreatic phospholipase, sPLA2 GIB, can also lead to probe activation. This will be explored in more detail in Chapter 4.

Chapter 4: *In Vitro* Evaluation of Probe Activation and Specificity

4.1 Introduction

cPLA2 is overexpressed in numerous cancers and is implicated in the development of resistance to estrogen receptor targeted therapy of breast cancer (Caiazza, Harvey, and Thomas 2010, Murakami et al. 2011, Meyer et al. 2004, Hong et al. 2001). In breast cancer, cPLA2 expression is correlated to the molecular subtype, with higher expression in basal-like cancer versus luminal-like cancer (Caiazza et al. 2011). In addition, levels of the downstream metabolite of cPLA2, glycerophosphocholine (GPC), have been found to be elevated in basal-like compared to luminal-like breast cancer, and this has been linked to elevations in cPLA2 gene expression (Moestue et al. 2010).

Molecular imaging of cancer offers the potential to probe alterations in enzyme expression and activity *in vivo*, providing potentially relevant functional information for clinical assessment. In a research setting, molecular imaging agents allow for the elucidation of unknown biological tumor pathways and can serve as companion diagnostics for the development of novel therapeutics (Weissleder 2006, Willmann et al. 2008). Activatable fluorophores for molecular imaging have been of increased interest (Tung et al. 2004, Kamiya et al. 2007, Beatty et al. 2013, Setsukinai et al. 2003, Urano et al. 2011). In contrast to targeted fluorophores, which rely on selective tumor accumulation in combination with rapid systemic clearance to facilitate contrast, activatable fluorophores generate high signal to noise due to selective activation in areas of interest, typically through specific enzymatic cleavage (Rao, Dragulescu-Andrasi, and

Yao 2007). This allows for the cleavage of multiple fluorescent substrates resulting in increased signal amplification and high detection sensitivity. In addition, this provides the ability to quantitate target activity in addition to enzyme expression.

Activatable fluorophores have been previously targeted towards phospholipases C and A2 through incorporation of fluorophores and complimentary quenchers into the backbone of a phospholipid (Popov et al. 2010, Mawn et al. 2011). In the design for PLC, Pyropheophorbide *a* (Pyro), a NIR fluorophore, was esterified to the *sn*-2 position and the head group was replaced with the NIR black hole quencher, BHQ-3. Further alteration of this structure found that incorporation of a 12-carbon spacer between Pyro and the glycerol backbone shifted specificity away from PLC and towards sPLA2 group IB. Utilizing this probe design to generate a cPLA2 selective agent proved challenging. cPLA2 structural based analysis has identified a small pocket where the head group lies during lipolysis and it is likely a large quencher would decrease activity (Dessen et al. 1999). In addition, arachidonic acid at the *sn*-2 position would be necessary to generate specificity for cPLA2. Therefore, a simpler probe design was needed.

Previous studies have shown that a caged fluorescent molecule, 7-HC is cleavable by purified cPLA2 resulting in the generation of fluorescence (Huang et al. 1994, Pickard et al. 1996). The fluorescence release occurred at an identical rate to enzymatic cleavage of ^{14}C-labeled endogenous phospholipids, suggesting that the glycerol backbone and head group are not absolutely required for cPLA2-mediated cleavage. Due to the chemical nature of fluorescence quenching, in which covalent molecular bonding alters the delocalized electronic structure necessary for fluorescence, caged fluorophores can

theoretically achieve higher levels of quenching than spatially FRET or contact quenched fluorophores, thus minimizing background signal. However, the low wavelength emission of 7-HC limits its *in vivo* potential. Fluorophores which fluoresce in the NIR window, a region of the electromagnetic spectrum with minimal absorption from hemoglobin and water, are more suitable for *in vivo* imaging (Weissleder 2001).

In this Chapter, we assess the three cPLA2 caged red-shifted fluorophores, described in Chapter 3, which were synthesized based on the design of 7-HC. In addition, we assess the functionality of the two control probes in which palmitic acid was esterified. Synthesized caged fluorophores contain only a fatty acid esterified to a small molecule fluorophore, therefore it must be evaluated for each fluorophore whether phospholipase activation can occur without the presence of a glycerol backbone and phosphorylated head group. Due to the ability of purified cPLA2 to cleave 7-HC, we hypothesized that similar small molecule fluorophores esterified to a fatty acid will also be cleavable by PLA2. Additionally, we hypothesized that arachidonic acid, but not palmitic acid, incorporated fluorophores will be cleavable by cPLA2.

Using purified porcine group IB sPLA2 (sPLA2 GIB), which has no specificity for arachidonic acid, we first assessed the activatable fluorophores for their ability to undergo enzyme-mediated cleavage *in vitro*. We then assessed whether incorporation of arachidonic acid conferred selectivity towards cPLA2 in live cell assays using breast cancer cell lines that express high levels of cPLA2. The enzymatic specificity to cPLA2 was assessed using inducing agents and inhibitors of the enzyme. In addition, we probed whether varying the degrees of cPLA2 expression correlates with probe activation. In

breast cancer, it has been shown that cPLA2 varies with breast cancer subtype, with basal-like cancer expressing higher levels than luminal-like cancer (Caiazza et al. 2011). We therefore used cell lines representing the three major subtypes of breast cancer to evaluate whether activity correlates with cPLA2 expression. Finally, we utilized Cluster Regularly Interspaced Short Palindromic Repeats (CRISPR) knockdown to more specifically assess the role of cPLA2 in probe activation.

The fatty acid caged fluorophores are not soluble in aqueous media. Therefore a method of solubilization was needed for delivery and enzymatic evaluation. Since cPLA2 acts preferentially on phosphatidylcholine rich biological membranes (Murakami et al. 2011), we decided to use artificial phosphatidylcholine rich liposomes for *in vitro* analysis with purified enzyme. Egg phosphatidylcholine liposomes were therefore used as a delivery vehicle for phospholipase probes. For *in vitro* studies, egg phosphatidylcholine liposomes were generated (see Chapter 2: Methods) with the probe incorporated at a mole fraction of 0.1. For experimental studies the amount of agent added is referred to in nmol of activatable probe.

4.2 Results

Activation in the presence of sPLA2 GIB

sPLA2 GIB is a pancreatic digestive enzyme that functions to break down ingested phospholipids for intestinal absorption (Dennis et al. 2011). sPLA2 GIB has no specificity for incorporated fatty acids, however it has high phospholipase activity.

Therefore, using purified sPLA2 GIB, we evaluated the ability of synthesized caged fluorophores to undergo phospholipase-mediated cleavage.

To test for sensitivity to phospholipase cleavage, 1 nmol of probe was incubated with varying concentrations of sPLA2 GIB in pH 7.4 Tris buffer containing 1.1 mM $CaCl_2$. Fluorescence generation was monitored as a function of time (Figure 4.1). Naphthofluorescein diarachidonate displayed a low initial fluorescence (Figure 4.1A).

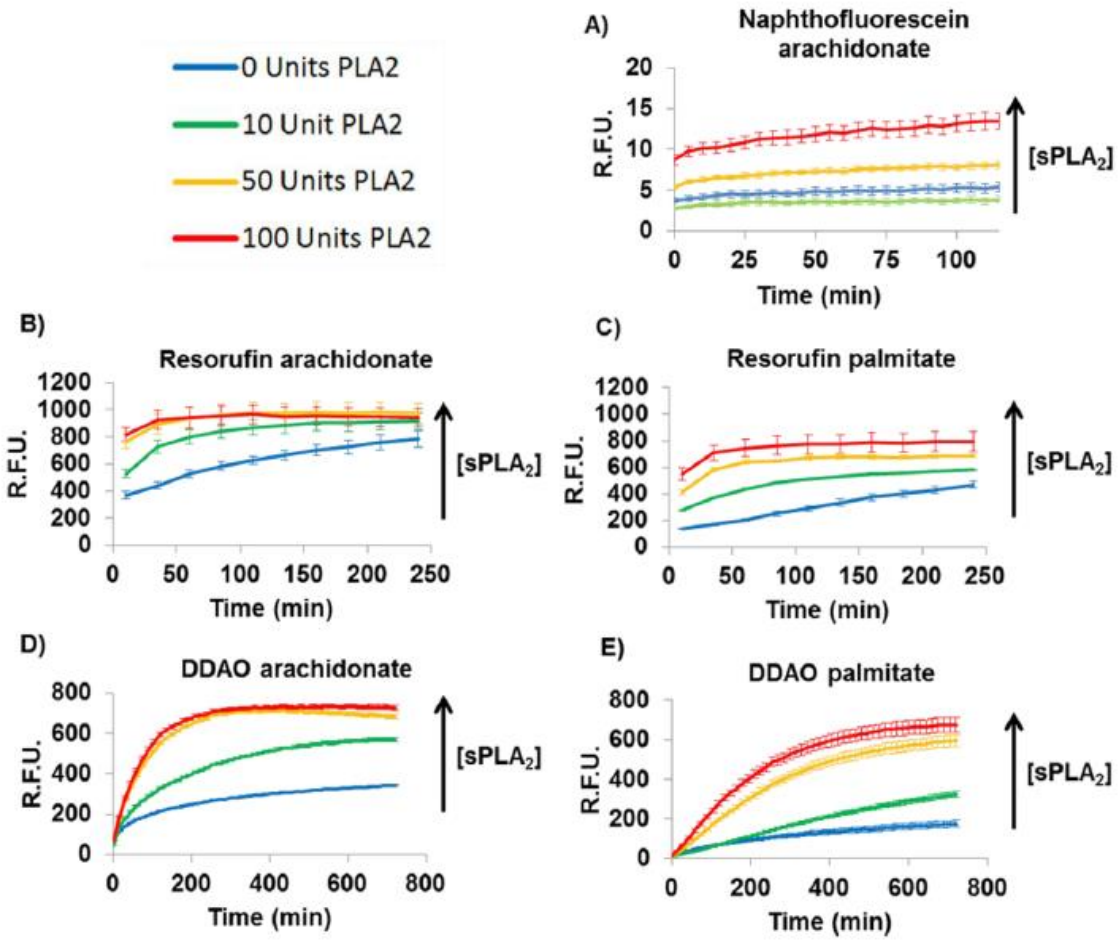

Figure 4.1. Cleavage and fluorescence generation of candidate probes by a nonselective phospholipase (sPLA2 GIB). Fluorescence generation is shown with time in the presence of increasing concentrations of sPLA2 GIB for naphthofluorescein arachidonate (A), resorufin arachidonate (B), resorufin palmitate (C), DDAO arachidonate (D), and DDAO palmitate (E). One unit is equivalent to the amount of enzyme producing 1 μmol of free fatty acid per minute at pH 8 and at 40 °C.

Addition of sPLA2 GIB resulted in increased fluorescence generation that positively correlated with enzyme concentration. However, the relative fluorescence units (R.F.U.) were low, remaining under 20 R.F.U. even for the maximum concentration of enzyme added.

Resorufin arachidonate and resorufin palmitate both resulted in increased fluorescence with time, which was positively correlated with the concentration of sPLA2 GIB (Figure 4.1B,C). A high initial fluorescence was observed in both arachidonate and palmitate activation studies. Initial fluorescence was higher in the presence of enzyme than in control wells without added phospholipase. However, even in enzyme-free controls, initial fluorescence was fairly high and increased with time.

DDAO arachidonate and palmitate both showed activation in the presence of sPLA2 GIB that positively correlated with enzyme concentration (Figure 4.1D,E). Initial fluorescence of both DDAO arachidonate and DDAO palmitate was low (less than 100 R.F.U.), and a significant time-dependent increase in fluorescence was observed in the presence of sPLA2 ($p = 5.7 \times 10^{-26}$ and $p = 2.8 \times 10^{-14}$, respectively, for 100 units sPLA2 at 720 min).

In order to confirm that DDAO arachidonate and palmitate fluorescence activation resulted directly from phospholipase activity, experiments were performed using a sPLA2 inhibitor, LY311727 (Figure 4.2). In the presence of LY311727, fluorescence generation was reduced for both probes (Figure 4.2A,B). Quantitation of the final fluorescence intensity at 720 min (Figure 4.2C) showed that both DDAO arachidonate and DDAO palmitate fluorescence were significantly ($p = 1.4 \times 10^{-11}$ and p

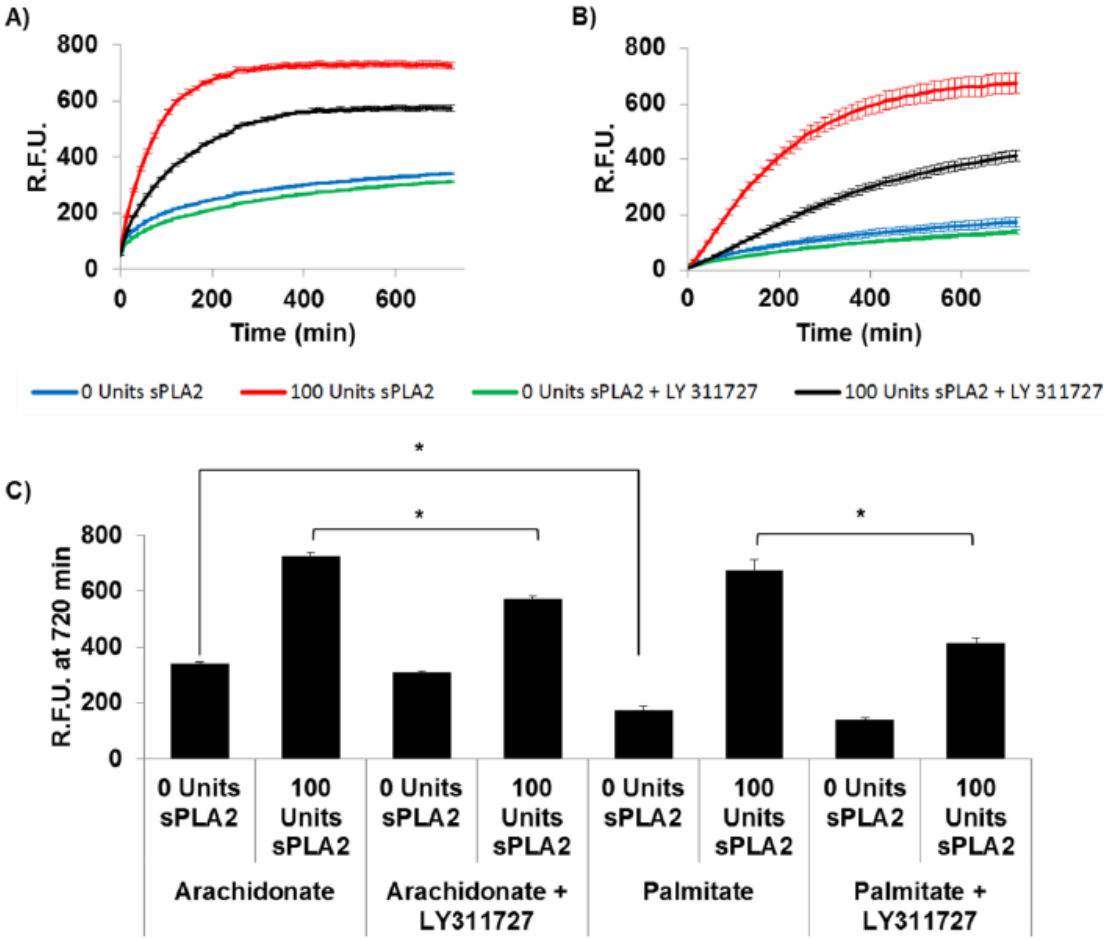

Figure 4.2. DDAO fluorescence generation is attenuated by the sPLA2 inhibitor LY311727. The fluorescence generated by 100 units of sPLA2 was inhibited by the addition of 100 μM of the sPLA2 inhibitor LY311727 for both DDAO arachidonate (A) and DDAO palmitate (B). (C) Quantifying the fluorescence at 720 min shows that LY311727 significantly inhibits the final fluorescence intensity of DDAO arachidonate ($p = 1.4 \times 10^{-11}$) and DDAO palmitate ($p = 3.2 \times 10^{-7}$). In the absence of enzyme, DDAO arachidonate gives significantly higher fluorescence ($p = 3.1 \times 10^{-11}$) than DDAO palmitate. No significant difference exists in the final fluorescence between DDAO arachidonate and DDAO palmitate in the presence of 100 units of sPLA2.

$= 3.2 \times 10^{-7}$, respectively) reduced in the presence of LY311727. The final fluorescence intensity of DDAO arachidonate was not significantly different from that of DDAO palmitate. Due to the high degree of activation, high initial quenching, and low aqueous

hydrolysis observed, DDAO arachidonate was chosen for future analysis of cPLA2 activity in combination with the control probe, DDAO palmitate.

Optimization of liposomal formulation

In order to optimize DDAO arachidonate activation and to minimize aqueous hydrolysis, the formulation of the liposomes was varied and probe cleavage in the presence of sPLA2 GIB was assessed. Delivery of probe in DMSO was also assessed as an additional control. In all cases, the concentration of probe was kept constant at 0.2 nmol of probe per well in a 96 well plate. Mole fractions of 0.01, 0.05, 0.1, and 0.2 were tested (Figure 4.3).

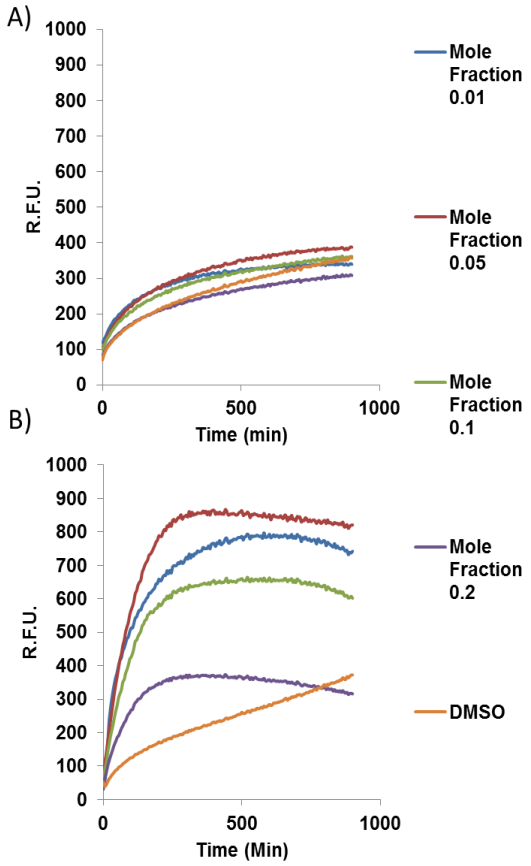

Figure 4.3. Optimization of liposomal formulation. A) Aqueous hydrolysis of DDAO arachidonate incorporated into egg phosphatidylcholine liposomes at varying mole fractions. B) sPLA2 mediated hydrolysis (100 Units) of DDAO arachidonate incorporated into liposomes of varying mole fractions.

There were no large differences in aqueous mediated hydrolysis for all conditions tested including a DMSO vehicle control (Figure 4.3A). However, a high difference in cleavage sensitivity was noted when incubated in the presence of 100 units sPLA2 GIB (Figure 4.3B). It was observed that a DDAO arachidonate mole fraction of 0.05 resulted in the highest levels of cleavage. Increasing the mole fraction to 0.1 or 0.2 resulted in

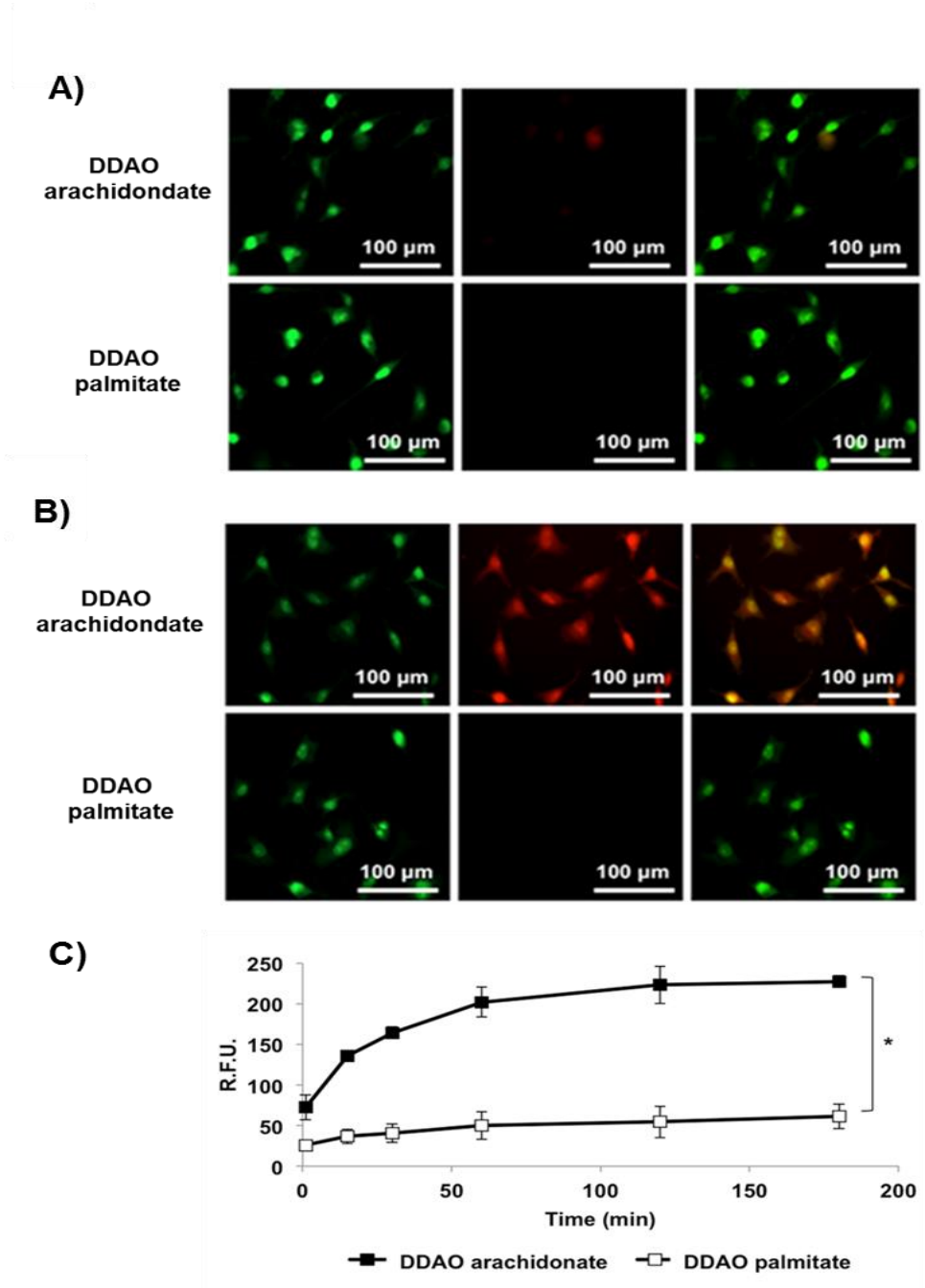

Figure 4.4. Cellular activation of DDAO arachidonate and DDAO palmitate. DDAO arachidonate and DDAO palmitate were incubated with 4175-Luc+ cells for 30 min (A) and for 3 h (B). Wide field fluorescent microscopy was performed to visualize free DDAO fluorescence. Nuclei were counterstained with Syto 9. Separate and merged fluorescence images are shown with yellow indicating overlap of fluorescence in the merged image. (C) Fluorimetry was used to quantify DDAO fluorescence as a function of time and demonstrated significantly increased fluorescence at 3 h from DDAO arachidonate relative to DDAO palmitate ($p = 1.3 \times 10^{-6}$).

decreased fluorescence generation with time. The DDAO arachidonate / DMSO vehicle control showed slow activation with time that was comparable to aqueous mediated hydrolysis. This is consistent with PLA2 requiring a phospholipid membrane in order to act. Egg phosphatidylcholine liposomes with a mole fraction of 0.05 probe were further assessed for the effects of extrusion on fluorescence generation. Liposomes were prepared as previously described (see Chapter 2: Methods) and then subjected to extrusion through a sterile 0.2 μm filter. Following extrusion it was found that fluorescence activation in the presence of sPLA2 was significantly decreased (data not shown). Therefore, polydisperse liposomes without extrusion were used in future experiments at a mole fraction of 0.05. Dynamic light scattering indicating an average size of 295.55 nm with a polydispersity of 187.65 nm.

DDAO arachidonate activation in a cPLA2 expressing breast cancer cell line

The activity of DDAO arachidonate was further evaluated in a breast cancer cell line expressing high levels of cPLA2. 4175-Luc+ is a triple-negative breast cancer cell line derived from a murine lung metastasis of the MDA-MB-231 line and engineered to express luciferase (Minn et al. 2005). MDA-MB-231 cells have previously been shown to have increased cPLA2 activity consistent with the increased cPLA2 expression in triple negative basal-like breast cancer (Caiazza, Harvey, and Thomas 2010). 4175-Luc+ cells were incubated with DDAO arachidonate or DDAO palmitate for up to 3 h and co-stained with the nuclear stain Syto 9. The cells were analyzed with wide field fluorescence microscopy (Figure 4.4). At 30 min, weak intracellular fluorescence from DDAO arachidonate was observable with no fluorescence visible from DDAO palmitate (Figure 4.4 A). At 3 hours, strong intracellular fluorescence was seen from DDAO

arachidonate; however, there was still no fluorescence in cells incubated with DDAO palmitate. DDAO arachidonate fluorescence was dispersed throughout the cytoplasm but with high perinuclear fluorescence, consistent with the subcellular location of cPLA2 activity (Figure 4.4B). In order to quantitate activation, the experiment was repeated using fluorimetry to measure fluorescence (ex/em: 600/660 nm) with time (Figure 4.4C). Quantitation showed a strong time-dependent increase in fluorescence in cells incubated with DDAO arachidonate, whereas little change was observed in DDAO palmitate incubated cells. Unlike the nonselective sPLA2 GIB cleavage studies shown in Figure 4.2, DDAO arachidonate displayed a significantly ($p = 1.3 \times 10^{-6}$) higher final fluorescence intensity in cells compared to that of DDAO palmitate.

In order to visualize the time dependence of fluorescence activation, a wide field fluorescence microscope (EVOS FL Auto) equipped with a 37°C stage and a 5% CO_2 incubation chamber was utilized. Following addition of DDAO arachidonate, the plate was placed in the chamber for 30 minutes to adjust to the environment. Fluorescence activation was then measured over the course of 70 minutes (Figure 4.5A,B). Small vesicles with high fluorescence were seen to appear and then disappear as fluorescence became dispersed throughout the cytoplasm. Vesicles appeared to be localized around the peri-nuclear region where cPLA2 is known to act (Evans et al. 2001, Nakamura et al. 2010). In one cell, vesicles can be seen forming initially close to the nucleus, then migrated out towards the cytoplasm and dispersing (Figure 4.5B).

To determine whether the observed differences in probe activation were the result of cPLA2, two agents that induce cPLA2 activity were employed: ionomycin and

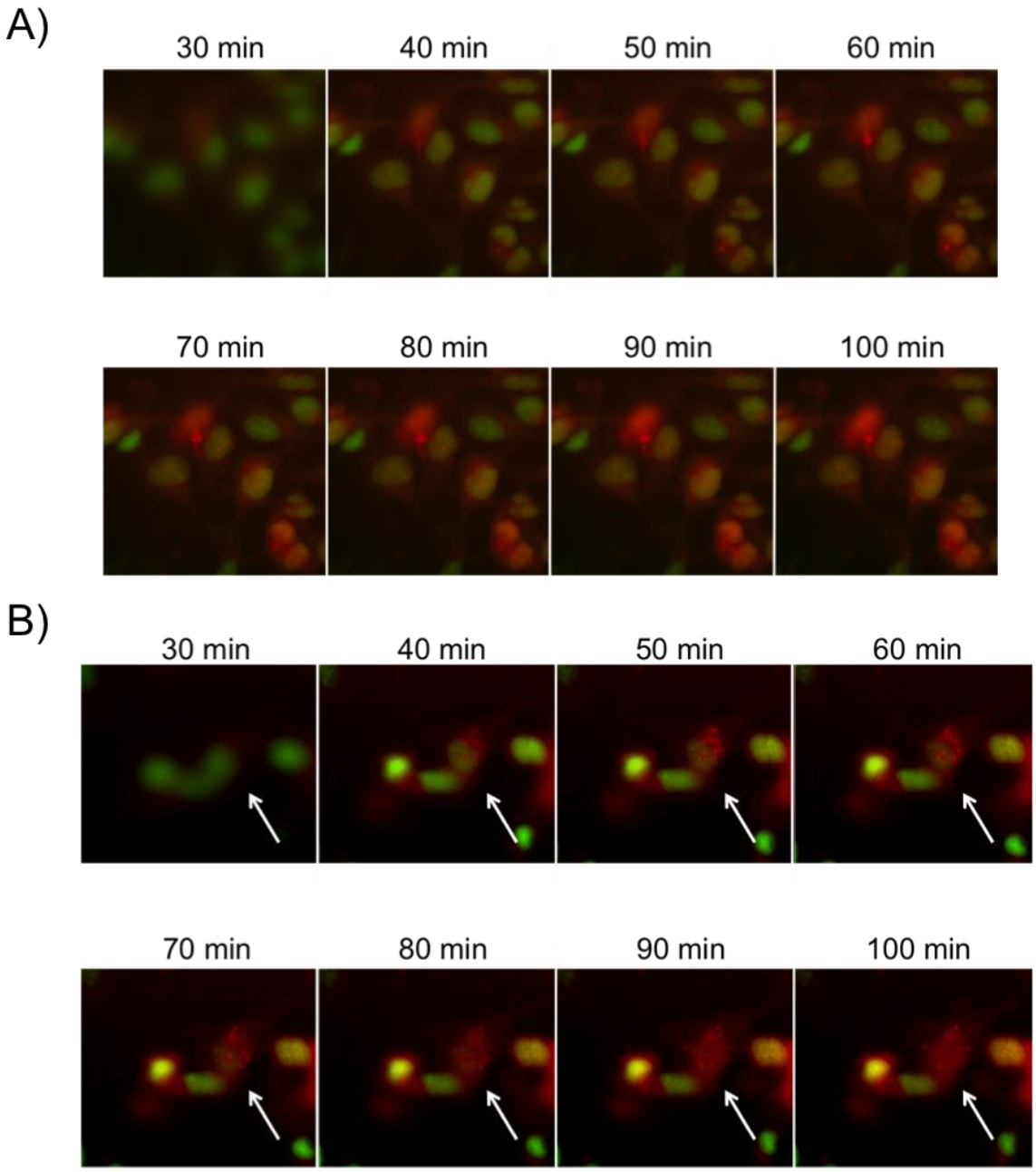

Figure 4.5. DDAO arachidonate activation with time. Wide field fluorescence microscopy was used to visualize the subcellular activation of DDAO arachidonate with time. DDAO activation is shown in red, Syto 9 nuclear staining is shown in green. A) Fluorescence accumulation can be seen with time dispersed throughout the cytoplasm and in small vesicles surrounding the nucleus B) Cellular activation of DDAO arachidonate in one cell showed initial appearance of bright vesicles surrounding the nucleus which migrated to the cytoplasm resulting in dispersed fluorescence accumulation.

hydrogen peroxide. Ionomycin is a calcium ionophore, which when incubated with cells leads to calcium release from intracellular stores into the cytosol. cPLA2, which resides in the cytosol, requires calcium for translocation to membranes where it can act on membrane localized phospholipids (Burke and Dennis 2009, Murray-Whelan et al. 1995).

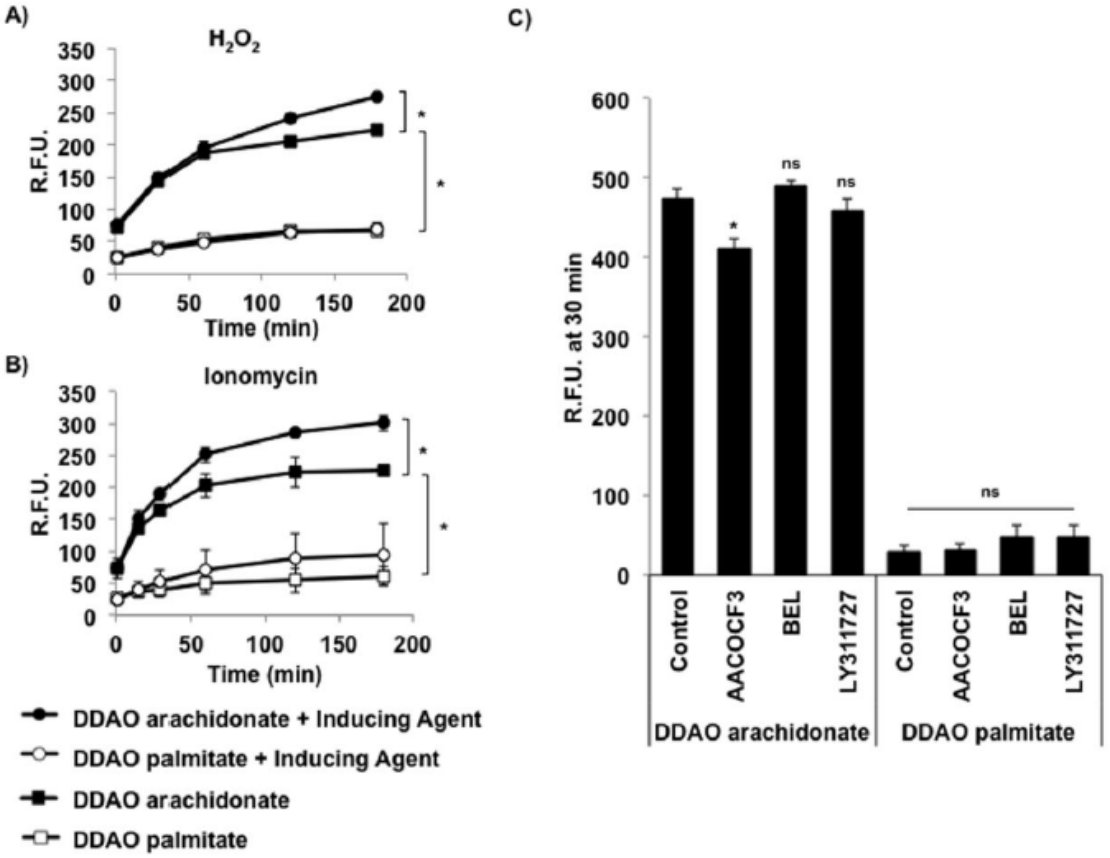

Figure 4.6. cPLA2 enzymatic induction and inhibition. cPLA2 activity was induced through either H_2O_2 (A) or ionomycin (B). Fluorescence generation was monitored with time. DDAO arachidonate showed significant enhancement of fluorescence in the presence of H_2O_2 ($p = 2.9 \times 10^{-6}$) and ionomycin ($p = 1.9 \times 10^{-7}$), whereas DDAO palmitate did not show any significant changes in fluorescence. (C) Phospholipase inhibitors were incubated with cells for 4 h, cells were washed in PBS, and fresh medium containing either DDAO arachidonate or DDAO palmitate was added. Fluorescence was recorded following 30 min of incubation. AACOCF3 treatment resulted in a significant ($p = 0.003$) reduction of fluorescence relative to that of the control. BEL and LY311727 did not alter fluorescence significantly. No significant changes in fluorescence were recorded in the presence of DDAO palmitate.

Previous work has indicated hydrogen peroxide is a potent activator of cPLA2 activity, partly due to phosphorylation through the MAPK pathway (van Rossum et al. 2004). Incubation of 4175-Luc+ cells with either ionomycin (2 μM) or hydrogen peroxide (300 μM) in the presence of DDAO arachidonate resulted in a significant ($p = 1.9 \times 10^{-7}$ and $p = 2.9 \times 10^{-6}$, respectively) increase in the final relative fluorescence (Figure 4.6A,B). However, neither ionomycin nor hydrogen peroxide had a significant effect on DDAO palmitate fluorescence. It was noted that at 3 h, cells treated with ionomycin began showing signs of stress, most notably rounding of the cells and detachment from the plate to a small extent. It is possible that the slight nonsignificant increase in DDAO palmitate fluorescence could be attributed to increased light penetration resulting from rounded up cells. Phospholipase specificity was further evaluated by monitoring fluorescence following incubation with several phospholipase inhibitors (Figure 4.6C). Inhibitors were added to 4175-Luc+ cells for 4 h at a concentration of 10 μM, cells were then washed in PBS, and fresh medium containing either DDAO arachidonate or DDAO palmitate was added. Fluorescence (ex/em: 600/660 nm) was measured following 30 min of incubation. Arachidonyl trifluoromethyl ketone (AACOCF3), a cPLA2 and iPLA2 selective inhibitor, resulted in a significant reduction in DDAO arachidonate fluorescence compared to that of untreated controls ($p = 0.003$). Bromoenol lactone (BEL), an iPLA2 selective inhibitor, resulted in no significant change in fluorescence. These data indicate that the fluorescence inhibition caused by AACOCF3 is a direct result of cPLA2 activity and not iPLA2 activity. *In vitro* studies (Figures 4.1 and 4.2) indicated that DDAO arachidonate is also susceptible to cleavage by sPLA2. Therefore, to control for sPLA2 selective activation, the sPLA2 inhibitor LY311727 was used. A small decrease in

fluorescence was witnessed in the presence of LY311727; however, this was not significant. DDAO palmitate gave no significant changes in fluorescence in the presence of any of the inhibitors.

To further evaluate the specificity of DDAO arachidonate, a highly potent cPLA2 inhibitor, AVX-235, was used. Cells were incubated with 10 µM AVX-235 for two hours prior to analysis. DDAO arachidonate or DDAO palmitate was added to initiate

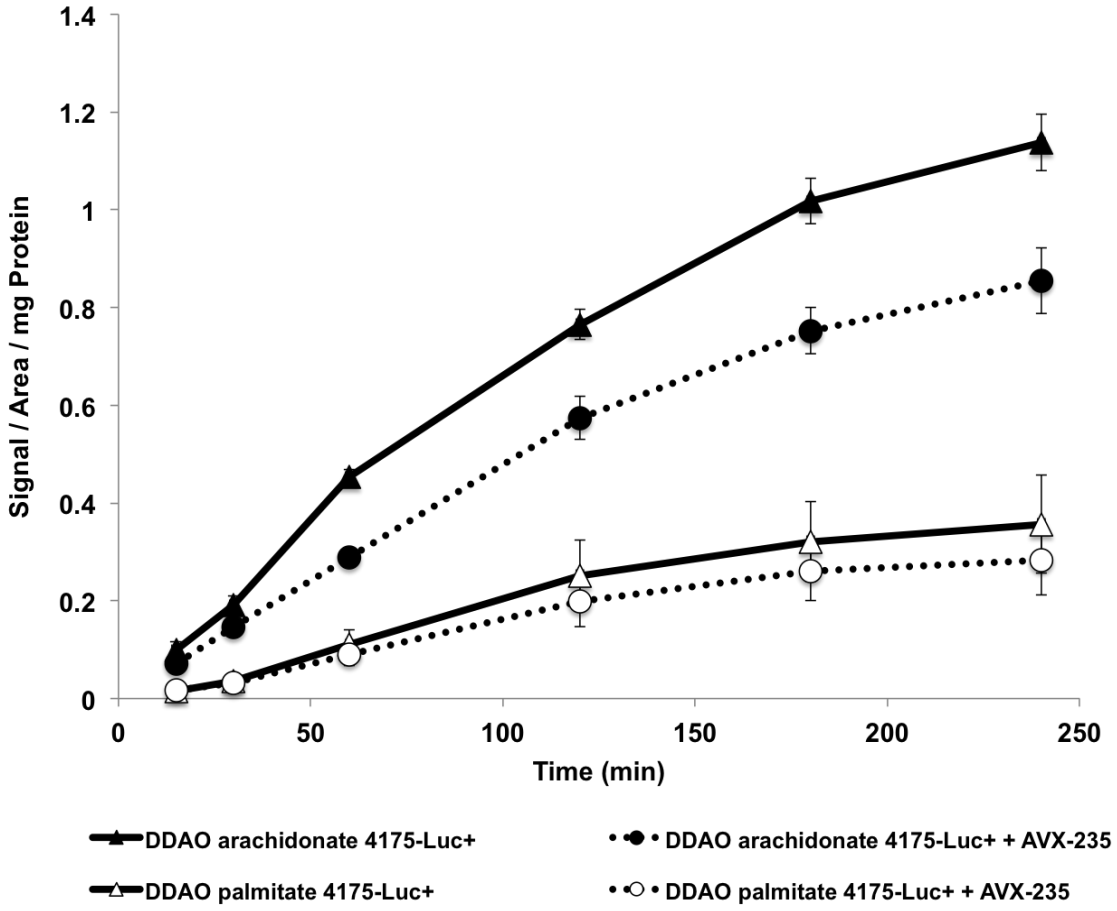

Figure 4.7. Inhibition of DDAO arachidonate by AVX-235. DDAO arachidonate and DDAO palmitate activation was measured as a function of time in 4175-Luc+ cells in the presence of 10 µM AVX-235, a potent cPLA2 inhibitor, or DMSO vehicle control. A significant decrease ($p=0.006$) of fluorescence corresponding with 20% inhibition was observed for DDAO arachidonate. No significant changes were seen for DDAO palmitate.

the reaction and fluorescence generation was monitored with time. AVX-235 resulted in a significant inhibition in the generation of fluorescence with time (p=0.006) with no significant inhibition of DDAO palmitate (Figure 4.7).

Activation of DDAO arachidonate in varying breast cancer subtypes

DDAO arachidonate was evaluated in a series of breast cancer cell lines previously described to differ in their expression of cPLA2. Three breast cancer cell lines were chosen to represent the three major subtypes of breast cancer. MDA-MB-231 is a basal-like cell line representing triple negative breast cancer. SKBR3 is a HER2 expressing cell line representing HER2-like breast cancer. MCF-7 is a estrogen receptor positive cell line representing luminal-like breast cancer. In addition, we also used the 4175-Luc+ cell line, a metastatic derivative of the MDA-MB-231 cell line, which is highly tumorigenic.

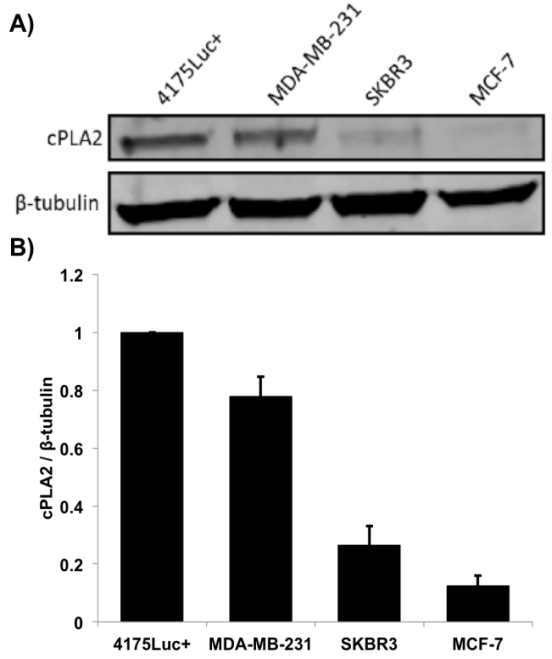

Figure 4.8. Immunoblot of cPLA2 in breast cancer cell lines. A) cPLA2 and β-tubulin protein expression levels. B) Quantitated ratio of cPLA2 / β-tubulin.

Cell lines were analyzed by immunoblot to determine the relative protein levels of cPLA2 (Figure 4.8). Consistent with previous literature, it was found that MCF-7 cells contain the lowest levels of cPLA2, with SKBR3 cells having two fold higher expression and MDA-MB-

231 cells having six fold higher expression. 4175-Luc+ cells have the highest cPLA2 expression, even greater than the parent cell line, MDA-MB-231.

To determine whether cellular protein levels correlated with cPLA2 activity we seeded cells in 96 well black-wall clear bottom plates at concentrations optimized to achieve ~80% confluency in 48 h. To test for specificity, the cPLA2 inhibitor AVX-235 or vehicle control was added 2 hours prior to the addition of either DDAO arachidonate or DDAO palmitate. Fluorescence was measured at four hours using the LI-COR Odyssey® CLx imaging system (700 nm channel) and quantitated relative to the mg of protein present per well determined using a Qubit® protein assay (Figure 4.9). 4175-Luc+ gave the highest fluorescence activation of DDAO arachidonate, followed by MDA-MB-231. SKBR3 displayed fluorescence less than that of MDA-MB-231 and MCF-7 cells displayed the lowest relative fluorescence. AVX-235 significantly inhibited the fluorescence of 4175-Luc+ and MDA-MB-231 ($p = 0.006$ and 0.03, respectively). A trend towards reduced fluorescence was seen for SKBR3 and MCF-7 cells in the presence of AVX-235, however this was not significant. In all cases, DDAO palmitate fluorescence was significantly less than that of DDAO arachidonate. Using the assumption that DDAO palmitate activation is a function of non-cPLA2 mediated hydrolysis, the R.F.U. / mg protein was adjusted by subtraction of the DDAO palmitate fluorescence and plotted as relative cPLA2 activity (Figure 4.10A). A close correlation ($R^2 = 0.9633$) between fluorescence activation and protein expression can be seen (Figure 4.10B).

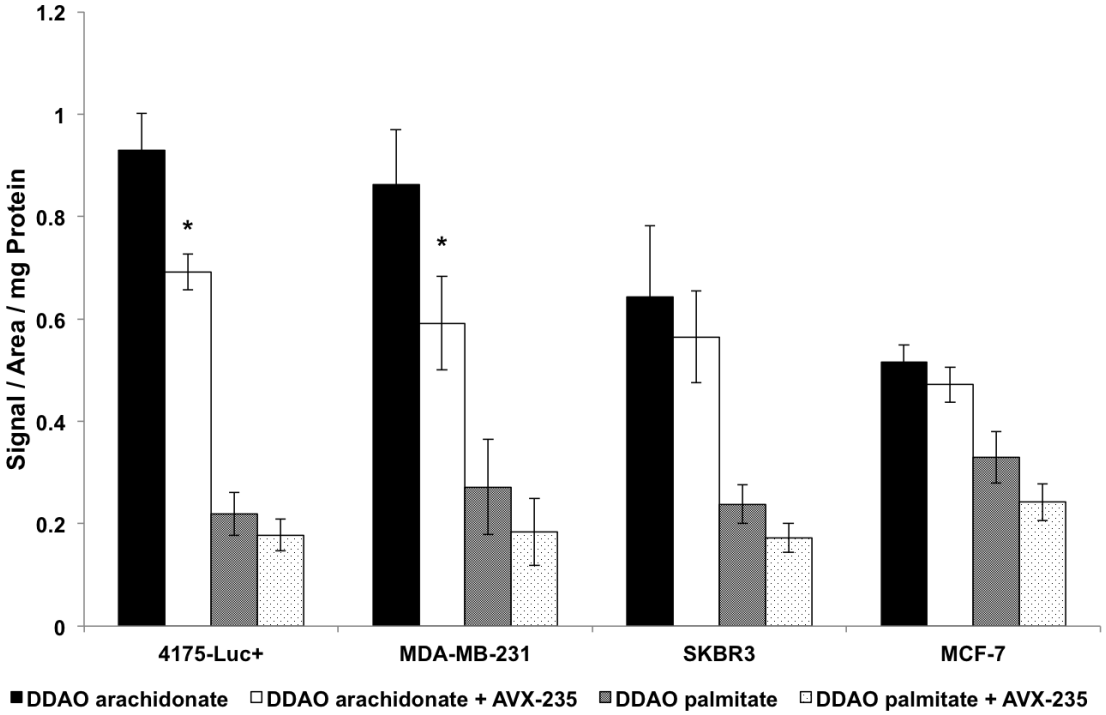

Figure 4.9. Inhibition of cPLA2 in a panel of breast cancer cell lines with AVX-235. Four breast cancer cell lines representing the three most common breast cancer subtypes were incubated with DDAO arachidonate or DDAO palmitate in the presence or absence of 10 μM AVX-235, a potent cPLA2 inhibitor. Fluorescence was acquired after four hours on a LI-COR Odyssey CLx imaging system (700 nm channel). Significant inhibition of DDAO arachidonate was observed for 4175-Luc+ and MDA-MB-231 cells when incubated with AVX-235 ($p = 0.006$ and 0.03, respectively). No significant changes in DDAO palmitate fluorescence were observed in all cell lines analyzed.

In order to confirm that measured signal is a result of cellular activation, we repeated this study in the MDA-MB-231, SKBR3, and MCF-7 cell lines using confocal fluorescence microscopy (Figure 4.11). Images were acquired at 4 hours and analyzed with Image J. MDA-MB-231 resulted in the brightest fluorescence, followed by SKBR3, with MCF-7 cells displaying the lowest fluorescence generation. AVX-235 treatment resulted in decreased fluorescence in all cell lines for DDAO arachidonate. As observed with spectroscopy, cells treated with DDAO palmitate displayed weak fluorescence making visualization difficult.

Analysis of images costained with nuclear HOESCHT2388 reveals differences in cytosolic distribution of fluorescence (Figure 4.12). MDA-MB-231 cells display fluorescence evenly dispersed throughout the cytosol. SKBR3 displays fluorescence concentrated in small cytosolic vesicles. MCF-7 displays low cytosolic fluorescence and uniquely shows evenly dispersed fluorescence in the cellular membrane.

Finally, a genetic knockdown using Cluster Regularly Interspaced Short Palindromic Repeats (CRISPR) technology was generated through transfection of 4175-Luc+ cells with a cPLA2 targeted knockout vector (Santa Cruz Biotechnology). This vector encoded for CRISPR associated protein 9 (Cas9), 3 Cas9 guide RNAs targeted towards cPLA2, and green fluorescent protein (GFP) (Figure 4.13A). Positively transfected cells, determined through the expression of GFP, were separated using fluorescence-activated cell sorting (Figure 4.13B). Cells were expanded and analyzed for protein expression (Figure 4.14A). A significant reduction in cPLA2 expression (approximately 40%) was observed in CRISPR treated cells versus non-transfected. DDAO arachidonate and DDAO palmitate activation within these cells was determined with time (Figure 4.15A) and cPLA2 activity was quantitated at 120 min (Figure 4.15B). A significant decrease in fluorescence was observed in cells treated with CRISPR/Cas9 knockout vector ($p = 1.58 \times 10^{-6}$).

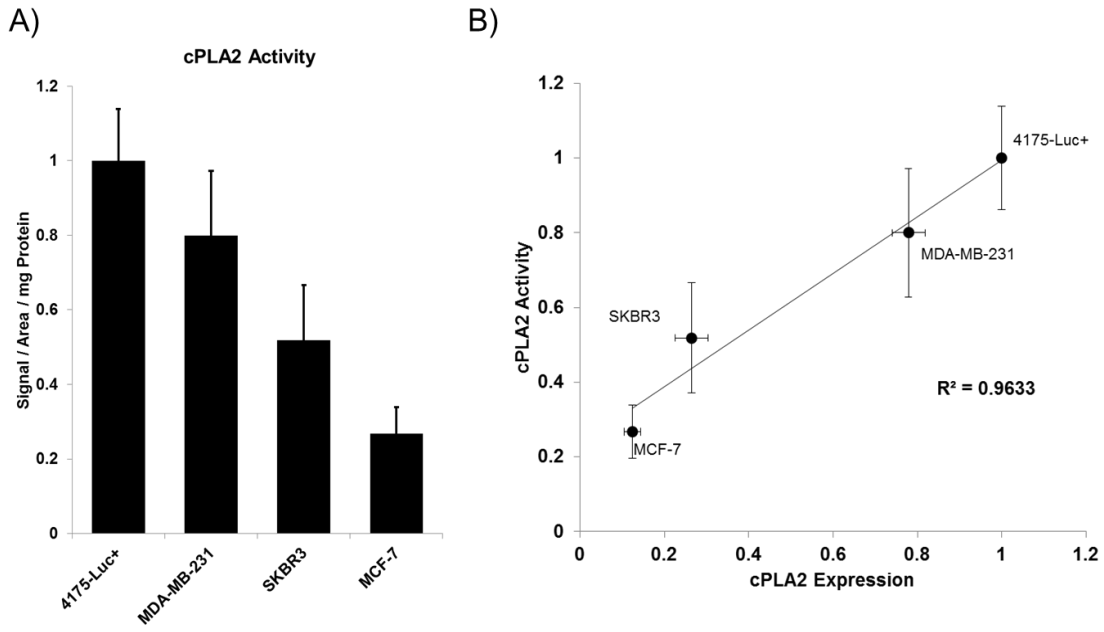

Figure 4.10. cPLA2 activity in breast cancer cell lines. A) cPLA2 activity in breast cancer cell lines was calculated from Figure 4.9 by subtracting non-selective cleavage from the fluorescence of DDAO palmitate. B) Activity levels relative to 4175-Luc+ were plotted versus cPLA2 expression relative to 4175-Luc+ (taken from Figure 4.8). A close correlation (R^2 = 0.9633) between activity and expression was observed.

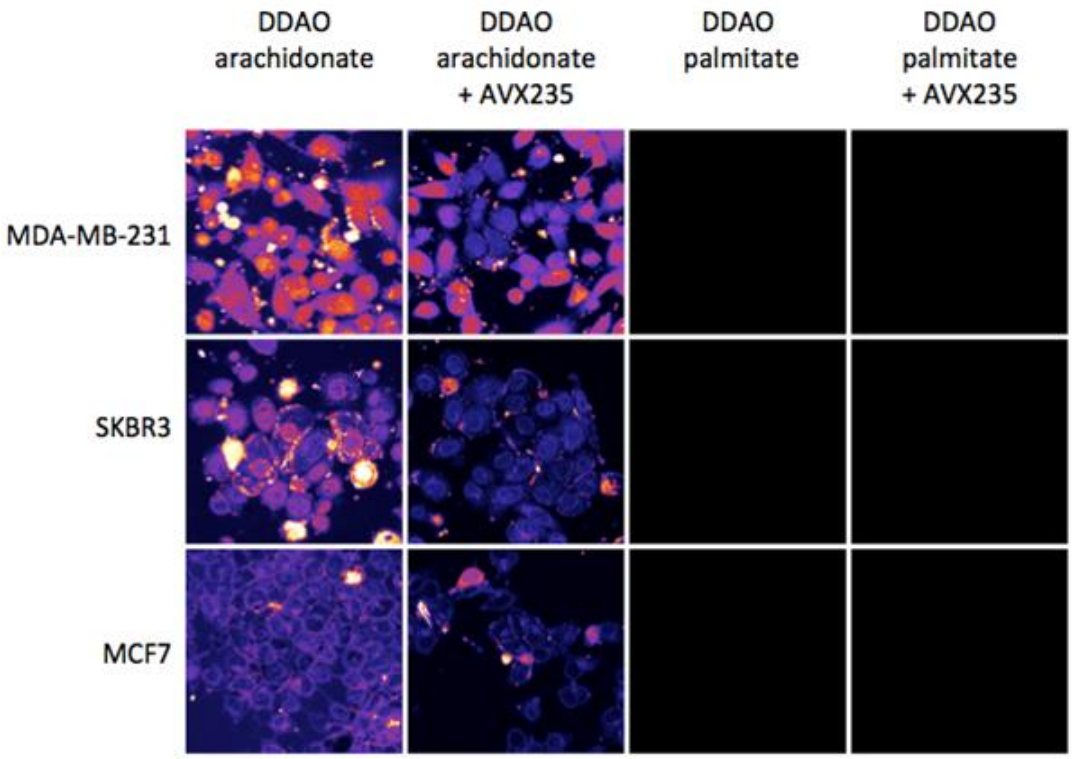

Figure 4.11. Confocal fluorescence microscopy of DDAO arachidonate and palmitate activation and inhibition. Fluorescence at four hours is shown as a heat map with brighter areas indicating high fluorescence signal.

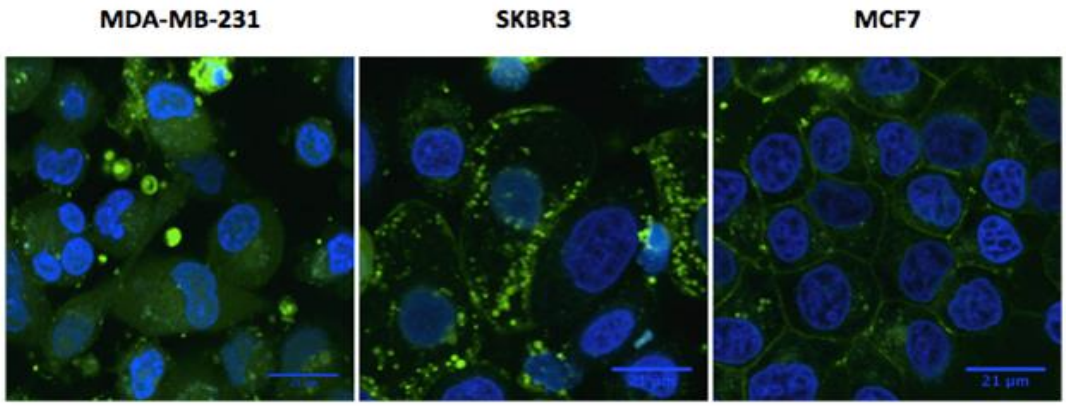

Figure 4.12. Confocal fluorescence microscopy of the subcellular distribution of DDAO arachidonate. Fluorescence at four hours with DDAO fluorescence in green, and HOESCHT 33342 nuclear staining in blue. Images are not optimized for intensity comparison but for analysis of subcellular distribution.

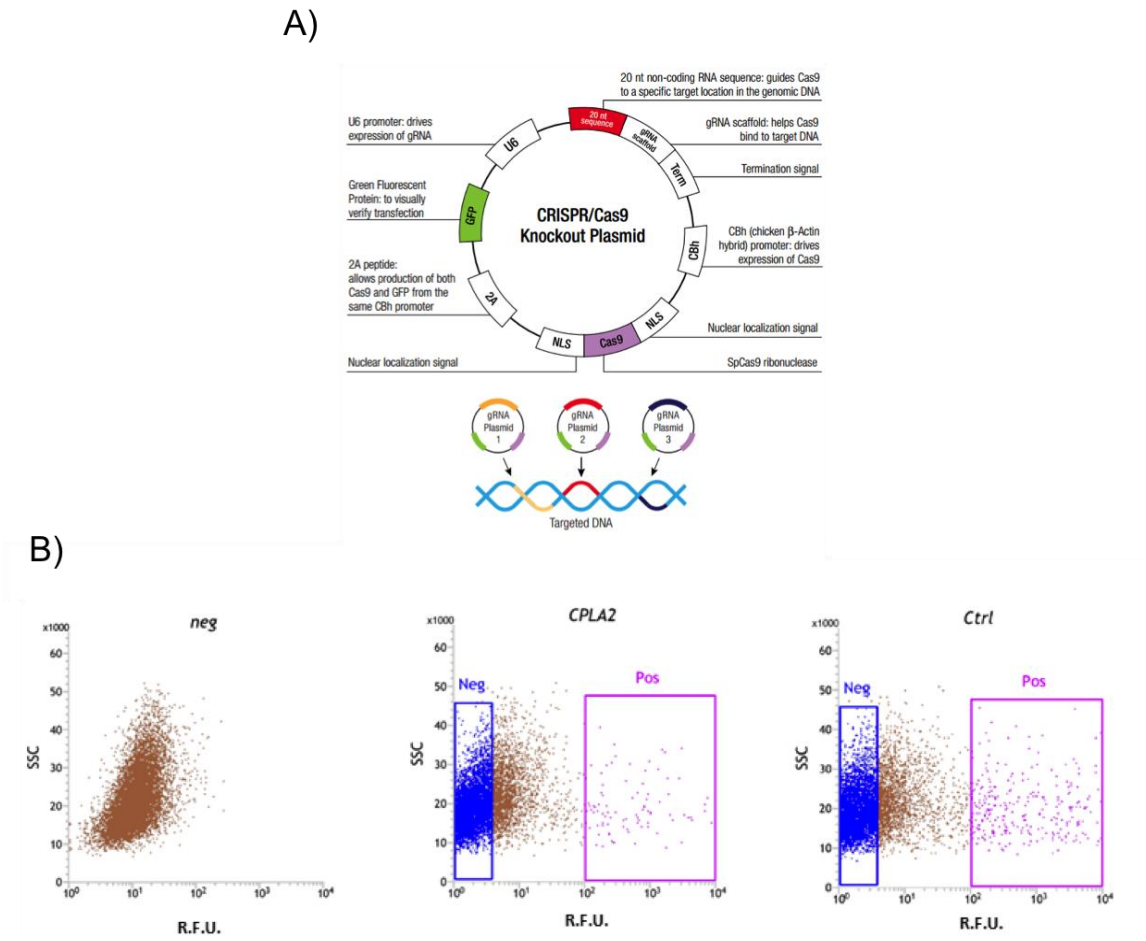

Figure 4.13. cPLA2 genetic knockdown through CRISPR/Cas9. A) A cPLA2 targeted CRISPR/Cas9 vector encoding Cas9, 3 cPLA2 targeted guide RNAs, and GFP was purchased from Santa Cruz Biotechnology. A vector containing scrambled guide RNAs was also purchased. B) Vector was transfected into 4175-Luc+ cells and GFP expressing cells were separated using fluorescence-activated cell sorting. A fluorescence cut-off of 10^2 was chosen based on the auto-fluorescence of non-transfected cells (neg) and positive populations of cPLA2 (cPLA2) and scrambled (Ctrl) transfected cells were isolated.

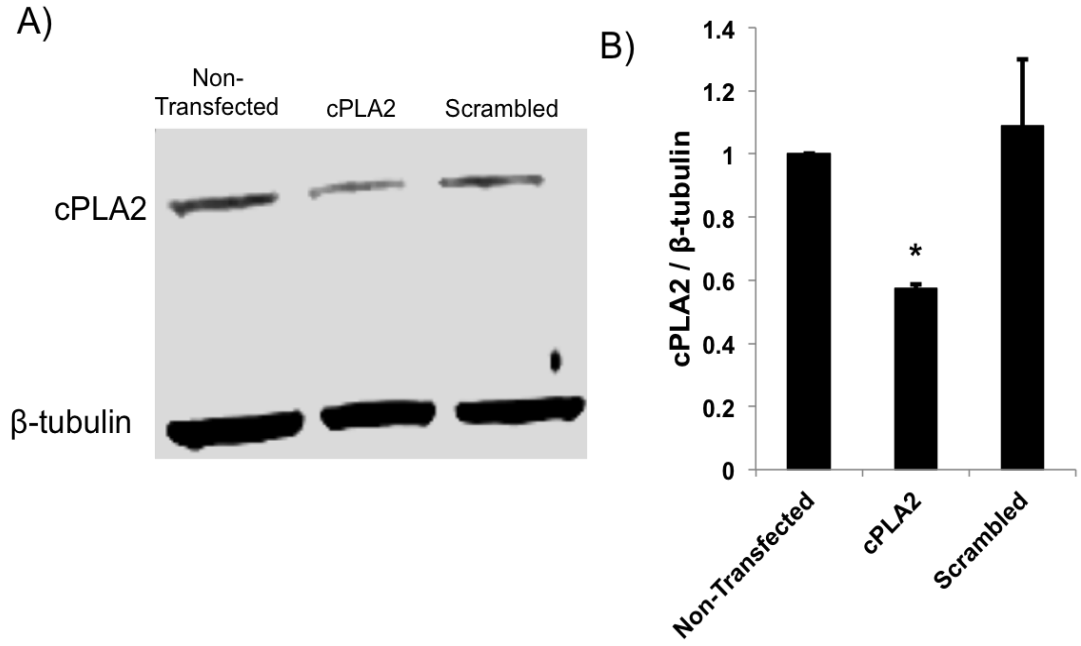

Figure 4.14. cPLA2 expression in CRISPR transfected cells. A) Immunoblot of cPLA2 and β-tubulin in non-transfected, cPLA2 CRISPR transfected, and scrambled CRISPR transfected cells. B) Quantitation of relative cPLA2 expression in cell lines. Significant reduction of protein expression is observed for cPLA2 transfected cells ($p = 8.2 \times 10^{-7}$).

4.3 Discussion

In this Chapter, we determined the sensitivity of our synthesized DDAO probes to phospholipase activation using purified enzyme and cells. Prior to the analysis for specificity to cPLA2 activation, it needed to be ascertained whether all probes, including the palmitic acid controls, were susceptible to phospholipase mediated cleavage. To determine this, the probes were tested against sPLA2 GIB, a pancreatic digestive phospholipase with no specificity towards arachidonic acid. It was observed that all probes were activated with time in proportion to the concentration of sPLA2 added. Similar to what was observed in the literature for 7-HC (Huang et al. 1994), these data supports the concept that a glycerol backbone and phosphorylated head group are not

necessary for probe activation by PLA2. However, modification of the fluorophore and fatty acid both led to observable effects on the degree of cleavage.

Naphthofluorescein diarachidonate displayed poor enzymatic activation, with the final fluorescence intensity remaining under 20 R.F.U.s, even for the maximum concentration of enzyme added. Naphthofluorescein diarachidonate was the largest fluorophore synthesized, and it is possible that steric hindrance contributed to poor enzymatic cleavage. In addition, naphthofluorescein has a pKa of 7.6, which may contribute to the poor relative fluorescence observed at pH 7.4. At a pH of 8.0, it was possible to increase the relative fluorescence generation 9-fold. Because of these observed limitations, a naphthofluorescein dipalmitate control probe was not synthesized.

Resorufin arachidonate and resorufin palmitate both gave increased fluorescence generation with time. However, a high initial fluorescence was observed indicating either poor intramolecular quenching or rapid enzymatic hydrolysis. Even in controls conducted without the addition of enzyme, initial fluorescence was fairly high and increased over time. This would indicate that resorufin-conjugated fatty acids may be susceptible to nonspecific aqueous hydrolysis in addition to enzymatic cleavage.

Similar to resorufin, DDAO arachidonate and palmitate both gave increased fluorescence activation with time. Initial fluorescence of both DDAO arachidonate and DDAO palmitate was low (less then 100 R.F.U.) indicating a high degree of initial fluorescence quenching. In addition, minimal aqueous hydrolysis was observed indicating DDAO arachidonate would be likely to give the largest signal to noise ratio.

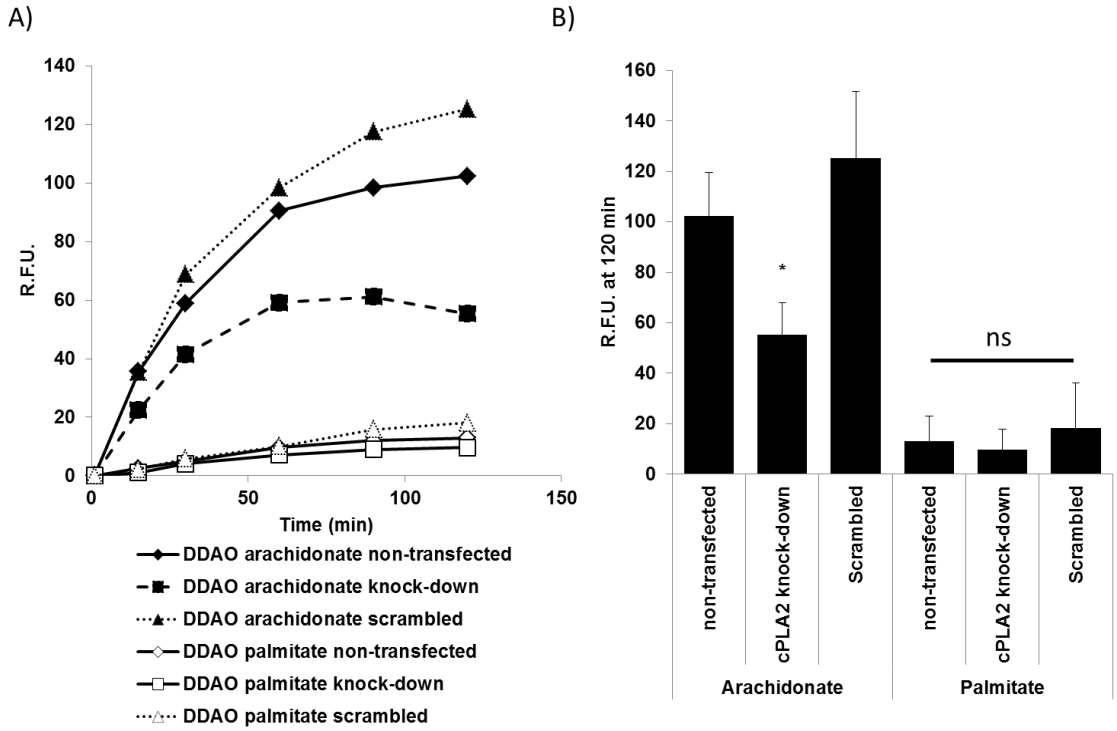

Figure 4.15. DDAO arachidonate and DDAO palmitate activation in CRISPR transfected cell lines. A) Activation with time of DDAO arachidonate and DDAO palmitate in cPLA2, scrambled, and non-transfected cells. B) Quantitation of relative fluorescence at 120 min showing significant reduction in cPLA2 targeted CRISPR transfected vector ($p = 1.58 \times 10^{-6}$)

The large difference in initial fluorescence observed between DDAO and resorufin conjugates may be due to steric or electrostatic protection by the two chloride groups ortho to the ester bond in DDAO. This is consistent with previous literature showing that 2,6-dichlorophenyl acetate has a hydrolysis constant that is 1.5 times lower than that of phenol acetate (Nottebohm 2010). For DDAO arachidonate, a more rapid initial rate of fluorescence activation was observed compared to the palmitate probe, suggesting that arachidonate conjugation results in a more readily hydrolyzable fluorophore. Because of DDAO's high initial quenching and significant increase in

fluorescence versus other fluorophores, it was chosen as our candidate cPLA2 probe for further studies.

Inhibition of sPLA2 with LY311727 resulted in a significant decrease in the generation of DDAO arachidonate and DDAO palmitate generated fluorescence indicating activation is a direct result of enzyme activity. The final fluorescence intensity was not significantly different between DDAO arachidonate and palmitate probes indicating both probes are hydrolyzed to the same degree, albeit at different rates. As expected, because sPLA2 GIB has no selectivity for arachidonic acid, no difference in final fluorescence was observed. However, DDAO arachidonate in the absence of enzyme did give significantly ($p = 3.1 \times 10^{-11}$) higher fluorescence than that of DDAO palmitate indicating that DDAO arachidonate may be more sensitive to aqueous hydrolysis. This may be an additional factor contributing to the differing rates of enzymatic hydrolysis observed.

In a triple negative breast cancer cell line expressing high levels of cPLA2, fluorescence generation in the presence of DDAO arachidonate and DDAO palmitate was assessed with fluorescence microscopy and spectroscopy. To minimize the presence of sPLA2, cells were washed 2x with PBS immediately prior to addition of probe. It was observed that unlike sPLA2 mediated cleavage studies, breast cancer cells led to significantly increased activation of DDAO arachidonate relative to DDAO palmitate. Microscopy showed that the activation occurred intracellularly, with probe dispersed throughout the cytoplasm but with high perinuclear fluorescence, consistent with the subcellular location of cPLA2. The final fluorescence intensity, measured with

fluorescence spectroscopy, was noted to be lower than the relative fluorescence achieved through *in vitro* studies. This may be attributed to a combination of increased scattering and absorption of light by cells and differences in enzyme concentration, along with variations in cellular uptake. However, these results indicate that DDAO arachidonate was specifically activated in 4175-Luc+ breast cancer cells, whereas DDAO palmitate was not.

The specificity of the cPLA2 activity was probed through the use of cPLA2 inducing agents and inhibitors. Ionomycin and hydrogen peroxide, two known inducers of cPLA2 resulted in a significant increase of DDAO arachidonate fluorescence but not DDAO palmitate. AACOCF3, a mixed inhibitor for cPLA2 and iPLA2, resulted in significant reduction of fluorescence generation implicating either cPLA2 or iPLA2 to be, at least partially, responsible for cleavage. BEL, an iPLA2 selective inhibitor, had no effect on fluorescence generation, nor did LY311727, a sPLA2 selective inhibitor. In addition, we explored the use of a highly potent cPLA2 inhibitor, AVX-235. In repeating DDAO activation in the presence of inhibitor, we found a higher percentage of fluorescence inhibition, compared to that with AACOCF3, was achievable with AVX-235. Together these results suggest that although DDAO arachidonate is susceptible to sPLA2 mediated cleavage *in vitro,* the fluorescence observed in cancer cells directly results from cPLA2 activity. DDAO palmitate, being activated by sPLA2 to the same extent as DDAO arachidonate, but not by cPLA2, served as a useful control for nonselective cleavage when assaying cPLA2 activity. This was used further to assess differences in cPLA2 in breast cancer subtypes.

cPLA2 has been shown to vary in breast cancer subtypes with higher expression in basal-like vs. luminal-like cancer. Through immunoblot analysis, we measured cPLA2 expression in four breast cancer cell lines ranging in molecular subtype. In agreement with previously reported studies (Caiazza, Harvey, and Thomas 2010), we found that triple negative breast cancer cells had the highest cPLA2 expression, HER2 expressing cells had intermediate expression, and luminal-like cells had low expression. Analysis of DDAO arachidonate activation in these cell lines correlated closely with relative cPLA2 expression levels, thus lending further evidence to the specificity of DDAO arachidonate for cPLA2.

Inhibition of cPLA2 in cell lines using the inhibitor AVX-235 was shown to significantly decrease the fluorescence generation of DDAO arachidonate in 4175-Luc+ and MDA-MB-231 cells. Although a trend towards decreased fluorescence was seen in MCF-7 and SKBR3 cells, this was not significant. It is likely the lower fluorescence signal present in MCF-7 and SKBR3 decreases the ability to measure significant inhibition. When experiments were repeated using fluorescence confocal microscopy, a clear drop in fluorescence was observed in all cell lines when incubated with AVX-235.

Confocal microscopy of the cell lines provided valuable insight into the variability that is present in the sub-cellular location of DDAO arachidonate activation. Differences in vesicle appearance and activation between cell lines may be an effect of time, as was observed in Figure 4.5. The nature of these vesicles requires further investigation. Liposomes can be incorporated into cells through two main processes (Düzgünes and Nir 1999). Membrane fusion can occur between the cellular membrane

and the liposomal membrane resulting in dispersion of probe throughout the cell. Alternatively endocytosis of liposomes followed by fusion or lipid exchange could occur. Depending on the extent of lipid exchange which occurs, transfer to lysosomal vesicles and subsequent degradation is also possible and may be a cause of non-specific activation. The presence of fluorescent vesicles in microscopic analysis indicates endocytosis may be the main uptake mechanism employed.

Interestingly, confocal microscopy also revealed the presence of several bright cells which saturated the image in all three cell lines analyzed. These cells all had characteristic signs of stress including rounding up and detachment from the plate. cPLA2 activation has previously been shown to be involved in apoptotic activation and shown to be required for tumor necrosis factor (TNFα) induced apoptosis (Enari et al. 1996). Lipid droplet accumulation, a characteristic of cancer cells exposed to apoptosis inducing anti-cancer agents (Delikatny et al. 2011), has also been linked to cPLA2 activity (Gubern et al. 2008). Whether the high fluorescence observed in microscopic images is a result of cPLA2 activity associated with apoptosis requires further investigation. However, this result highlights the potential utility of DDAO arachidonate in the investigation of cell signaling and therapeutic response.

Finally, we sought to obtain a genetic knockout of cPLA2 through transfection with a cPLA2 targeted CRISPR/Cas9 vector. Isolation and expansion of transfected cells resulted in a partial knockdown of cPLA2 expression. Based on the mechanism of action for CRISPR, it is likely we obtained a mixed population of 100% knockout and fully cPLA2 expressing cells. However, this mixed population did result in reduced DDAO

arachidonate fluorescence indicating that cPLA2 gene expression is correlated to probe activation. Future work will include isolation of a 100% knockout cell line that will be used to determine the degree of non-specific activation involved in DDAO arachidonate activation.

In summary, DDAO arachidonate appears to be specifically activated due to the actions of cPLA2 in breast cancer cell lines. DDAO palmitate is not activated by cPLA2 and therefore serves as a useful control for non-cPLA2 mediated cleavage, including the assessment of sPLA2 activity and aqueous hydrolysis. Analysis of DDAO arachidonate in a panel of breast cancer cell lines indicates it may be useful for the *in vivo* molecular imaging of cPLA2 in triple negative breast cancer.

Chapter 5: *In Vivo* Activation of DDAO Arachidonate

5.1 Introduction

This Chapter explores the use of DDAO arachidonate for *in vivo* imaging of breast cancer and the evaluation of its potential as a contrast agent for NIR fluorescence guided surgery. *In vivo* molecular imaging of cancer allows for the phenotypic and genotypic analysis of cancer while also providing anatomical tumor location. In a research setting, this allows for the assessment of tumor biology while also providing a model for the investigation of anti-cancer therapeutics (Willmann et al. 2008). In a clinical setting, this allows for the real-time determination, monitoring and alteration of treatment protocols (Weissleder 2006).

Fluorescence guided surgery is a field rapidly gaining momentum for its ability to aid in the surgical resection of tumors. Fluorescence guidance has been shown to reduce positive margins following resection and has been correlated to reduced risk of reoccurrence and metastasis (Nguyen and Tsien 2013). Though promising, the majority of contrast agents which have been evaluated accumulate through the EPR effect and provide little functional information outside of vasculature disruption. Activatable fluorophores have been shown to be capable of engineering specificity towards cancer markers and because they do not rely on accumulation they can generate a higher theoretical signal to noise (Rao, Dragulescu-Andrasi, and Yao 2007).

Improved contrast agents for breast cancer are desperately needed as the percentage of positive margins seen following surgery range from 5-49% based on the

study performed (Vahrmeijer et al. 2013). cPLA2 has been shown to be a molecular target associated with breast cancer. cPLA2 varies between subtypes with higher expression in basal-like triple negative breast cancer (Caiazza, Harvey, and Thomas 2010). Elevated levels of cPLA2 in luminal-like breast cancer have been implicated in the development of resistance to hormonal therapy. In support of this, luminal-like breast cancer patients with elevated cPLA2 had a statistically decreased rate of overall survival (Caiazza et al. 2011). Therefore, activatable fluorophores targeted towards cPLA2 may prove useful in the surgical resection of breast cancer and the discernment of aggressive breast cancer from less aggressive forms in real-time.

In Chapter 4, we identified DDAO arachidonate as an activatable fluorophore with specificity towards cPLA2. In this chapter, we explore DDAO arachidonate for its use in the *in vivo* imaging of breast cancer. We first explore the effects of systemic delivery of DDAO arachidonate. Next we compare different tumor tissues for activation in *ex vivo* fluorescence studies. Final we explore DDAO arachidonate in a surgical model through *i.p.* injections close to the tumor site.

5.2 Results

4175-Luc+ breast cancer cells were previously derived from MDA-MB-231 cells through harvesting and re-culturing of a lung metastasis from mice bearing tumor xenografts (Minn et al. 2005). As a result, 4175-Luc+ breast cancer cells grow readily in mice and metastasize to lung. We have shown that 4175-Luc+ cells have high levels of cPLA2 and can activate DDAO arachidonate but not the DDAO palmitate control probe.

In order to assess the efficacy of DDAO arachidonate *in vivo*, 4175-Luc+ cells were grown as tumor xenografts in the hind right flank of athymic mice.

Following the establishment of a palpable tumor, mice were switched to a low fluorescence chow (LabDiet 5V02) for 48 hours to reduce background fluorescence. DDAO arachidonate or DDAO palmitate (40 nmol) was injected in egg phosphatidylcholine liposomes (MF 0.05). Fluorescence images (ex/em: 640/680) were acquired over 48 hours (Figure 5.1). The results show that high fluorescence is observable throughout the entire mouse making discernment of tumor fluorescence

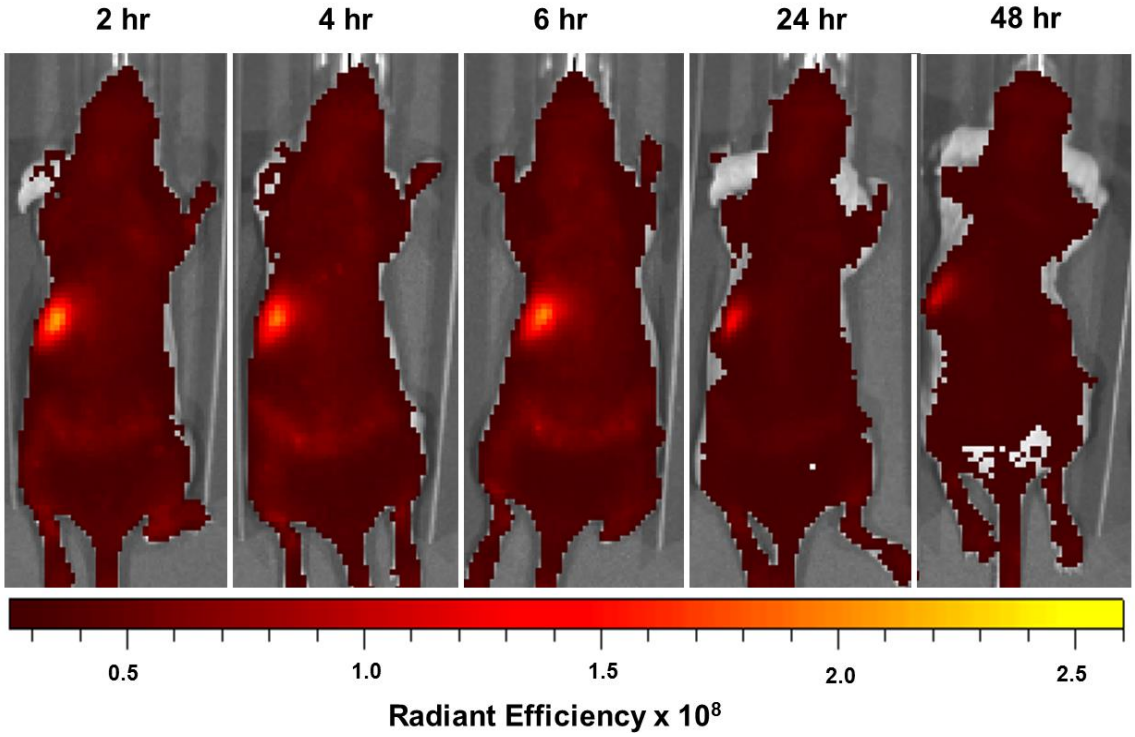

Figure 5.1. Challenges of whole body fluorescence imaging. Mice bearing 4175-Luc+ tumor xenografts were injected *i.v.* with 40 nmol of DDAO arachidonate containing liposomes (MF 0.05). Fluorescence is shown with time (ex/em: 640/680). High background fluorescence is seen throughout the mouse which decreases slightly up to 48 hours.

difficult. This initial result highlights the challenges associated with whole body fluorescence imaging. DDAO fluorescence lies on the lower wavelength edge of the NIR window, where there may still be significant absorption from tissue. In addition, tissue auto-fluorescence from elastin, collagen, and other endogenous biological fluorophores is high at wavelengths less than 600 nm and the tails of the emission spectra may overlap with DDAO fluorescence (Hilderbrand and Weissleder 2010). Finally, we have shown *in vitro* that pancreatic sPLA2 GIB can activate both DDAO arachidonate and DDAO palmitate. As a result, probe activation by sPLA2 GIB in the small intestines can occur resulting in signal overlap with surrounding tissue, increasing overall background.

Spectral unmixing techniques have been developed for the separation of different fluorescent signals *in vivo* based on their characteristic spectra (Xu and Rice 2009). By imaging fluorophores separately using various different emission and/or excitation filters, characteristic fluorescence spectra can be generated and saved for each fluorophore. *In vivo*, these spectra can be applied to images with multiple fluorophores containing overlapping emission spectra in order to unmix the individual fluorescence signals. This technique can be used to separate auto-fluorescence from actual signal, increasing detection specificity.

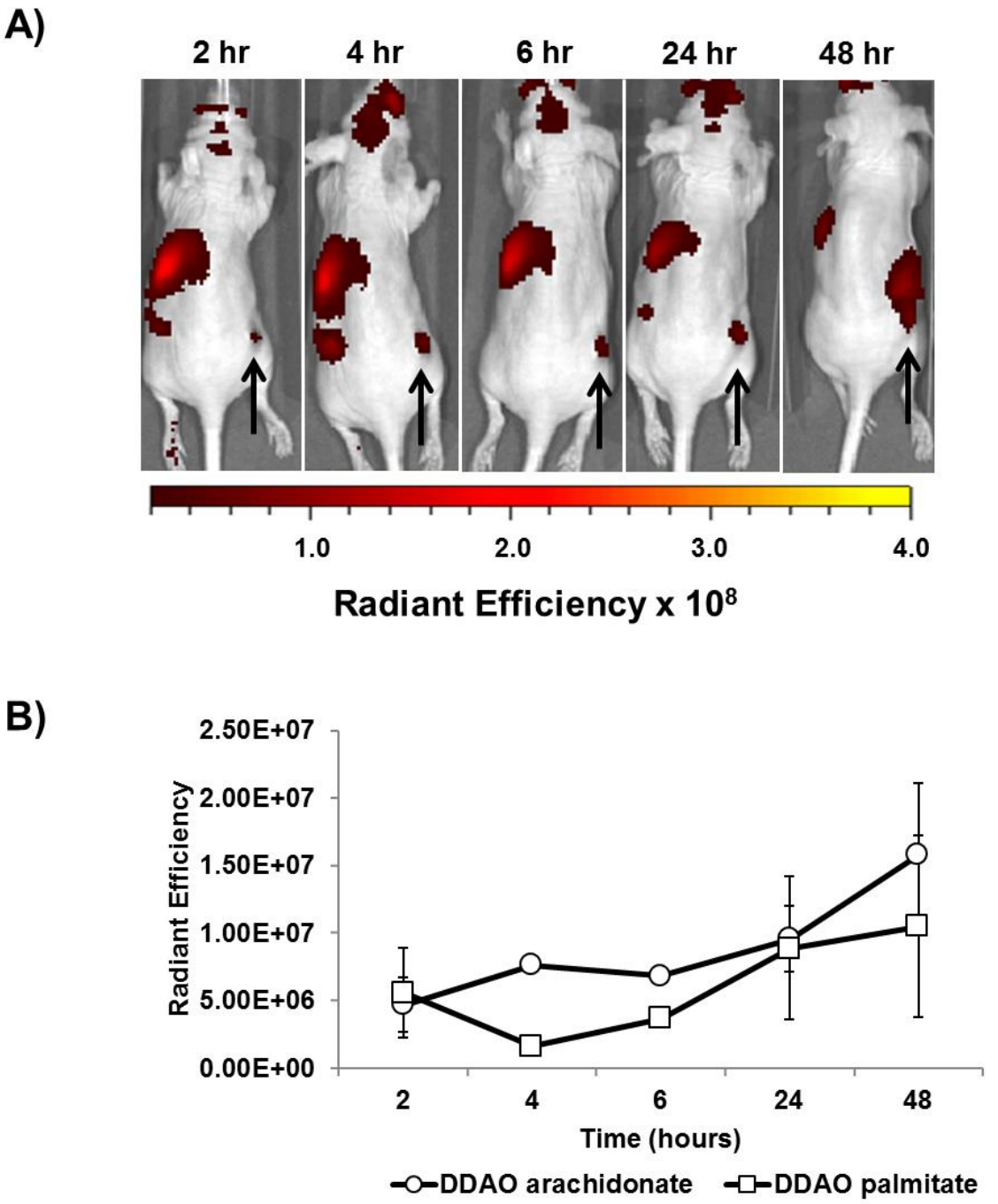

Figure 5.2. Whole body fluorescence imaging of DDAO arachidonate with spectral unmixing. A) Mice bearing 4175-Luc+ tumor xenografts were injected *i.v.* with 40 nmol of DDAO arachidonate containing liposomes (MF 0.05). Fluorescence is shown with time (ex/em: 640/680) using spectral unmixing post-processing to remove auto-fluorescence. The tumor can be seen in the bottom right flank of the mouse indicated with an arrow. B) Quantification of tumor fluorescence with time.

A filter scan was performed using two excitation filters (570 and 640 nm) and a series of emission filters separated by 20 nm for each excitation (excitation 570 nm: emission 620 - 780 nm; excitation 640 nm: emission 680 - 780 nm). A spectral signal was acquired for DDAO in a 1.5 mL Eppendorf in PBS, pH 7.4, and auto-fluorescence using a dorsal facing mouse with no treatment. Using the PerkinElmer LivingImage software, these spectra were applied to the images in Figure 5.1 and an unmixed fluorescence image of DDAO arachidonate and palmitate was obtained (Figure 5.2). Spectral unmixing resulted in a substantial reduction in auto-fluorescence. As expected, intestinal fluorescence was observed as a result of DDAO arachidonate or palmitate activation in the intestines. Because this signal arises from DDAO fluorescence, it was not removed through spectral unmixing. However, the location of the tumor far from the

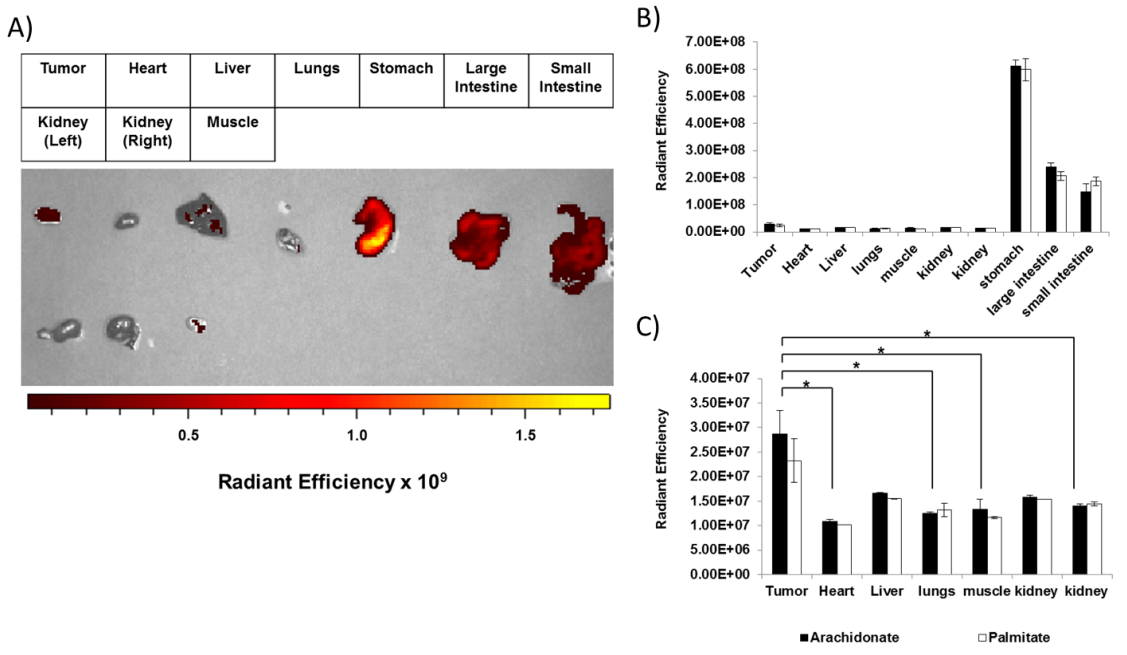

Figure 5.3. Biodistribution of DDAO arachidonate and DDAO palmitate. A) Fluorescence (ex/em: 640/680) of DDAO arachidonate in excised tissue. B) Quantification of the radiant efficiency for excised tissue. C) Expanded view of organ fluorescence with digestive organs removed.

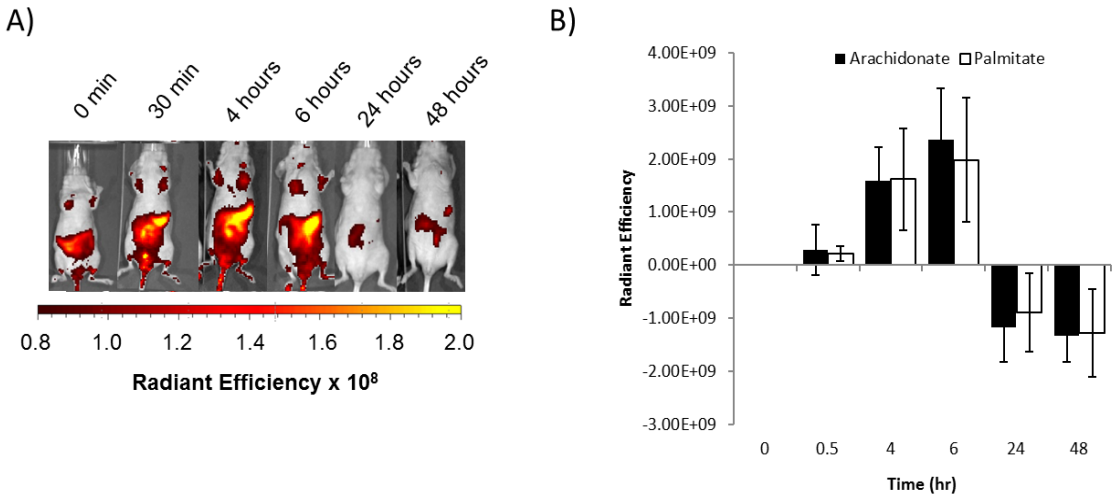

Figure 5.4. Elimination of DDAO arachidonate and DDAO palmitate. A) Whole body spectrally unmixed fluorescence of ventral facing mice over 2 days following injection *i.v.* with 40 nmol of DDAO arachidonate. B) Quantification of DDAO arachidonate and DDAO palmitate elimination through measurement of whole body fluorescence spectrally unmixed signal from ventral facing mice.

intestinal fluorescence allows the tumor signal to be resolved. As digestion of fluorophore occurs, it is passed further down the intestines, and the signals begin to overlap (seen most notably at 48 hours). Regardless, tumor fluorescence can be observed from both DDAO arachidonate and DDAO palmitate fluorophores (n=3 DDAO arachidonate, n=2 DDAO palmitate). This fluorescence was significantly higher for DDAO arachidonate fluorescence at 4 and 6 hours relative to DDAO palmitate fluorescence ($p = 0.002$ and 0.02, respectively). This significance is lost at 24 and 48 hours as both signals increase.

Following the image acquisition at 48 hours, mice were euthanized and individual organs were excised, rinsed in PBS, and imaged for fluorescence (ex/em: 640/680 nm) (Figure 5.3). As expected, strong fluorescence was observed in both the small and large intestines. In addition, stomach fluorescence was shown to also be high. Tumor fluorescence was observed from both DDAO arachidonate and DDAO palmitate and was

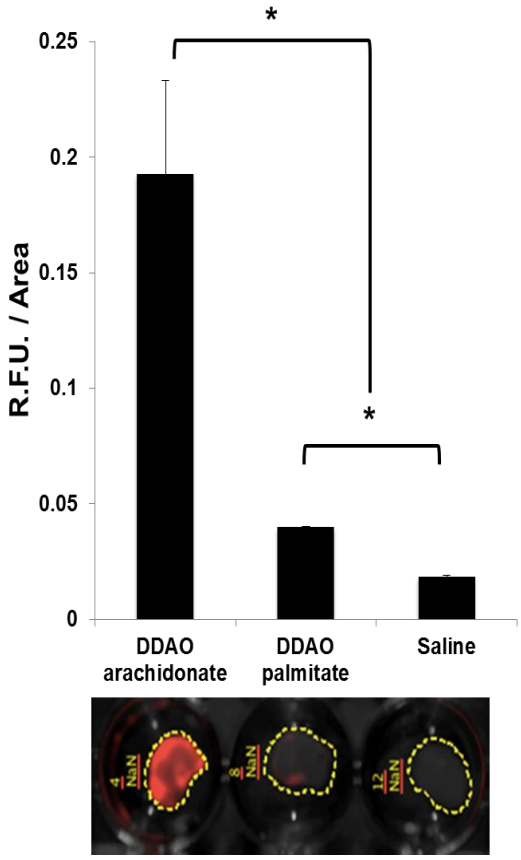

Figure 5.5. *Ex Vivo* tumor painting. Orthotopic 4175-Luc+ tumors were excised from mice, sliced, and cultured *ex vivo* in DMEM (5% CO2, 37°C). DDAO arachidonate, DDAO palmitate, or saline was painted onto tumors and left to incubate 3 hours. Tumors were then imaged for fluorescence in the LI-COR Pearl Impulse imaging system (700 nm channel).

greater than other non-digestive organs analyzed. Though not significant, DDAO arachidonate fluorescence was slightly greater than DDAO palmitate in excised organs at 48 h. In analysis of other organs, DDAO arachidonate tumor fluorescence was significantly higher than heart, lungs, kidney, and muscle ($p = 0.02, 0.03, 0.04, 0.04$, respectively). DDAO palmitate trended towards higher fluorescence but was not significantly larger than any other organ. The calculated tumor / muscle ratio of DDAO arachidonate was found to be significant and determined to be 2.14.

In a separate study, whole body fluorescence imaging with spectral unmixing of ventral facing mice was conducted as a function of time following injection of either DDAO arachidonate ($n = 4$) or DDAO palmitate ($n = 4$) (Figure 5.4). There was high variability of the total fluorescence between each mouse in this experiment leading to larger error bars in the data. However, a common trend of significantly decreased fluorescence was observed at 24 hours relative to the maximum signal at 6 hours for

DDAO arachidonate (p = 0.02). Therefore the majority of probe was cleared within this time.

Despite the ability to resolve tumor fluorescence with spectral unmixing, high background and intestinal fluorescence remained challenging. Furthermore, the low tumor signal intensity at 48 hours compared to intestinal signal indicated a relatively low delivery of fluorophore to tumor. In order to assess tumor activation of probe directly and to avoid issues of delivery and background fluorescence, *ex vivo* tumor painting studies were conducted.

For these experiments, mice were injected orthotopically with 4175-Luc+ cells. Following the formation of a palpable tumor, mice were euthanized. Tumor tissue (n=2) was excised, sliced into approximately 1 mm thick sections for the appropriate number of conditions, and placed into 24 well plates containing DMEM. The tissue was placed at 37°C, 5% CO_2 and 20 nmol of DDAO arachidonate, DDAO palmitate, or saline was pipetted evenly over the surface of the tumor. The tumor was incubated for 3 hours, washed twice in PBS, and fluorescence was acquired in a LI-COR Pearl Impulse imaging system

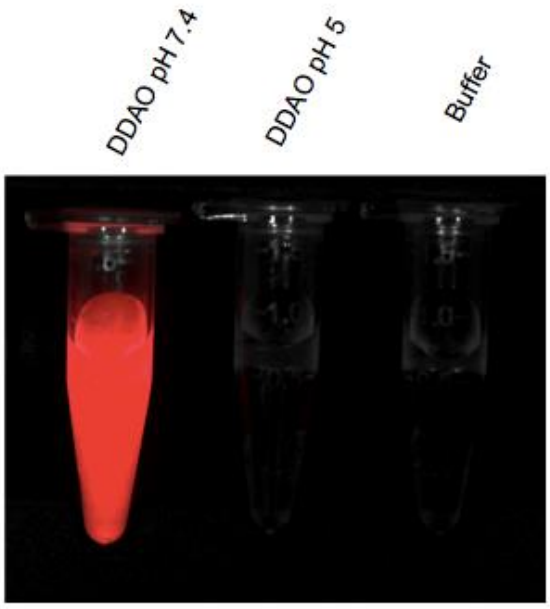

Figure 5.6. Analysis of DDAO fluorescence in the LI-COR Pearl Impulse Imaging system (700 nm channel). DDAO was assessed for fluorescence in TRIS buffer at pH 7.4 and pH 5. Free buffer is shown as a control.

(700 nm channel) (Figure 5.5). Significantly greater fluorescence from tumors (n =2) painted with DDAO arachidonate was observed compared to either DDAO palmitate or saline ($p = 7 \times 10^{-6}$ and 6.5×10^{-6} respectively). A small activation was observed from DDAO palmitate, which was significant over saline control ($p = 4.5 \times 10^{-4}$). Due to the non-optimal excitation wavelengths in the Pearl Impulse imaging system, fluorescence of DDAO was confirmed to be visible at pH 7.4 using this system (Figure 5.6).

Expanding on this study, we analyzed the differences in activation between 4175-

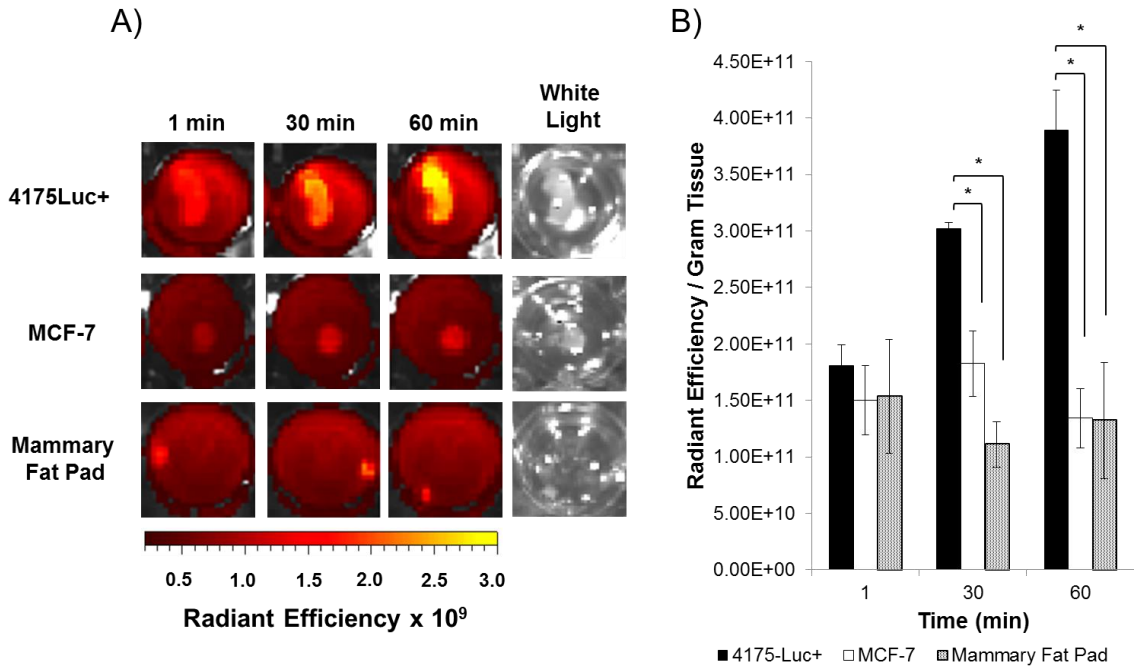

Figure 5.7. *Ex Vivo* Tumor Painting for comparison of breast cancer subtypes. A) 4175-Luc+, MCF-7, and non-inoculated mammary fat pad were excised from mice, sliced and cultured *ex vivo.* 20 nmol DDAO arachidonate containing liposomes (MF 0.05) were pipetted evenly onto the surface of tumors. Fluorescence (ex/em: 640/680) was acquired with time. B) The final fluorescence relative to the amount of tissue was quantitated.

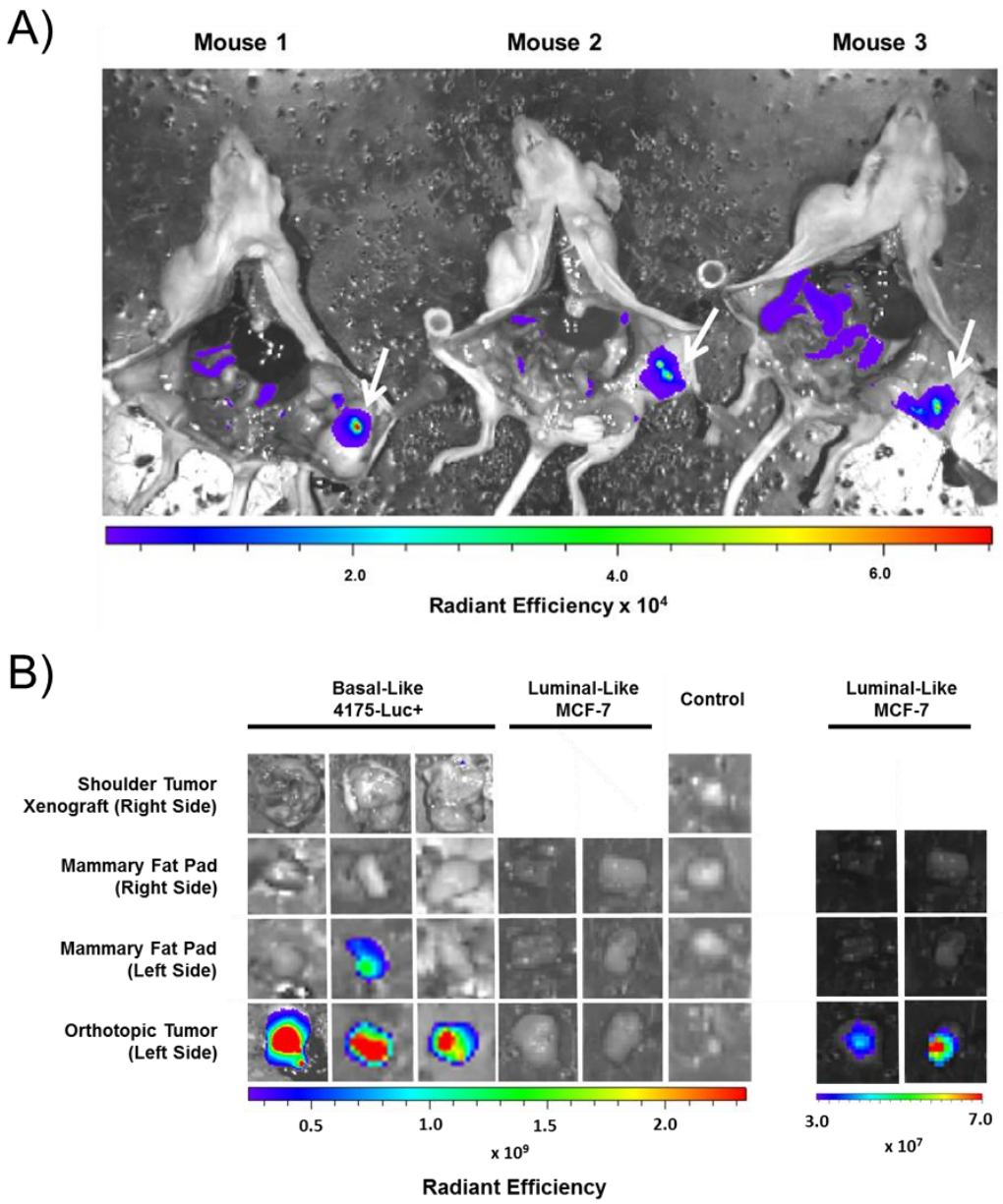

Figure 5.8. Intraoperative study of DDAO arachidonate. A) 4175-Luc+ cells were inoculated into the lower left mammary fat pad and into the right shoulder. Following formation of a palpable tumor, 40 nmol of DDAO arachidonate containing egg phosphatidylcholine liposomes (MF 0.05) were injected *i.p.* directly under the tumor. After one hour the mice were euthanized, and dissected to reveal the peritoneal cavity. The entire cavity was washed 1x in PBS and fluorescence (ex/em: 640/680) was acquired. White arrows indicate the location of tumor. B) The orthotopic tumor, tumor bearing mammary fat pat, non-inoculated mammary fat pad, and shoulder tumor xenograft were excised, rinsed in PBS and imaged for fluorescence (ex/em: 640/680). The experiment was repeated with MCF-7 luminal-like cells. The images are shown on the same vertical scale in the central Figure, and again on the right with the vertical scale expanded to optimize tumor fluorescence.

Luc+ (basal-like) and MCF-7 (luminal-like) orthotopic tumors. MCF-7 cells require estrogen for growth. Therefore, one week prior to tumor inoculation, mice were implanted subcutaneously with a slow release 17β-estradiol tablet. Following development of palpable tumors, mice were euthanized. Tumor and non-inoculated mammary fat pad (n = 3) were excised, sliced into approximately 1 mm thick sections for the appropriate number of conditions, and placed in DMEM at 37°C, 5% CO_2. DDAO arachidonate (20 nmol) was pipetted evenly over the surface of the tumor. Fluorescence was imaged on the IVIS spectrum as a function of time (ex/em: 640/680) (Figure 5.7). Significant activation of DDAO arachidonate was observed in 4175-Luc+ tumor slices versus MCF-7 and mammary fat pad at 30 min ($p = 0.002$ and 0.04 respectively) and 1 hour ($p = 0.001$ and 0.04 respectively).

It appears evident that high activation of DDAO arachidonate can be achieved in triple negative breast cancer, however high background fluorescence following systemic injection has thus far limited our ability to unequivocally determine tumor fluorescence *in vivo*. Unlike targeted fluorophores that rely on selective accumulation, DDAO arachidonate has the advantage that it can activate selectively in cancerous tissue. Therefore, during surgical resection it may be possible to paint DDAO arachidonate onto the tumor versus delivering *i.v.* In order to explore this, we sought to develop an experimental model that could mimic this surgical painting.

Tumors were grown orthotopically in the lower mammary fat pad. Shoulder tumor xenografts were also implanted on the opposing side of the mouse. Following 21 days of growth, 40 nmol of DDAO arachidonate containing liposomes (MF 0.05) were injected *i.p.* directly under the tumor in order to enhance delivery. After one hour, mice (n = 3) were euthanized and the peritoneal cavity was exposed. The cavity was washed with PBS to remove non-absorbed fluorophore and fluorescence (ex/em: 640/680) was acquired on the IVIS Spectrum (Figure 5.8). Strong fluorescence from the area of the tumor was observed (Figure 5.8A). Surgical resection of orthopic tumor, shoulder tumor xenograft, inoculated mammary fat pad, and non-inoculated mammary fat pad was

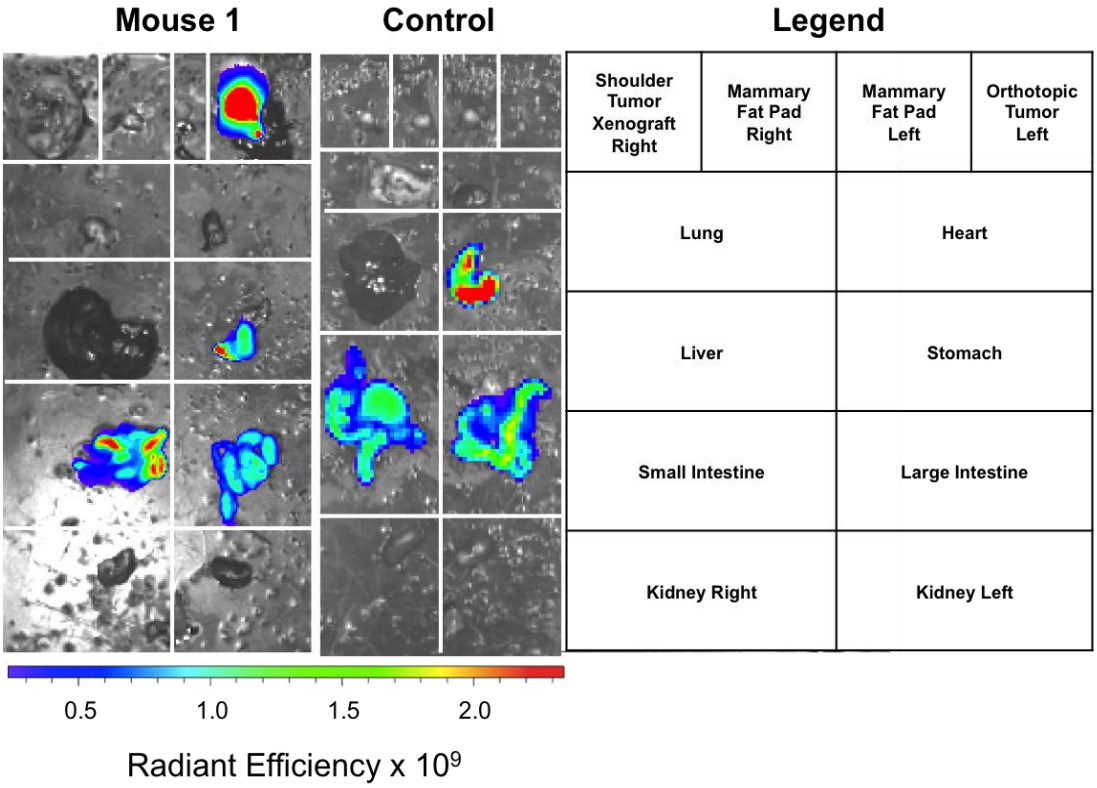

Figure 5.9. Biodistribution of DDAO arachidonate 1 hour following *i.p.* injection. Organ distribution of DDAO arachidonate is shown in under "Mouse 1". A control mouse was injected with an equal volume of saline. The legend of organs is shown on the right.

performed. Organs were washed in PBS and *ex vivo* fluorescence (ex/em: 640/680) indicated strong fluorescence from the orthotopic tumor, which was significantly greater than fluorescence from the inoculated mammary fat pad, non-inoculated mammary fat pad, and the shoulder tumor xenograft (outside the area of DDAO arachidonate injection) ($p = 0.002$, 0.001, 0.001, respectively) (Figure 5.8B). One inoculated mammary fat pad was noted to display high fluorescence. Repeating this experiment in mice bearing luminal-like orthotopic tumors ($n = 2$) revealed significantly less activation ($p = 0.01$). However, when viewed on an expanded scale, there was significant activation of MCF-7 tumors seen versus non-inoculated and inoculated mammary fat pad ($p = 0.009$ and 0.01, respectively). Comparison of individual organs following *i.p.* injection of DDAO arachidonate revealed high intestinal and stomach fluorescence as was observed previously. This signal was also present in a non-treated control mouse ($n = 1$), suggesting chow (despite being low fluorescence) still contributes to background fluorescence (Figure 5.9).

5.3 Discussion

Following *i.v.* administration of DDAO arachidonate and DDAO palmitate control, we were able to visualize time dependent changes in tumor fluorescence. However, high background signal was apparent from fluorescence dispersed throughout the animal. This fluorescence appeared with strong intensity in the upper left abdominal quadrant, possibly due to stomach or intestinal fluorescence, which was confirmed in *ex vivo* analysis. Several factors can decrease the ability to resolve fluorescence *in vivo*. Absorption due to hemoglobin is prevalent up until 650 nm where it begins to decrease

(Weissleder 2001). DDAO arachidonate is optimal just above this wavelength and therefore it is possible we still face signal loss from hemoglobin absorbance. Increased background can also result from auto-fluorescence of tissue, which is higher at lower wavelengths (Hilderbrand and Weissleder 2010). Finally, chow fluorescence can increase background signal resulting in loss of detectable signal. Though we attempt to minimize the contribution of chow by feeding mice a low fluorescence diet, it is possible this is still a contributing factor.

In vitro analysis in Chapter 4 showed that DDAO arachidonate and DDAO palmitate are activated readily by sPLA2 GIB. Therefore, high fluorescence background in the digestive tract is also possible through activation by pancreatic phospholipases. In support of this, whole body fluorescence does appear to decrease at 24 and 48 hours as probe is eliminated.

Establishment of a spectral unmixing algorithm for the separation of DDAO fluorescence from auto-fluorescence was performed using the IVIS LivingImage software. Upon application of the unmixing algorithm, we were able to reduce auto-fluorescence. Following removal of auto-fluorescence, high fluorescence remained from intestinal fluorescence. Because DDAO fluorescence in the intestines will not be removed through an unmixing algorithm, this implies intestinal fluorescence is a result of activated DDAO, possibly through the actions of sPLA2 GIB, which is secreted into the small intestine from the pancreas. Despite this, following adjustment for auto-fluorescence, tumor fluorescence was visualized at two hours and increased over two days showing DDAO arachidonate can be used for tumor imaging in mice.

The effects of intestinal signal overlap must be considered in interpreting increased fluorescence in the tumor region of interest (ROI). It was observed that intestinal fluorescence shifts in location over the course of two days, likely due to the elimination of the bulk probe. By day 2, intestinal fluorescence was more closely overlapped with the tumor and could be the cause of the increase of signal observed.

Despite this, upon quantification of the tumor ROI, we showed that DDAO arachidonate fluorescence was significantly higher than DDAO palmitate fluorescence at 4 and 6 hours post injection ($p = 0.002$ and 0.02, respectively). This significance was lost at 24 and 48 hours, possibly due to overlap with intestinal fluorescence or slow activation of DDAO palmitate with time. Both DDAO arachidonate and DDAO palmitate liposomes are expected to accumulate within tumors to the same degree and so we rely on differences in activation to visualize signal. Therefore it is possible that at time points greater than 6 hours, DDAO palmitate that is present in the tumor but not activated, may activate through a number of mechanisms including sPLA2 and aqueous hydrolysis. The higher rate of activation of DDAO arachidonate supports the hypotheses that this is due to increased cPLA2 within the tumor.

After 48 hours, organs were resected and analyzed. Intestinal fluorescence was observed to be much higher than that of tumor fluorescence, showing most of the probe is being excreted by this time with relatively small amounts remaining in the tumor. Fluorescence activation in the intestine is likely a result of the actions of sPLA2 GIB. Interestingly, high fluorescence was also observable in the stomach. Though it is possible that intestinal reflux or fecophagy could contribute to probe accumulation in the

stomach, the low pH of the stomach should minimize this fluorescence signal. Chow fluorescence may be an additional contributing factor to the high fluorescence seen in stomach and intestines. Analysis of tumor fluorescence with non-digestive organs showed significant activity from DDAO arachidonate tumor fluorescence compared to other organs ($p = 0.02, 0.03, 0.04, 0.04$ for heart, lungs, kidney, and muscle respectively), but not for DDAO palmitate. However, fluorescence intensity was low for all organs and after 48 hours no significance was seen between DDAO arachidonate and DDAO palmitate. These results indicate effective probe removal and relatively low tumor delivery combined with non-selective activation with time.

Using *ex vivo* tumor painting experiments we were able to show that significant activation of DDAO arachidonate versus DDAO palmitate was achievable in tumor tissue ($p = 7x\ 10^{-6}$). Furthermore, activity was observed on both the IVIS and Pearl Impulse imaging systems, which is important for future research utilizing DDAO arachidonate. A significant difference in activation could also be seen between basal-like and luminal-like tumors ($p = 0.001$). In addition, activation was significantly greater in basal-like tumors compared to healthy mammary fat pad ($p = 0.04$). These data indicate that if the problems associated with delivery and high background can be addressed, DDAO arachidonate could be a highly useful contrast agent for the guided surgical resection of triple negative breast cancer.

Because DDAO arachidonate is activatable, *i.v.* injection may not be necessary in a surgical procedure. Instead, similar to the *ex vivo* tumor painting experiments performed, DDAO arachidonate could be painted onto tissue in the operating room. This

would reduce the high background fluorescence seen during *i.v.* injection. Since rapid activation in *ex vivo* studies was observed, it is likely that visualization of tumor fluorescence would be possible at a much earlier time point using painting compared to *i.v.* injection.

To test this in a model system, we inoculated mice with 4175-Luc+ cells in the lower left mammary fat pad that lays in close proximity to the peritoneal cavity. We then injected probe *i.p.* directly under the tumor. We euthanized mice after just 1 hour, exposed the peritoneal cavity and looked for fluorescence activation. Using this procedure, we observed high fluorescence in the tumor area relative to surrounding cavity. Dissection of individual organs revealed that the tumor activated probe significantly compared to surrounding mammary fat pad ($p = 0.002$). One mouse displayed high fluorescence from the healthy portion of the inoculated mammary fat pad (albeit lower than tumor fluorescence). Whether this fluorescence is a result of residual tumor or alternative mechanisms requires further analysis. However, this highlights the potential use of DDAO arachidonate as a surgical guide to ensure complete recession of tissue with high cPLA2 activity. In this experiment, a shoulder tumor xenograft lying far from the area of injection was also analyzed and shown to have significantly lower fluorescence ($p = 0.001$). We repeated this experiment in mice using the luminal-like MCF-7 cell line. Unlike the 4175-Luc+ tumors, MCF-7 tumors gave significantly less activation in comparison ($p = 0.01$). However, when analyzing tumor and healthy mammary fat pad a significant difference could still be observed ($p = 0.01$), suggesting MCF-7 tumors do activate DDAO arachidonate, albeit at a much lower rate than that of

4175-Luc+ tumors. Analysis of all organs revealed high digestive fluorescence as observed previously. However, high levels of digestive fluorescence were also observed in control mice. Therefore, we can contribute observed digestive fluorescence partially to chow fluorescence. Because our measurements take place after only 1 hour of incubation, it is likely that intestinal signal due to probe activation would increase with time as observed previously.

Together, we conclude that DDAO arachidonate is a promising fluorophore for the imaging of cancerous tissue *in vivo* and is worthy of further investigation for its use as a contrast agent in NIR fluorescence guided surgery. DDAO arachidonate should be used topically during surgery to visualize tumor margins and not injected *i.v.*. Though alternative delivery vehicles could be explored to enhance tumor delivery, topical delivery would also reduce the amount of probe needed, thus reducing potential systemic side effects, and decrease the wait time needed for optimal fluorescence. Furthermore, our results suggest DDAO arachidonate would be most useful in the NIR fluorescence guided surgery of basal-like breast cancer. However, cPLA2 activity has been suggested to vary in luminal-like cancers with increased expression being correlated with higher probability of developing resistance to estrogen receptor therapy (Caiazza et al. 2011). Therefore, use of DDAO arachidonate may be useful in staging luminal-like cancers and serve as an indicator for patients who may eventually develop resistance. Finally, because cPLA2 is associated with more aggressive breast cancer, DDAO arachidonate may also be useful in analysis of tumor heterogeneity, separating more aggressive from less aggressive tumor areas.

CHAPTER 6: Conclusions and Future Directions

6.1 Conclusions and Potential Applications

Despite numerous discoveries related to the treatment of breast cancer, it remains a disease with high prevalence and cancer related mortality in women (DeSantis et al. 2014). Increasing the armamentarium of available therapeutics along with developing more sensitive imaging methods to identify and characterize breast cancer at an early stage are both critical to increasing cure rates. Molecular based therapeutics have emerged that target unique molecular signatures of breast cancer through both traditional small molecule compounds and antibody-based therapeutics. Despite this, surgical intervention remains the first line of defense for the treatment of breast cancer and the accuracy of surgery has been shown to correlate closely with the probability of reoccurrence and metastasis (Singletary 2002). Methods of improving surgical resection are therefore vital to the continued treatment of this disease.

Within this dissertation, we introduced a novel activatable fluorophore, DDAO arachidonate, selective to the breast cancer associated protein, cPLA2. Through a series of *in vitro* and *in vivo* studies we have evaluated this probe's specificity for cPLA2 and for its ability to serve as a molecular imaging agent in breast cancer. Our results indicate several advantages and potential limitations to the use of DDAO arachidonate for NIR fluorescence guided surgery. In addition, our studies open the door for future research of cPLA2 activity in cancer and other diseases using DDAO arachidonate. However, our results also identify areas of concern, which will be a focus in the future design of activatable fluorophores.

The use of activatable probes in NIR fluorescence guided surgery deserves future study. We have shown a high ability to distinguish healthy from cancerous tissue using DDAO arachidonate. In addition, we have shown the ability to differentiate breast cancer subtypes with this probe, with higher activation observed in more aggressive cancer. Therefore, the intraoperative use of DDAO arachidonate may be able to accurately delineate tumor margins in real-time while providing functional information on variations in tissue heterogeneity.

DDAO arachidonate activation was shown to correlate closely with cPLA2 expression. Despite this, it was also shown that DDAO arachidonate is susceptible to aqueous hydrolysis, sPLA2 GIB mediated hydrolysis, and possible activation through unidentified sources. In a research setting, we proposed the use of DDAO palmitate as a control probe to account for non-cPLA2 mediated cleavage. However, for the potential use of DDAO arachidonate in clinical settings, this may be a confounding issue. This is especially evident when administered *i.v.* We observed high background fluorescence, partially due to activation outside the area of the tumor, especially in the digestive tract. In addition, we saw relatively low tumor accumulation with respect to probe clearance with the maximum measurable cPLA2 signal at 4 and 6 hours after administration. This presents additional potential problems as the higher amounts of time necessary to generate signal increases the likelihood of non-cPLA2 mediated cleavage.

DDAO arachidonate is an activatable fluorophore, dependent on enzymatic cleavage for the generation of signal. Unlike non-specific and targeted fluorophores, DDAO arachidonate does not depend to the same extent on tumor accumulation for

enhanced signal/noise. This allows for the possible topical application of DDAO arachidonate in a surgical setting. This would reduce the problems observed with non-specific activation as less time would be needed between administration and visualization. In addition, topical application would reduce the amount of probe needed to generate contrast thus limiting potential systemic side effects, which might occur through *i.v.* administration of larger concentrations. For these reasons, we believe this mechanism of activatable fluorescence is of high value and should be utilized in the design of future contrast agents for NIR fluorescence guided surgery.

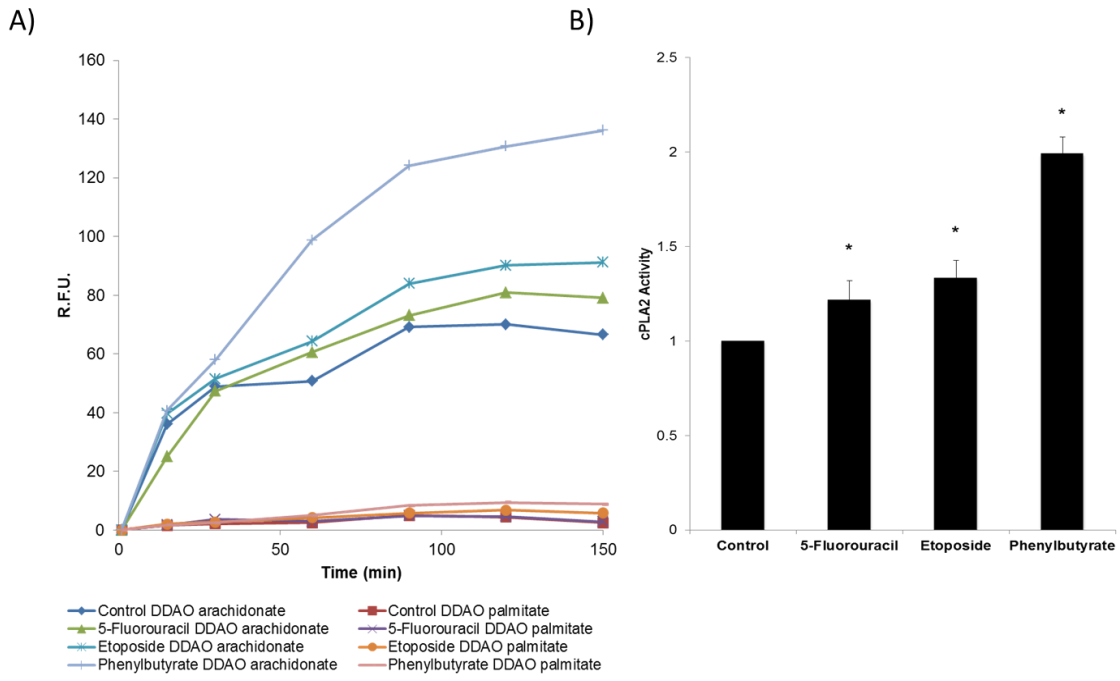

Figure 6.1. Effects of anti-cancer drug treatment on cPLA2 activation. A) MCF-7 cells were treated with 10 µM 5-fluorouracil, 40 µM etoposide, 10 mM phenylbutryate, or DMSO control for 12 hours. DDAO arachidonate activation was plotted with time. B) Relative cPLA2 activity was calculated at 150 min by adjusting DDAO arachidonate activation for non-specific cleavage measured with DDAO palmitate.

6.2 cPLA2 Activation During Apoptosis

In our attempts to define the specificity of DDAO arachidonate, we have made several observations related to the function of cPLA2, which warrant further investigation. In confocal microscopy experiments presented in Chapter 4, we showed subcellular activation of DDAO arachidonate in various cell lines. It was noted that in all cell lines analyzed, there were a small percentage of cells that gave much higher fluorescence than the general population. These cells were all similar in morphology in that they were rounded up and beginning to detach from the tissue culture plastic, a characteristic of stressed or early apoptotic cells.

cPLA2 has been previously shown to be required in TNF-α induced apoptosis (Enari et al. 1996). Furthermore, cPLA2 has been implicated in the formation of lipid droplets, which form in the early stages of the apoptotic response to anti-cancer therapy (Gubern et al. 2008, Delikatny et al. 2011, Guijas et al. 2014). Therefore, if the fluorescence that was observed in confocal microscopy was a result of cPLA2 activation as part of the apoptotic process, then DDAO arachidonate may prove to have some utility in measuring tumor response to therapy. Furthermore, if the high level of fluorescence activation seen in cellular studies translates to apoptosis in tumor bearing mice, some of the issues of signal to noise outlined earlier would be reduced.

In a preliminary study, we analyzed three apoptosis inducing agents for their effect on DDAO arachidonate activation. We chose the MCF-7 cell line for analysis as it contains the lowest levels of cPLA2 and therefore offers the greatest potential for

increased signal generation. MCF-7 cells were plated in 96-well black wall, clear bottom plates at 2.5 x 10^5 cells / mL in 100 µL media 24 hours prior to drug treatment. 12 hours prior to experiment, the media was replaced with phenol red- and FBS-free media containing 10 µM 5-fluorouracil, 40 µM etoposide, or 10 mM phenylbutyrate. Drug concentrations for 5-fluorouracil and etoposide were chosen based on previously reported literature values (Hernandez-Vargas et al. 2006, Alpsoy, Yasa, and Gunduz 2014). Drug concentrations for phenylbutyrate was chosen based on previous performed toxicity studies of the prostate cancer cell line, DU145 (Milkevitch et al. 2005, Milkevitch et al. 2007, Milkevitch, Beardsley, and Delikatny 2010). To initiate the assay, 10 µL of DDAO arachidonate or DDAO palmitate in liposomes (MF 0.05) were added to each well. Fluorescence was acquired with time and relative cPLA2 activity was calculated (Figure 6.1A and B). Significant enhancement of cPLA2 activity was observed following administration of 5-fluorouracil, etoposide, and phenylbutyrate ($p = 0.02, 0.003, 0.0004$, respectively). 5-Fluorouracil, etoposide, and phenylbutyrate gave a 1.2, 1.3, and 2 fold increase in activity, respectively, when compared to control. Together, this provides further evidence for the role of cPLA2 in apoptosis and supports further investigation of DDAO arachidonate for the *in vivo* imaging of tumor response to therapy.

6.3 cPLA2 Involvement In Alternative Disease Models

DDAO arachidonate shows promise in its potential to serve as a contrast agent for fluorescence guided surgery in breast cancer. We have focused on breast cancer within this thesis for reasons including relatively high light penetration in breast tissue and variations of cPLA2 expression levels related to breast cancer subtype. However, cPLA2 overexpression is not unique to the breast and has been observed in other cancers. In non-small cell lung cancer, cPLA2 expression was found to be elevated in relation to induction of the RAS oncogene (Heasley et al. 1997). In addition, it has been shown that cPLA2 deficient mice have decreased lung tumor formation following urethane exposure

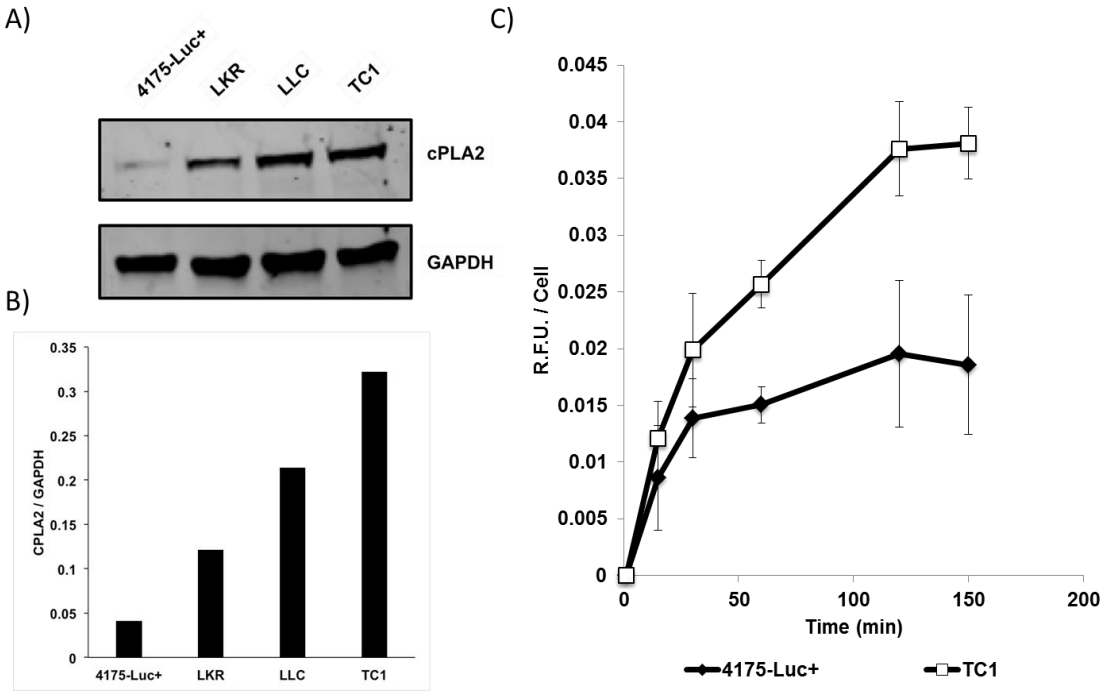

Figure 6.2. cPLA2 activity in lung cancer cell lines. A) Immunoblot of cPLA2 and GAPDH (control) in 4175-Luc+ and three murine lung cancer lines. B) Quantification of immunoblot showing expression relative to control. C) cPLA2 activity in 4175-Luc+ and TC1 cells as measured through activation of DDAO arachidonate (adjusted for DDAO palmitate activation) with respect to time. Significant activity in TC1 vs. 4175-Luc+ cells was observed ($p = 2.4 \times 10^{-7}$)

(Meyer et al. 2004).

In order to explore cPLA2 in a lung cancer model, we utilized 3 murine non-small cell lung cancer cell lines (LKR, LLC, and TC1), generously provided by Dr. Sunil Singhal in the Department of Surgery at the University of Pennsylvania. Immunoblot of cPLA2, carried out by Sofya Osharovich, showed a remarkable elevation in expression in all lung cancer cell lines relative to 4175-Luc+. Most dramatic was the TC1 line, which showed 9 fold increased expression of cPLA2 compared to the 4175-Luc+ cell line (Figure 6.2A and B). To investigate the activity of cPLA2 within this cell line, 4175-Luc+ and TC1 were plated at 2.5 x 10^5 and 1.25 x 10^5 cell/mL, respectively, in 100 µL media. Plating concentrations were chosen to result in approximately 80% confluency at

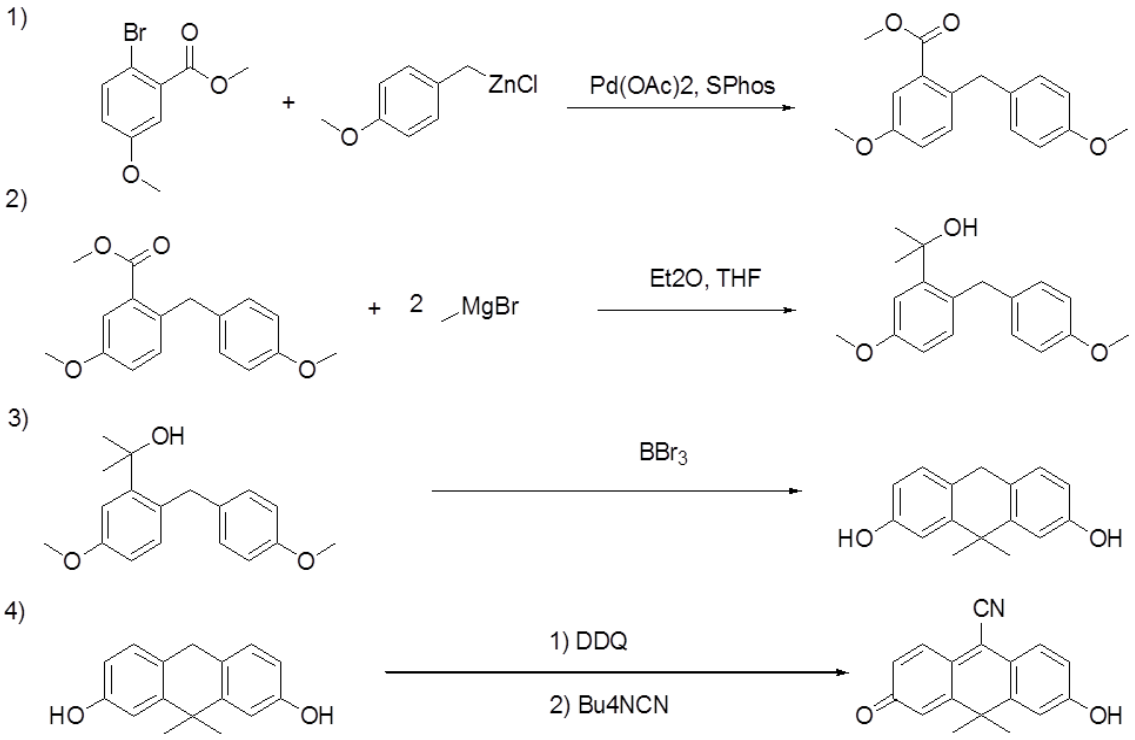

Figure 6.3. Four step synthetic scheme for nitriloanthracenone.

time of analysis. Following 24 hours of incubation, DDAO arachidonate or DDAO palmitate in liposomes (MF 0.05) were added to each well. cPLA2 activity with time was determined and data was plotted by subtraction of DDAO palmitate fluorescence from DDAO arachidonate and scaled relative to the final number of cells (Figure 6.2C). A significant increase of fluorescence was observed from the TC1 cell line relative to the 4175-Luc+ cell line ($p = 2.4 \times 10^{-7}$). Therefore, we believe non-small cell lung cancer could be evaluated as a potential target for DDAO arachidonate mediated NIR fluorescence guided surgery. Our preliminary results suggest lung cancers may provide even higher levels of contrast than triple-negative breast cancer.

6.4 Second-Generation Long-Wavelength Activatable Fluorophores

Despite the success we have observed for DDAO arachidonate, signal to noise resulting from tissue absorbance, scattering, and auto-fluorescence remain problematic.

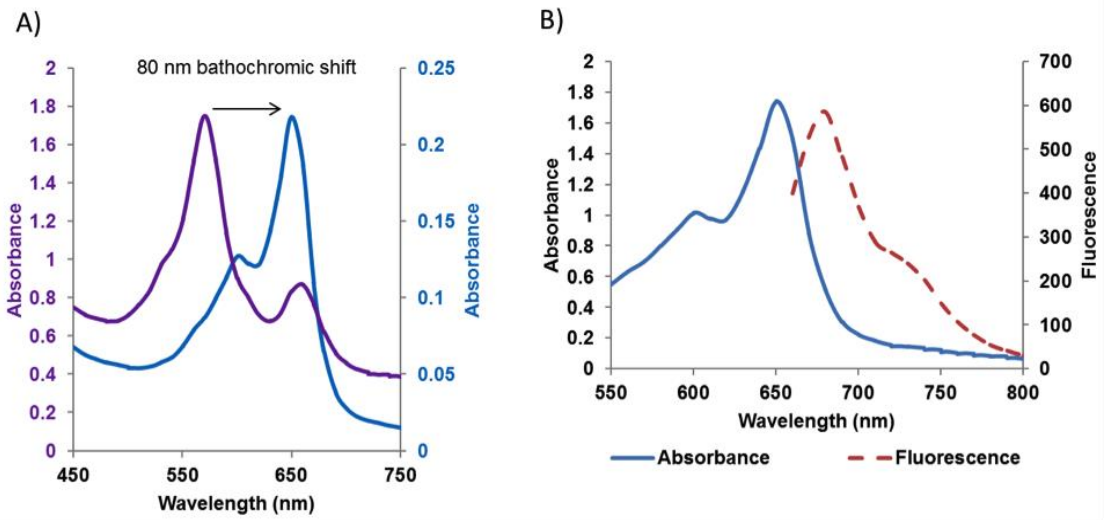

Figure 6.4. Spectral properties of nitriloanthracenone. A) The addition of a nitrilo moiety to an existing tricyclic fluorophore induced an 80 nm bathochromic shift in the final product. B) Fluorescence (excitation 650 nm) results in fluorescence maximum at 680 nm and a large shoulder that persists to 750 nm, suitable for *in vivo* NIR imaging.

DDAO lies at the edge of the NIR window and if fluorescence could be shifted farther into the NIR, higher signal could potentially be acquired. Longer wavelength fluorophores tend to be large in size, which may prevent cPLA2 mediated cleavage as observed with naphthofluorescein diarachidonate. In addition, the structures of NIR fluorophores typically do not allow for the caging of fluorescence. Therefore, we sought to synthesize small tricyclic fluorophores with chemical modifications which might result in longer wavelength fluorescence emission.

Through a four step synthesis, we introduced a nitrilo substitution to the central ring of an anthracene scaffold to generate a fluorophore called nitriloanthracenone (Figure 6.3). Though similar in structure to DDAO, nitriloanthracenone displayed altered fluorescence properties, shifted further in the NIR region (Figure 6.4). Addition of the nitrilo moiety (Figure 6.3 step 4), resulted in an 80 nm bathochromic shift of absorbance resulting in an excitation at 650 nm, and a maximum emission at 680 nm (Figure 6.4). The emission spectrum has a prominent shoulder which extended out to 750 nm. The large Stokes shift in this fluorescence profile along with the extended emission wavelength into the NIR makes nitriloanthracenone an excellent potential platform for the design of NIR caged activatable fluorophores. Further modifications will include the addition of dichloro and dimethoxy substituents ortho to the resonant active hydroxyl similar to DDAO. We hypothesize that these substitutions will reduce non-specific and aqueous hydrolysis of the esterified derivatives, a necessary characteristic in the design of biological imaging agents. Furthermore, dichloro and dimethoxy substituents may shift fluorescence further into the NIR to give enhanced *in vivo* properties. Efforts are

currently underway to cage nitriloanthracenone to arachidonic acid in order to explore its use for cPLA2 imaging.

6.5 Final Remarks

In conclusion, we have supplied evidence for a new molecular imaging agent specific to cPLA2. We believe this will prove to be a valuable platform for the exploration of the function of cPLA2 in disease progression. In breast cancer, DDAO arachidonate warrants further investigation for its ability to aid in NIR fluorescence guided surgery. The application of this probe to other purposes such as apoptotic imaging or the molecular imaging of lung cancer will become clearer as more studies are performed. Finally, second generation fluorophores, with enhanced *in vivo* optical properties, offer the potential to greatly increase the capabilities of molecular imaging. Taken together, we believe the future of activatable fluorophores is bright.

BIBLIOGRAPHY

Abe, A, Poucher, HK, Hiraoka, M, and Shayman, JA. (2004). Induction of lysosomal phospholipase A2 through the retinoid X receptor in THP-1 cells. *J Lipid Res* **45** (4):667-73.

Alpsoy, A, Yasa, S, and Gunduz, U. (2014). Etoposide resistance in MCF-7 breast cancer cell line is marked by multiple mechanisms. *Biomed Pharmacother* **68** (3):351-5.

Aurilio, G, Disalvatore, D, Pruneri, G, Bagnardi, V, Viale, G, Curigliano, G, Adamoli, L, Munzone, E, Sciandivasci, A, De Vita, F, Goldhirsch, A, and Nole, F. (2014). A meta-analysis of oestrogen receptor, progesterone receptor and human epidermal growth factor receptor 2 discordance between primary breast cancer and metastases. *Eur J Cancer* **50** (2):277-89.

Baeten, J, Haller, J, Shih, H, and Ntziachristos, V. (2009). In vivo investigation of breast cancer progression by use of an internal control. *Neoplasia* **11** (3):220-7.

Beatty, KE, Williams, M, Carlson, BL, Swarts, BM, Warren, RM, van Helden, PD, and Bertozzi, CR. (2013). Sulfatase-activated fluorophores for rapid discrimination of mycobacterial species and strains. *Proc Natl Acad Sci U S A* **110** (32):12911-6.

Berridge, MJ. (2009). Inositol trisphosphate and calcium signalling mechanisms. *Biochim Biophys Acta* **1793** (6):933-40.

Berry, DA, Cronin, KA, Plevritis, SK, Fryback, DG, Clarke, L, Zelen, M, Mandelblatt, JS, Yakovlev, AY, Habbema, JD, Feuer, EJ, Cancer, I, and Surveillance Modeling Network, C. (2005). Effect of screening and adjuvant therapy on mortality from breast cancer. *N Engl J Med* **353** (17):1784-92.

Boren, J, and Brindle, KM. (2012). Apoptosis-induced mitochondrial dysfunction causes cytoplasmic lipid droplet formation. *Cell Death Differ* **19** (9):1561-70.

Borin, TF, Zuccari, DA, Jardim-Perassi, BV, Ferreira, LC, Iskander, AS, Varma, NR, Shankar, A, Guo, AM, Scicli, G, and Arbab, AS. (2014). HET0016, a selective inhibitor of 20-HETE synthesis, decreases pro-angiogenic factors and inhibits growth of triple negative breast cancer in mice. *PLoS One* **9** (12):e116247.

Bremer, C, Tung, CH, and Weissleder, R. (2001). In vivo molecular target assessment of matrix metalloproteinase inhibition. *Nat Med* **7** (6):743-8.

Burke, JE, and Dennis, EA. (2009). Phospholipase A2 structure/function, mechanism, and signaling. *J Lipid Res* **50 Suppl**:S237-42.

Caiazza, F, Harvey, BJ, and Thomas, W. (2010). Cytosolic phospholipase A2 activation correlates with HER2 overexpression and mediates estrogen-dependent breast cancer cell growth. *Mol Endocrinol* **24** (5):953-68.

Caiazza, F, McCarthy, NS, Young, L, Hill, AD, Harvey, BJ, and Thomas, W. (2011). Cytosolic phospholipase A2-alpha expression in breast cancer is associated with EGFR expression and correlates with an adverse prognosis in luminal tumours. *Br J Cancer* **104** (2):338-44.

Chen, X, Li, N, Wang, S, Wu, N, Hong, J, Jiao, X, Krasna, MJ, Beer, DG, and Yang, CS. (2003). Leukotriene A4 hydrolase in rat and human esophageal adenocarcinomas and inhibitory effects of bestatin. *J Natl Cancer Inst* **95** (14):1053-61.

Clapper, ML, Hensley, HH, Chang, WC, Devarajan, K, Nguyen, MT, and Cooper, HS. (2011). Detection of colorectal adenomas using a bioactivatable probe specific for matrix metalloproteinase activity. *Neoplasia* **13** (8):685-91.

Das, S, Rafter, JD, Kim, KP, Gygi, SP, and Cho, W. (2003). Mechanism of group IVA cytosolic phospholipase A(2) activation by phosphorylation. *J Biol Chem* **278** (42):41431-42.

Day, KE, Beck, LN, Deep, NL, Kovar, J, Zinn, KR, and Rosenthal, EL. (2013). Fluorescently labeled therapeutic antibodies for detection of microscopic melanoma. *Laryngoscope* **123** (11):2681-9.

Delikatny, EJ, Chawla, S, Leung, DJ, and Poptani, H. (2011). MR-visible lipids and the tumor microenvironment. *NMR Biomed* **24** (6):592-611.

Dennis, EA, Cao, J, Hsu, YH, Magrioti, V, and Kokotos, G. (2011). Phospholipase A2 enzymes: physical structure, biological function, disease implication, chemical inhibition, and therapeutic intervention. *Chem Rev* **111** (10):6130-85.

DeSantis, CE, Lin, CC, Mariotto, AB, Siegel, RL, Stein, KD, Kramer, JL, Alteri, R, Robbins, AS, and Jemal, A. (2014). Cancer treatment and survivorship statistics, 2014. *CA Cancer J Clin* **64** (4):252-71.

Dessen, A, Tang, J, Schmidt, H, Stahl, M, Clark, JD, Seehra, J, and Somers, WS. (1999). Crystal structure of human cytosolic phospholipase A2 reveals a novel topology and catalytic mechanism. *Cell* **97** (3):349-60.

Dreyling, KW, Hoppe, U, Peskar, BA, Morgenroth, K, Kozuschek, W, and Peskar, BM. (1986). Leukotriene synthesis by human gastrointestinal tissues. *Biochim Biophys Acta* **878** (2):184-93.

Duncan, RE, Sarkadi-Nagy, E, Jaworski, K, Ahmadian, M, and Sul, HS. (2008). Identification and functional characterization of adipose-specific phospholipase A2 (AdPLA). *J Biol Chem* **283** (37):25428-36.

Duo, T, Goddard-Borger, ED, and Withers, SG. (2014). Fluoro-glycosyl acridinones are ultra-sensitive active site titrating agents for retaining beta-glycosidases. *Chem Commun (Camb)* **50** (66):9379-82.

Düzgünes, N, and Nir, S. (1999). Mechanisms and kinetics of liposome-cell interactions. *Adv Drug Deliv Rev* **40** (1-2):3-18.

Eberhart, CE, Coffey, RJ, Radhika, A, Giardiello, FM, Ferrenbach, S, and DuBois, RN. (1994). Up-regulation of cyclooxygenase 2 gene expression in human colorectal adenomas and adenocarcinomas. *Gastroenterology* **107** (4):1183-8.

Edge, SB, and Compton, CC. (2010). The American Joint Committee on Cancer: the 7th edition of the AJCC cancer staging manual and the future of TNM. *Ann Surg Oncol* **17** (6):1471-4.

Ellis-Davies, GC. (2007). Caged compounds: photorelease technology for control of cellular chemistry and physiology. *Nat Methods* **4** (8):619-28.

Enari, M, Hug, H, Hayakawa, M, Ito, F, Nishimura, Y, and Nagata, S. (1996). Different apoptotic pathways mediated by Fas and the tumor-necrosis-factor receptor. Cytosolic phospholipase A2 is not involved in Fas-mediated apoptosis. *Eur J Biochem* **236** (2):533-8.

Eroles, P, Bosch, A, Perez-Fidalgo, JA, and Lluch, A. (2012). Molecular biology in breast cancer: intrinsic subtypes and signaling pathways. *Cancer Treat Rev* **38** (6):698-707.

Evans, JH, Spencer, DM, Zweifach, A, and Leslie, CC. (2001). Intracellular calcium signals regulating cytosolic phospholipase A2 translocation to internal membranes. *J Biol Chem* **276** (32):30150-60.

Fang, Y, Vilella-Bach, M, Bachmann, R, Flanigan, A, and Chen, J. (2001). Phosphatidic acid-mediated mitogenic activation of mTOR signaling. *Science* **294** (5548):1942-5.

Funk, CD. (2001). Prostaglandins and leukotrienes: advances in eicosanoid biology. *Science* **294** (5548):1871-5.

Gao, Q, Yan, L, Chiorazzo, M, Delikatny, EJ, Tsourkas, A, and Cheng, Z. (2015). PLA2-responsive and SPIO-loaded phospholipid micelles. *Chem Commun (Camb)* **51** (61):12313-5.

Gijon, MA, and Leslie, CC. (1999). Regulation of arachidonic acid release and cytosolic phospholipase A2 activation. *J Leukoc Biol* **65** (3):330-6.

Greenhough, A, Smartt, HJ, Moore, AE, Roberts, HR, Williams, AC, Paraskeva, C, and Kaidi, A. (2009). The COX-2/PGE2 pathway: key roles in the hallmarks of cancer and adaptation to the tumour microenvironment. *Carcinogenesis* **30** (3):377-86.

Griner, EM, and Kazanietz, MG. (2007). Protein kinase C and other diacylglycerol effectors in cancer. *Nat Rev Cancer* **7** (4):281-94.

Gross, S, and Piwnica-Worms, D. (2005). Spying on cancer: molecular imaging in vivo with genetically encoded reporters. *Cancer Cell* **7** (1):5-15.

Gubern, A, Casas, J, Barcelo-Torns, M, Barneda, D, de la Rosa, X, Masgrau, R, Picatoste, F, Balsinde, J, Balboa, MA, and Claro, E. (2008). Group IVA phospholipase A2 is necessary for the biogenesis of lipid droplets. *J Biol Chem* **283** (41):27369-82.

Guijas, C, Rodriguez, JP, Rubio, JM, Balboa, MA, and Balsinde, J. (2014). Phospholipase A2 regulation of lipid droplet formation. *Biochim Biophys Acta* **1841** (12):1661-71.

Gupta, S, Srivastava, M, Ahmad, N, Bostwick, DG, and Mukhtar, H. (2000). Over-expression of cyclooxygenase-2 in human prostate adenocarcinoma. *Prostate* **42** (1):73-8.

Haque, R, Ahmed, SA, Inzhakova, G, Shi, J, Avila, C, Polikoff, J, Bernstein, L, Enger, SM, and Press, MF. (2012). Impact of breast cancer subtypes and treatment on survival: an analysis spanning two decades. *Cancer Epidemiol Biomarkers Prev* **21** (10):1848-55.

Harris, RC, Homma, T, Jacobson, HR, and Capdevila, J. (1990). Epoxyeicosatrienoic acids activate Na+/H+ exchange and are mitogenic in cultured rat glomerular mesangial cells. *J Cell Physiol* **144** (3):429-37.

Heasley, LE, Thaler, S, Nicks, M, Price, B, Skorecki, K, and Nemenoff, RA. (1997). Induction of cytosolic phospholipase A2 by oncogenic Ras in human non-small cell lung cancer. *J Biol Chem* **272** (23):14501-4.

Hennig, R, Ding, XZ, Tong, WG, Schneider, MB, Standop, J, Friess, H, Buchler, MW, Pour, PM, and Adrian, TE. (2002). 5-Lipoxygenase and leukotriene B(4) receptor are expressed in human pancreatic cancers but not in pancreatic ducts in normal tissue. *Am J Pathol* **161** (2):421-8.

Hernandez-Vargas, H, Ballestar, E, Carmona-Saez, P, von Kobbe, C, Banon-Rodriguez, I, Esteller, M, Moreno-Bueno, G, and Palacios, J. (2006). Transcriptional profiling of MCF7 breast cancer cells in response to 5-Fluorouracil: relationship

with cell cycle changes and apoptosis, and identification of novel targets of p53. *Int J Cancer* **119** (5):1164-75.

Hilderbrand, SA, and Weissleder, R. (2010). Near-infrared fluorescence: application to in vivo molecular imaging. *Curr Opin Chem Biol* **14** (1):71-9.

Hong, KH, Bonventre, JC, O'Leary, E, Bonventre, JV, and Lander, ES. (2001). Deletion of cytosolic phospholipase A(2) suppresses Apc(Min)-induced tumorigenesis. *Proc Natl Acad Sci U S A* **98** (7):3935-9.

Hope-Ross, M, Yannuzzi, LA, Gragoudas, ES, Guyer, DR, Slakter, JS, Sorenson, JA, Krupsky, S, Orlock, DA, and Puliafito, CA. (1994). Adverse reactions due to indocyanine green. *Ophthalmology* **101** (3):529-33.

Horska, A, and Barker, PB. (2010). Imaging of brain tumors: MR spectroscopy and metabolic imaging. *Neuroimaging Clin N Am* **20** (3):293-310.

Huang, Z, Laliberte, F, Tremblay, NM, Weech, PK, and Street, IP. (1994). A continuous fluorescence-based assay for the human high-molecular-weight cytosolic phospholipase A2. *Anal Biochem* **222** (1):110-5.

Hudis, CA. (2007). Trastuzumab--mechanism of action and use in clinical practice. *N Engl J Med* **357** (1):39-51.

Inoue, Y, Izawa, K, Kiryu, S, Tojo, A, and Ohtomo, K. (2008). Diet and abdominal autofluorescence detected by in vivo fluorescence imaging of living mice. *Mol Imaging* **7** (1):21-7.

Jares-Erijman, EA, and Jovin, TM. (2003). FRET imaging. *Nat Biotechnol* **21** (11):1387-95.

Jiang, JG, Chen, CL, Card, JW, Yang, S, Chen, JX, Fu, XN, Ning, YG, Xiao, X, Zeldin, DC, and Wang, DW. (2005). Cytochrome P450 2J2 promotes the neoplastic phenotype of carcinoma cells and is up-regulated in human tumors. *Cancer Res* **65** (11):4707-15.

Judy, RP, Keating, JJ, DeJesus, EM, Jiang, JX, Okusanya, OT, Nie, S, Holt, DE, Arlauckas, SP, Low, PS, Delikatny, EJ, and Singhal, S. (2015). Quantification of tumor fluorescence during intraoperative optical cancer imaging. *Sci Rep* **5**:16208.

Kamiya, M, Kobayashi, H, Hama, Y, Koyama, Y, Bernardo, M, Nagano, T, Choyke, PL, and Urano, Y. (2007). An enzymatically activated fluorescence probe for targeted tumor imaging. *J Am Chem Soc* **129** (13):3918-29.

Ke, S, Wen, X, Gurfinkel, M, Charnsangavej, C, Wallace, S, Sevick-Muraca, EM, and Li, C. (2003). Near-infrared optical imaging of epidermal growth factor receptor in breast cancer xenografts. *Cancer Res* **63** (22):7870-5.

Keating, J, Tchou, J, Okusanya, O, Fisher, C, Batiste, R, Jiang, J, Kennedy, G, Nie, S, and Singhal, S. (2016). Identification of breast cancer margins using intraoperative near-infrared imaging. *J Surg Oncol* **113** (5):508-14.

Kelloff, GJ, Hoffman, JM, Johnson, B, Scher, HI, Siegel, BA, Cheng, EY, Cheson, BD, O'Shaughnessy, J, Guyton, KZ, Mankoff, DA, Shankar, L, Larson, SM, Sigman, CC, Schilsky, RL, and Sullivan, DC. (2005). Progress and promise of FDG-PET imaging for cancer patient management and oncologic drug development. *Clin Cancer Res* **11** (8):2785-808.

Khuri, FR, Wu, H, Lee, JJ, Kemp, BL, Lotan, R, Lippman, SM, Feng, L, Hong, WK, and Xu, XC. (2001). Cyclooxygenase-2 overexpression is a marker of poor prognosis in stage I non-small cell lung cancer. *Clin Cancer Res* **7** (4):861-7.

Konda, SD, Aref, M, Wang, S, Brechbiel, M, and Wiener, EC. (2001). Specific targeting of folate-dendrimer MRI contrast agents to the high affinity folate receptor expressed in ovarian tumor xenografts. *MAGMA* **12** (2-3):104-13.

Kulkarni, S, Rader, JS, Zhang, F, Liapis, H, Koki, AT, Masferrer, JL, Subbaramaiah, K, and Dannenberg, AJ. (2001). Cyclooxygenase-2 is overexpressed in human cervical cancer. *Clin Cancer Res* **7** (2):429-34.

Lamour, NF, Subramanian, P, Wijesinghe, DS, Stahelin, RV, Bonventre, JV, and Chalfant, CE. (2009). Ceramide 1-phosphate is required for the translocation of group IVA cytosolic phospholipase A2 and prostaglandin synthesis. *J Biol Chem* **284** (39):26897-907.

Larre, S, Tran, N, Fan, C, Hamadeh, H, Champigneulles, J, Azzouzi, R, Cussenot, O, Mangin, P, and Olivier, JL. (2008). PGE2 and LTB4 tissue levels in benign and cancerous prostates. *Prostaglandins Other Lipid Mediat* **87** (1-4):14-9.

Lehmann, BD, Bauer, JA, Chen, X, Sanders, ME, Chakravarthy, AB, Shyr, Y, and Pietenpol, JA. (2011). Identification of human triple-negative breast cancer subtypes and preclinical models for selection of targeted therapies. *J Clin Invest* **121** (7):2750-67.

Liimatainen, TJ, Erkkila, AT, Valonen, P, Vidgren, H, Lakso, M, Wong, G, Grohn, OH, Yla-Herttuala, S, and Hakumaki, JM. (2008). 1H MR spectroscopic imaging of

phospholipase-mediated membrane lipid release in apoptotic rat glioma in vivo. *Magn Reson Med* **59** (6):1232-8.

Lim, E, Modi, KD, and Kim, J. (2009). In vivo bioluminescent imaging of mammary tumors using IVIS spectrum. *J Vis Exp* (26).

Lim, E, Vaillant, F, Wu, D, Forrest, NC, Pal, B, Hart, AH, Asselin-Labat, ML, Gyorki, DE, Ward, T, Partanen, A, Feleppa, F, Huschtscha, LI, Thorne, HJ, kConFab, Fox, SB, Yan, M, French, JD, Brown, MA, Smyth, GK, Visvader, JE, and Lindeman, GJ. (2009). Aberrant luminal progenitors as the candidate target population for basal tumor development in BRCA1 mutation carriers. *Nat Med* **15** (8):907-13.

Lin, DT, Subbaramaiah, K, Shah, JP, Dannenberg, AJ, and Boyle, JO. (2002). Cyclooxygenase-2: a novel molecular target for the prevention and treatment of head and neck cancer. *Head Neck* **24** (8):792-9.

Lin, LL, Wartmann, M, Lin, AY, Knopf, JL, Seth, A, and Davis, RJ. (1993). cPLA2 is phosphorylated and activated by MAP kinase. *Cell* **72** (2):269-78.

Lu, H, Chen, CS, and Waxman, DJ. (2009). Potentiation of methoxymorpholinyl doxorubicin antitumor activity by P450 3A4 gene transfer. *Cancer Gene Ther* **16** (5):393-404.

Marshall, MV, Rasmussen, JC, Tan, IC, Aldrich, MB, Adams, KE, Wang, X, Fife, CE, Maus, EA, Smith, LA, and Sevick-Muraca, EM. (2010). Near-Infrared Fluorescence Imaging in Humans with Indocyanine Green: A Review and Update. *Open Surg Oncol J* **2** (2):12-25.

Mawn, TM, Popov, AV, Beardsley, NJ, Stefflova, K, Milkevitch, M, Zheng, G, and Delikatny, EJ. (2011). In vivo detection of phospholipase C by enzyme-activated near-infrared probes. *Bioconjug Chem* **22** (12):2434-43.

Meric, F, Mirza, NQ, Vlastos, G, Buchholz, TA, Kuerer, HM, Babiera, GV, Singletary, SE, Ross, MI, Ames, FC, Feig, BW, Krishnamurthy, S, Perkins, GH, McNeese, MD, Strom, EA, Valero, V, and Hunt, KK. (2003). Positive surgical margins and ipsilateral breast tumor recurrence predict disease-specific survival after breast-conserving therapy. *Cancer* **97** (4):926-33.

Meyer, AM, Dwyer-Nield, LD, Hurteau, GJ, Keith, RL, O'Leary, E, You, M, Bonventre, JV, Nemenoff, RA, and Malkinson, AM. (2004). Decreased lung tumorigenesis in mice genetically deficient in cytosolic phospholipase A2. *Carcinogenesis* **25** (8):1517-24.

Milkevitch, M, Beardsley, NJ, and Delikatny, EJ. (2010). Phenylbutyrate induces apoptosis and lipid accumulations via a peroxisome proliferator-activated receptor gamma-dependent pathway. *NMR Biomed* **23** (5):473-9.

Milkevitch, M, Jeitner, TM, Beardsley, NJ, and Delikatny, EJ. (2007). Lovastatin enhances phenylbutyrate-induced MR-visible glycerophosphocholine but not apoptosis in DU145 prostate cells. *Biochim Biophys Acta* **1771** (9):1166-76.

Milkevitch, M, Shim, H, Pilatus, U, Pickup, S, Wehrle, JP, Samid, D, Poptani, H, Glickson, JD, and Delikatny, EJ. (2005). Increases in NMR-visible lipid and glycerophosphocholine during phenylbutyrate-induced apoptosis in human prostate cancer cells. *Biochim Biophys Acta* **1734** (1):1-12.

Minn, AJ, Gupta, GP, Siegel, PM, Bos, PD, Shu, W, Giri, DD, Viale, A, Olshen, AB, Gerald, WL, and Massague, J. (2005). Genes that mediate breast cancer metastasis to lung. *Nature* **436** (7050):518-24.

Mochizuki, N, Yamashita, S, Kurokawa, K, Ohba, Y, Nagai, T, Miyawaki, A, and Matsuda, M. (2001). Spatio-temporal images of growth-factor-induced activation of Ras and Rap1. *Nature* **411** (6841):1065-8.

Moestue, SA, Borgan, E, Huuse, EM, Lindholm, EM, Sitter, B, Borresen-Dale, AL, Engebraaten, O, Maelandsmo, GM, and Gribbestad, IS. (2010). Distinct choline metabolic profiles are associated with differences in gene expression for basal-like and luminal-like breast cancer xenograft models. *BMC Cancer* **10**:433.

Moon, WK, Lin, Y, O'Loughlin, T, Tang, Y, Kim, DE, Weissleder, R, and Tung, CH. (2003). Enhanced tumor detection using a folate receptor-targeted near-infrared fluorochrome conjugate. *Bioconjug Chem* **14** (3):539-45.

Mosior, M, Six, DA, and Dennis, EA. (1998). Group IV cytosolic phospholipase A2 binds with high affinity and specificity to phosphatidylinositol 4,5-bisphosphate resulting in dramatic increases in activity. *J Biol Chem* **273** (4):2184-91.

Murakami, M, Taketomi, Y, Miki, Y, Sato, H, Hirabayashi, T, and Yamamoto, K. (2011). Recent progress in phospholipase A(2) research: from cells to animals to humans. *Prog Lipid Res* **50** (2):152-92.

Murakoshi, H, Iino, R, Kobayashi, T, Fujiwara, T, Ohshima, C, Yoshimura, A, and Kusumi, A. (2004). Single-molecule imaging analysis of Ras activation in living cells. *Proc Natl Acad Sci U S A* **101** (19):7317-22.

Murray-Whelan, R, Reid, JD, Piuz, I, Hezareh, M, and Schlegel, W. (1995). The guanine-nucleotide-binding protein subunit G alpha i2 is involved in calcium activation of phospholipase A2. Effects of the dominant negative G alpha i2 mutant, [G203T]G alpha i2, on activation of phospholipase A2 in Chinese hamster ovary cells. *Eur J Biochem* **230** (1):164-9.

Muthalif, MM, Hefner, Y, Canaan, S, Harper, J, Zhou, H, Parmentier, JH, Aebersold, R, Gelb, MH, and Malik, KU. (2001). Functional interaction of calcium-/calmodulin-dependent protein kinase II and cytosolic phospholipase A(2). *J Biol Chem* **276** (43):39653-60.

Nakamura, H, Wakita, S, Suganami, A, Tamura, Y, Hanada, K, and Murayama, T. (2010). Modulation of the activity of cytosolic phospholipase A2alpha (cPLA2alpha) by cellular sphingolipids and inhibition of cPLA2alpha by sphingomyelin. *J Lipid Res* **51** (4):720-8.

Nebert, DW, and Dalton, TP. (2006). The role of cytochrome P450 enzymes in endogenous signalling pathways and environmental carcinogenesis. *Nat Rev Cancer* **6** (12):947-60.

Nguyen, QT, and Tsien, RY. (2013). Fluorescence-guided surgery with live molecular navigation--a new cutting edge. *Nat Rev Cancer* **13** (9):653-62.

Normanno, N, De Luca, A, Bianco, C, Strizzi, L, Mancino, M, Maiello, MR, Carotenuto, A, De Feo, G, Caponigro, F, and Salomon, DS. (2006). Epidermal growth factor receptor (EGFR) signaling in cancer. *Gene* **366** (1):2-16.

Nottebohm, M, Licha, T., Ghergut, I., Nödler, K., Sauter, M. 2010. Development of thermosensitive tracers for push-pull experiments in geothermal reservoir characterization. In *Proceedings World Geothermal Congerss*. Bali, Indonesia.

Ntziachristos, V. (2010). Going deeper than microscopy: the optical imaging frontier in biology. *Nat Methods* **7** (8):603-14.

O'Sullivan, CC, Bradbury, I, Campbell, C, Spielmann, M, Perez, EA, Joensuu, H, Costantino, JP, Delaloge, S, Rastogi, P, Zardavas, D, Ballman, KV, Holmes, E, de Azambuja, E, Piccart-Gebhart, M, Zujewski, JA, and Gelber, RD. (2015). Efficacy of Adjuvant Trastuzumab for Patients With Human Epidermal Growth Factor Receptor 2-Positive Early Breast Cancer and Tumors </= 2 cm: A Meta-Analysis of the Randomized Trastuzumab Trials. *J Clin Oncol* **33** (24):2600-8.

Oei, HH, van der Meer, IM, Hofman, A, Koudstaal, PJ, Stijnen, T, Breteler, MM, and Witteman, JC. (2005). Lipoprotein-associated phospholipase A2 activity is associated with risk of coronary heart disease and ischemic stroke: the Rotterdam Study. *Circulation* **111** (5):570-5.

Osborne, CK. (1998). Tamoxifen in the treatment of breast cancer. *N Engl J Med* **339** (22):1609-18.

Panel, V, Boelle, PY, Ayala-Sanmartin, J, Jouniaux, AM, Hamelin, R, Masliah, J, Trugnan, G, Flejou, JF, and Wendum, D. (2006). Cytoplasmic phospholipase A2 expression in human colon adenocarcinoma is correlated with cyclooxygenase-2 expression and contributes to prostaglandin E2 production. *Cancer Lett* **243** (2):255-63.

Panigrahy, D, Kaipainen, A, Greene, ER, and Huang, S. (2010). Cytochrome P450-derived eicosanoids: the neglected pathway in cancer. *Cancer Metastasis Rev* **29** (4):723-35.

Park, JB, Lee, CS, Jang, JH, Ghim, J, Kim, YJ, You, S, Hwang, D, Suh, PG, and Ryu, SH. (2012). Phospholipase signalling networks in cancer. *Nat Rev Cancer* **12** (11):782-92.

Park, JM, Kanaoka, Y, Eguchi, N, Aritake, K, Grujic, S, Materi, AM, Buslon, VS, Tippin, BL, Kwong, AM, Salido, E, French, SW, Urade, Y, and Lin, HJ. (2007). Hematopoietic prostaglandin D synthase suppresses intestinal adenomas in ApcMin/+ mice. *Cancer Res* **67** (3):881-9.

Pickard, RT, Chiou, XG, Strifler, BA, DeFelippis, MR, Hyslop, PA, Tebbe, AL, Yee, YK, Reynolds, LJ, Dennis, EA, Kramer, RM, and Sharp, JD. (1996). Identification of essential residues for the catalytic function of 85-kDa cytosolic phospholipase A2. Probing the role of histidine, aspartic acid, cysteine, and arginine. *J Biol Chem* **271** (32):19225-31.

Popov, AV, Mawn, TM, Kim, S, Zheng, G, and Delikatny, EJ. (2010). Design and synthesis of phospholipase C and A2-activatable near-infrared fluorescent smart probes. *Bioconjug Chem* **21** (10):1724-7.

Popovtzer, R, Agrawal, A, Kotov, NA, Popovtzer, A, Balter, J, Carey, TE, and Kopelman, R. (2008). Targeted gold nanoparticles enable molecular CT imaging of cancer. *Nano Lett* **8** (12):4593-6.

Prat, A, and Perou, CM. (2011). Deconstructing the molecular portraits of breast cancer. *Mol Oncol* **5** (1):5-23.

Rao, J, Dragulescu-Andrasi, A, and Yao, H. (2007). Fluorescence imaging in vivo: recent advances. *Curr Opin Biotechnol* **18** (1):17-25.

Regula, J, MacRobert, AJ, Gorchein, A, Buonaccorsi, GA, Thorpe, SM, Spencer, GM, Hatfield, AR, and Bown, SG. (1995). Photosensitisation and photodynamic therapy of oesophageal, duodenal, and colorectal tumours using 5 aminolaevulinic acid induced protoporphyrin IX--a pilot study. *Gut* **36** (1):67-75.

Rocha, S, De Keersmaecker, H, Hutchison, JA, Vanhoorelbeke, K, Martens, JA, Hofkens, J, and Uji-i, H. (2014). Membrane remodeling processes induced by phospholipase action. *Langmuir* **30** (16):4743-51.

Ross, JS, Fletcher, JA, Linette, GP, Stec, J, Clark, E, Ayers, M, Symmans, WF, Pusztai, L, and Bloom, KJ. (2003). The Her-2/neu gene and protein in breast cancer 2003: biomarker and target of therapy. *Oncologist* **8** (4):307-25.

Sarpara, GH, Si, JH, Palmer, DA, French, MT, Evans, M, and Miller, JN. (1999). A new long-wavelength fluorigenic substrate for alkaline phosphatase: synthesis and characterisation. *Anal Commun* **36** (1):19-20.

Schaafsma, BE, Mieog, JS, Hutteman, M, van der Vorst, JR, Kuppen, PJ, Lowik, CW, Frangioni, JV, van de Velde, CJ, and Vahrmeijer, AL. (2011). The clinical use of indocyanine green as a near-infrared fluorescent contrast agent for image-guided oncologic surgery. *J Surg Oncol* **104** (3):323-32.

Sertznig, P, Seifert, M, Tilgen, W, and Reichrath, J. (2007). Present concepts and future outlook: function of peroxisome proliferator-activated receptors (PPARs) for pathogenesis, progression, and therapy of cancer. *J Cell Physiol* **212** (1):1-12.

Setsukinai, K, Urano, Y, Kakinuma, K, Majima, HJ, and Nagano, T. (2003). Development of novel fluorescence probes that can reliably detect reactive oxygen species and distinguish specific species. *J Biol Chem* **278** (5):3170-5.

Shcherbakova, DM, and Verkhusha, VV. (2013). Near-infrared fluorescent proteins for multicolor in vivo imaging. *Nat Methods* **10** (8):751-4.

Shinoda, J, Yano, H, Yoshimura, S, Okumura, A, Kaku, Y, Iwama, T, and Sakai, N. (2003). Fluorescence-guided resection of glioblastoma multiforme by using high-dose fluorescein sodium. Technical note. *J Neurosurg* **99** (3):597-603.

Shu, X, Royant, A, Lin, MZ, Aguilera, TA, Lev-Ram, V, Steinbach, PA, and Tsien, RY. (2009). Mammalian expression of infrared fluorescent proteins engineered from a bacterial phytochrome. *Science* **324** (5928):804-7.

Simmons, DL, Botting, RM, and Hla, T. (2004). Cyclooxygenase isozymes: the biology of prostaglandin synthesis and inhibition. *Pharmacol Rev* **56** (3):387-437.

Singletary, SE. (2002). Surgical margins in patients with early-stage breast cancer treated with breast conservation therapy. *Am J Surg* **184** (5):383-93.

Slamon, DJ, Clark, GM, Wong, SG, Levin, WJ, Ullrich, A, and McGuire, WL. (1987). Human breast cancer: correlation of relapse and survival with amplification of the HER-2/neu oncogene. *Science* **235** (4785):177-82.

Stummer, W, Pichlmeier, U, Meinel, T, Wiestler, OD, Zanella, F, Reulen, HJ, and Group, AL-GS. (2006). Fluorescence-guided surgery with 5-aminolevulinic acid for resection of malignant glioma: a randomised controlled multicentre phase III trial. *Lancet Oncol* **7** (5):392-401.

Subbaramaiah, K, Norton, L, Gerald, W, and Dannenberg, AJ. (2002). Cyclooxygenase-2 is overexpressed in HER-2/neu-positive breast cancer: evidence for involvement of AP-1 and PEA3. *J Biol Chem* **277** (21):18649-57.

Subramanian, P, Stahelin, RV, Szulc, Z, Bielawska, A, Cho, W, and Chalfant, CE. (2005). Ceramide 1-phosphate acts as a positive allosteric activator of group IVA cytosolic phospholipase A2 alpha and enhances the interaction of the enzyme with phosphatidylcholine. *J Biol Chem* **280** (18):17601-7.

Terwisscha van Scheltinga, AG, van Dam, GM, Nagengast, WB, Ntziachristos, V, Hollema, H, Herek, JL, Schroder, CP, Kosterink, JG, Lub-de Hoog, MN, and de Vries, EG. (2011). Intraoperative near-infrared fluorescence tumor imaging with vascular endothelial growth factor and human epidermal growth factor receptor 2 targeting antibodies. *J Nucl Med* **52** (11):1778-85.

Theriot, JA, and Mitchison, TJ. (1991). Actin microfilament dynamics in locomoting cells. *Nature* **352** (6331):126-31.

Thun, MJ, Henley, SJ, and Patrono, C. (2002). Nonsteroidal anti-inflammatory drugs as anticancer agents: mechanistic, pharmacologic, and clinical issues. *J Natl Cancer Inst* **94** (4):252-66.

Tian, W, Wijewickrama, GT, Kim, JH, Das, S, Tun, MP, Gokhale, N, Jung, JW, Kim, KP, and Cho, W. (2008). Mechanism of regulation of group IVA phospholipase A2 activity by Ser727 phosphorylation. *J Biol Chem* **283** (7):3960-71.

Tjoelker, LW, Eberhardt, C, Unger, J, Trong, HL, Zimmerman, GA, McIntyre, TM, Stafforini, DM, Prescott, SM, and Gray, PW. (1995). Plasma platelet-activating

factor acetylhydrolase is a secreted phospholipase A2 with a catalytic triad. *J Biol Chem* **270** (43):25481-7.

Tucker, DE, Ghosh, M, Ghomashchi, F, Loper, R, Suram, S, John, BS, Girotti, M, Bollinger, JG, Gelb, MH, and Leslie, CC. (2009). Role of phosphorylation and basic residues in the catalytic domain of cytosolic phospholipase A2alpha in regulating interfacial kinetics and binding and cellular function. *J Biol Chem* **284** (14):9596-611.

Tung, CH, Zeng, Q, Shah, K, Kim, DE, Schellingerhout, D, and Weissleder, R. (2004). In vivo imaging of beta-galactosidase activity using far red fluorescent switch. *Cancer Res* **64** (5):1579-83.

Tyagi, S, and Kramer, FR. (1996). Molecular beacons: probes that fluoresce upon hybridization. *Nat Biotechnol* **14** (3):303-8.

Urano, Y, Sakabe, M, Kosaka, N, Ogawa, M, Mitsunaga, M, Asanuma, D, Kamiya, M, Young, MR, Nagano, T, Choyke, PL, and Kobayashi, H. (2011). Rapid cancer detection by topically spraying a gamma-glutamyltranspeptidase-activated fluorescent probe. *Sci Transl Med* **3** (110):110ra119.

Vahrmeijer, AL, Hutteman, M, van der Vorst, JR, van de Velde, CJ, and Frangioni, JV. (2013). Image-guided cancer surgery using near-infrared fluorescence. *Nat Rev Clin Oncol* **10** (9):507-18.

Valabrega, G, Montemurro, F, and Aglietta, M. (2007). Trastuzumab: mechanism of action, resistance and future perspectives in HER2-overexpressing breast cancer. *Ann Oncol* **18** (6):977-84.

van Dam, GM, Themelis, G, Crane, LM, Harlaar, NJ, Pleijhuis, RG, Kelder, W, Sarantopoulos, A, de Jong, JS, Arts, HJ, van der Zee, AG, Bart, J, Low, PS, and Ntziachristos, V. (2011). Intraoperative tumor-specific fluorescence imaging in ovarian cancer by folate receptor-alpha targeting: first in-human results. *Nat Med* **17** (10):1315-9.

van Rossum, GS, Drummen, GP, Verkleij, AJ, Post, JA, and Boonstra, J. (2004). Activation of cytosolic phospholipase A2 in Her14 fibroblasts by hydrogen peroxide: a p42/44(MAPK)-dependent and phosphorylation-independent mechanism. *Biochim Biophys Acta* **1636** (2-3):183-95.

von Burstin, J, Eser, S, Seidler, B, Meining, A, Bajbouj, M, Mages, J, Lang, R, Kind, AJ, Schnieke, AE, Schmid, RM, Schneider, G, and Saur, D. (2008). Highly sensitive detection of early-stage pancreatic cancer by multimodal near-infrared molecular imaging in living mice. *Int J Cancer* **123** (9):2138-47.

Wang, D, and Dubois, RN. (2010). Eicosanoids and cancer. *Nat Rev Cancer* **10** (3):181-93.

Warther, D, Bolze, F, Leonard, J, Gug, S, Specht, A, Puliti, D, Sun, XH, Kessler, P, Lutz, Y, Vonesch, JL, Winsor, B, Nicoud, JF, and Goeldner, M. (2010). Live-cell one- and two-photon uncaging of a far-red emitting acridinone fluorophore. *J Am Chem Soc* **132** (8):2585-90.

Weissleder, R. (2001). A clearer vision for in vivo imaging. *Nat Biotechnol* **19** (4):316-7.

Weissleder, R. (2006). Molecular imaging in cancer. *Science* **312** (5777):1168-71.

Weissleder, R, and Pittet, MJ. (2008). Imaging in the era of molecular oncology. *Nature* **452** (7187):580-9.

Weissleder, R, Tung, CH, Mahmood, U, and Bogdanov, A, Jr. (1999). In vivo imaging of tumors with protease-activated near-infrared fluorescent probes. *Nat Biotechnol* **17** (4):375-8.

Willmann, JK, Kimura, RH, Deshpande, N, Lutz, AM, Cochran, JR, and Gambhir, SS. (2010). Targeted contrast-enhanced ultrasound imaging of tumor angiogenesis with contrast microbubbles conjugated to integrin-binding knottin peptides. *J Nucl Med* **51** (3):433-40.

Willmann, JK, van Bruggen, N, Dinkelborg, LM, and Gambhir, SS. (2008). Molecular imaging in drug development. *Nat Rev Drug Discov* **7** (7):591-607.

Wilson, T, and Hastings, JW. (1998). Bioluminescence. *Annu Rev Cell Dev Biol* **14**:197-230.

Winstead, MV, Balsinde, J, and Dennis, EA. (2000). Calcium-independent phospholipase A(2): structure and function. *Biochim Biophys Acta* **1488** (1-2):28-39.

Xu, H, and Rice, BW. (2009). In-vivo fluorescence imaging with a multivariate curve resolution spectral unmixing technique. *J Biomed Opt* **14** (6):064011.

Xu, Y, Fang, XJ, Casey, G, and Mills, GB. (1995). Lysophospholipids activate ovarian and breast cancer cells. *Biochem J* **309 (Pt 3)**:933-40.

Zardavas, D, Irrthum, A, Swanton, C, and Piccart, M. (2015). Clinical management of breast cancer heterogeneity. *Nat Rev Clin Oncol* **12** (7):381-94.

Zhang, L, and Zhao, D. (2013). Liposomal encapsulation enhances in vivo near infrared imaging of exposed phosphatidylserine in a mouse glioma model. *Molecules* **18** (12):14613-28.

Zhao, C, Du, G, Skowronek, K, Frohman, MA, and Bar-Sagi, D. (2007). Phospholipase D2-generated phosphatidic acid couples EGFR stimulation to Ras activation by Sos. *Nat Cell Biol* **9** (6):706-12.